ANL-7255

ANL-7255

Argonne National Laboratory

REACTOR DEVELOPMENT PROGRAM

PROGRESS REPORT

SEPTEMBER 1966

DISCLAIMER

LEGAL NOTICE

Printed in USA. Price $4.00 . Available from the Clearinghouse for Federal Scientific and Technical Information, National Bureau of Standards, U. S. Department of Commerce, Springfield, Virginia 22151

ANL-7255
Reactor Technology
(TID-4500)
AEC Research and
Development Report

ARGONNE NATIONAL LABORATORY
9700 South Cass Avenue
Argonne, Illinois 60439

REACTOR DEVELOPMENT PROGRAM PROGRESS REPORT

September 1966

Albert V. Crewe, Laboratory Director
Stephen Lawroski, Associate Laboratory Director

Division	Director
Chemical Engineering	R. C. Vogel
Idaho	M. Novick
Metallurgy	M. V. Nevitt
Reactor Engineering	L. J. Koch
Reactor Physics	R. Avery
Remote Control	R. C. Goertz

Report coordinated by
R. M. Adams and A. Glassner

Issued October 26, 1966

Operated by The University of Chicago
under
Contract W-31-109-eng-38
with the
U. S. Atomic Energy Commission

FOREWORD

The Reactor Development Program Progress Report, issued monthly, is intended to be a means of reporting those items of significant technical progress which have occurred in both the specific reactor projects and the general engineering research and development programs. The report is organized in a way which, it is hoped, gives the clearest, most logical overall view of progress. The budget classification is followed only in broad outline, and no attempt is made to report separately on each sub-activity number. Further, since the intent is to report only items of significant progress, not all activities are reported each month. In order to issue this report as soon as possible after the end of the month editorial work must necessarily be limited. Also, since this is an informal progress report, the results and data presented should be understood to be preliminary and subject to change unless otherwise stated.

The issuance of these reports is not intended to constitute publication in any sense of the word. Final results either will be submitted for publication in regular professional journals or will be published in the form of ANL topical reports.

The last six reports issued in this series are:

March 1966	ANL-7193
April 1966	ANL-7204
May 1966	ANL-7219
June 1966	ANL-7230
July 1966	ANL-7245
August 1966	ANL-7249

REACTOR DEVELOPMENT PROGRAM

Highlights of Project Activities for September 1966

EBWR Plutonium Recycle Program

To achieve a 40-MW level of power in the EBWR, reactivity was added by replacing eight 6% enriched uranium assemblies with fully enriched uranium spike assemblies. For the revised loading, the boric acid and control rod worths were measured, for both the eight-rod shutdown and the nine-rod shutdown cases.

EBR-II

Maintenance and modifications planned during the current scheduled shutdown are almost completed as projected. Fuel handling for the next power run early in October also is essentially completed.

The new rotating reactivity oscillator and drive are being installed.

ZPR-3

Corrections have been applied to refine the measurements made on Assembly 48. The critical mass of the heterogeneous composition has been measured as 272 ± 2 kg Pu^{239}. Reactivity measurements of various small samples continued.

ZPPR

Thirteen piling holes have been completed, the foundation for the outside equipment building has been poured, and excavation for the service wing is about 90% complete.

AARR

The final project review of the Title I report has been completed.

Flow coastdown calculations on the primary system indicate that the flowrate is down to 50% in 2.3 sec and 25% in 7.0 sec. Addition of a flywheel to the primary pumps would increase the coastdown time.

The burnable poison addition backup study for the AARR fuel has indicated that 4 w/o and 6 w/o B_2O_3 additions to SiO_2 yields a boron-bearing glass particle that experiences very little distortion when fabricated into the UO_2-SS cermet fuel plates.

Fuel specimens have been successfully irradiated to a calculated peak burnup of 48.9% of the U^{235} fissionable material at a calculated peak heat flux of 2.6×10^6 Btu/hr-ft^2.

Computations show that the combined shell stresses in or near the beltline region of the reactor vessel are approximately one-half of the yield strength of either SA-302B or SA-212B steel.

TABLE OF CONTENTS

TABLE OF CONTENTS

TABLE OF CONTENTS

THIS PAGE
WAS INTENTIONALLY
LEFT BLANK

I. PLUTONIUM UTILIZATION

A. Research and Development

1. Reactor Physics

a. Calibration of Control Rods and Boric Acid Systems. Measurements showed that to achieve 40 MW of power in the EBWR it would be necessary to add reactivity. This was achieved by replacing eight 6% enriched uranium assemblies with fully enriched uranium spike assemblies. For the revised loading, measurements have been made of the boric acid and control-rod worths, including determinations of the minimum boric acid concentration for the eight-rod shutdown case and the nine-rod shutdown case for the unborated system.

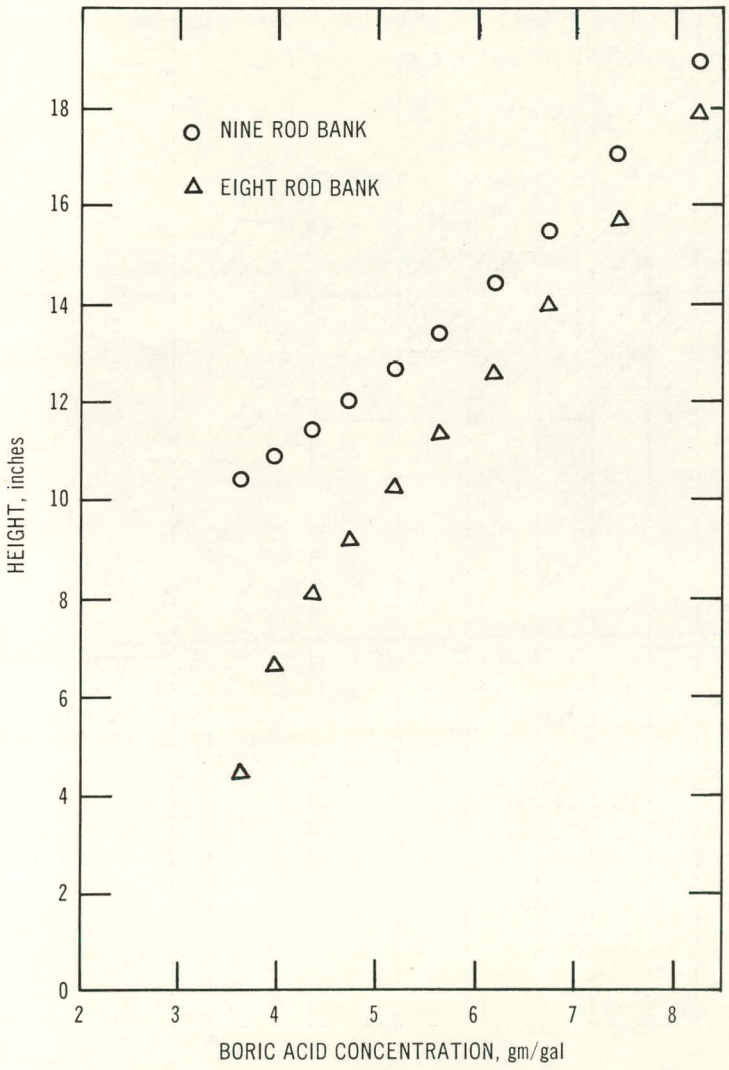

Fig. 1. Critical Nine-rod Bank and Critical Eight-rod Bank Heights (with Center Rod at 39.5 in.) vs. Boric Acid Concentration

In Fig. 1, the critical nine-rod and the critical eight-rod bank heights, obtained by raising the center rod to its maximum allowable height, are plotted as functions of boric acid concentration. For the nine-rod shutdown operation criterion to be satisfied, the nine-rod bank should be partly withdrawn when the reactor water is unborated. From Fig. 1, it is seen that this criterion is satisfied as the critical nine-rod bank height has a positive intercept when extrapolated to zero boric acid concentration. The minimum boric acid concentration required for eight-rod shutdown is obtained by extrapolating the critical eight-rod bank curve to zero bank height. From Fig. 1, this minimum allowable boric acid concentration is found to be 3.4 g/gal.

The reactivity effect of the eight spike assemblies can be estimated from the

change in the critical height of the nine-rod bank for a given boric acid concentration. At a boric acid concentration of 6.68 g/gal the critical nine-rod bank height had to be lowered from 18.65 to 15.5 in. For this range of bank heights, the bank worth has been found to be 0.55 ± 0.12%k/in. Thus the replacement of eight shim assemblies with spike assemblies is estimated to result in an increase in reactivity of 1.73 ± 0.37%k. Computations by two-dimensional, four-group, diffusion theory predicted an increase in reactivity of 1.95%k for this replacement.

Measurements were made of the boric acid worth as a function of boric acid concentration between 8.2 and 3.6 g/gal and of the nine-rod bank worth as a function of bank height between 19 and 10 in. The results are summarized in Figs. 2 and 3, in which the shading represents the

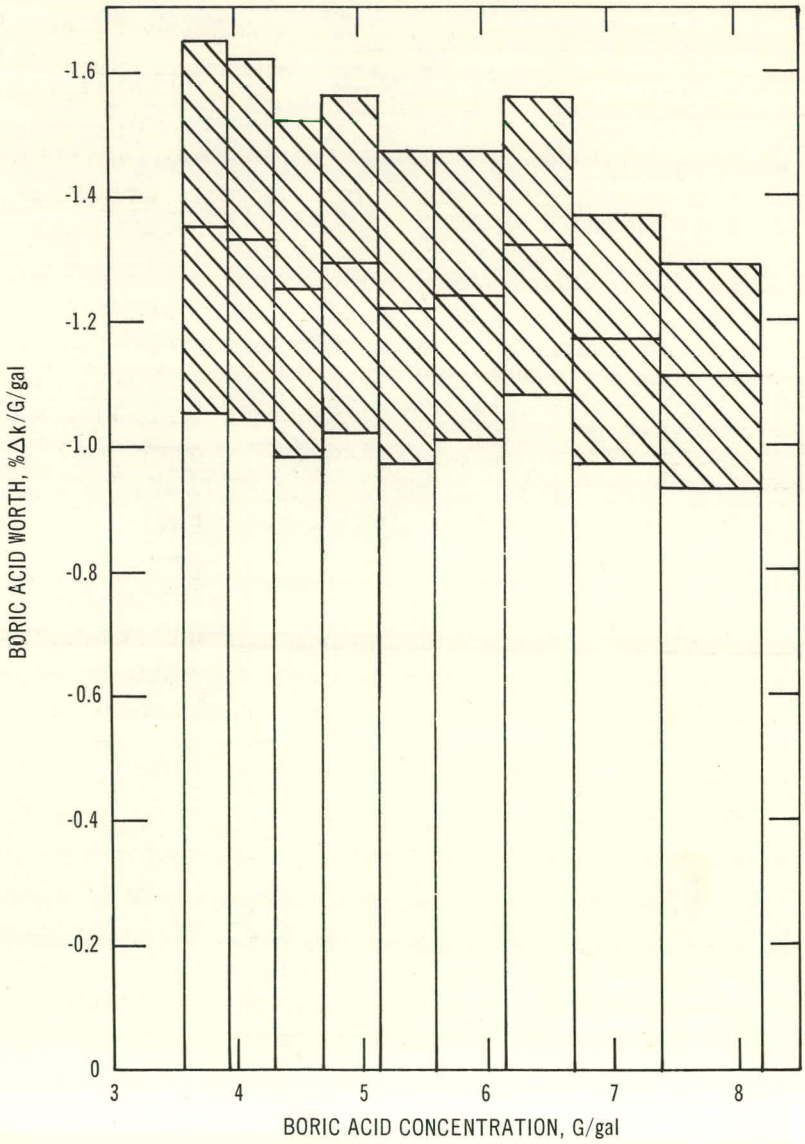

Fig. 2. Boric Acid Worth vs. Boric Acid Concentration for Full EBWR Fuel Loading with Eight Spikes

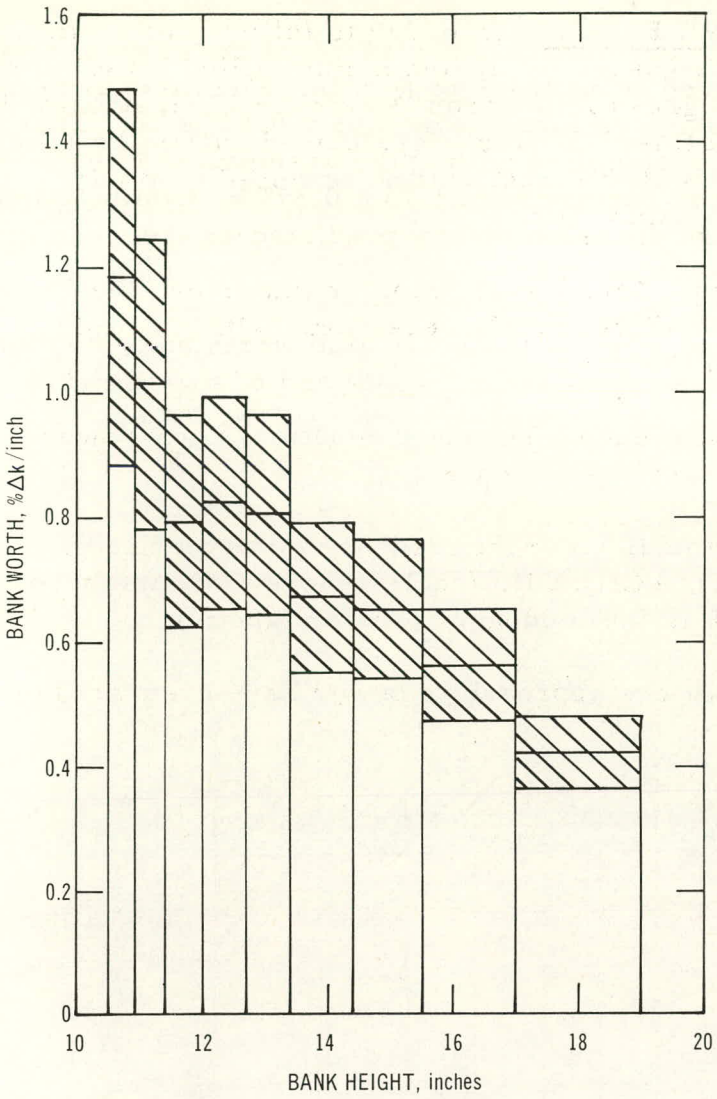

Fig. 3. Nine-rod Bank Worth vs. Bank Height for Full EBWR Fuel Loading with Eight Spikes

experimental error. Because of the relatively large experimental error we can only report an average boric acid worth of $(-1.25 \pm 0.30)\%\Delta k/g/gal$ although a trend toward increasing worth with decreasing concentration is discernible. This measured boric acid worth is slightly higher than the predicted value of approximately $-1.0\%\Delta k/g/gal$. The nine-rod bank reactivity worths increase as the bank is lowered. The explanation for this effect is that as the rods are inserted the active portion of the core becomes progressively flattened and therefore an incremental movement of the bank has a progressively greater reactivity effect.

2. Operations

a. EBWR Facility. After closing the EBWR pressure vessel, preparatory to heat generation with a plutonium core, the vessel was subjected to the following treatment: After a warm hydrostatic pressure test (975 psi at 150°F), which is in accordance with the new EBWR safety criterion pertaining to an unirradiated steel pressure vessel, the vessel was heated to 370°F by means of the startup heater. This test was executed to ascertain if the heater could raise the temperature of the vessel to a minimum of 350°F. At the end of the experimental lifetime of the Plutonium Recycle Facility, the NDT is expected to rise from ~80°F (at present time) to a maximum 230°F and in accordance with safety considerations, the vessel should be heated to NDT of 230 + 120 or 350°F before subjecting the pressure vessel to normal operating stress. The necessary heat to attain 350°F is supplied at each startup by the heater.

b. Irradiation of EBWR Facility. In order to follow plutonium irradiation damage to pressure vessel steel, five helium-filled irradiation surveillance capsules (see Progress Report for December 1964, ANL-6997, p. 47) containing EBWR vessel SA-212B steel were placed within the reactor vessel before closure. Samples of the steel will be removed (and NDT checked) after various neutron exposures.

c. Transfer Functions. Zero power transfer functions (see Progress Report for June 1966, ANL-7230, p. 47) were rerun with the eight spiked elements placed around the core.

The data have been reduced, but the theoretical zero-power curve has not been fit to the experimental data.

Digital programs to calculate the feedback characteristics have been written to calculate $(1+GH)$, GH, and H, where G is the zero-power transfer function and H is the feedback transfer function.

Test procedures for the approach to power have been written.

II. LIQUID METAL FAST BREEDER REACTORS

A. EBR-II

1. Operations

The scheduled reactor shutdown period, planned to accomplish numerous maintenance and modifications tasks, has proceeded as projected during the reporting period. Most of the fuel handling for Run No. 22, currently scheduled to begin October 11 for 1000 MWd, has been accomplished. Nineteen subassemblies were removed from the core: these include 7 core-type, 8 inner blanket, 2 control rod, 1 experimental and 1 source subassembly. Seventeen subassemblies were loaded into the core: 8 core-type, 5 inner blanket, 1 control rod, and 3 outer blanket subassemblies. The fuel subassemblies removed had all reached their burnup limit of 1.2 a/o max. One inner blanket subassembly will be loaded, when available, later in the shutdown period and control rod position No. 8 is reserved for installation of the rotating oscillator rod.

Cooling down of the primary system to 350°F in preparation for refilling the secondary sodium system was underway at month's end.

The main turbine was disassembled for routine inspection as part of the planned program this month. Damaged blading was found in the second and third stages, with slight damage apparent as far down as the seventh stage. Apparently this was caused by a portion of a spill strip which broke from the turbine casing in the vicinity of the first stage. A manufacturer's specialist (GE) has replaced or repaired all of the blading in the first or second stages, and the turbine is being reassembled. The remainder of the turbine appears to be in good condition.

An inspection of the turbine end of the main generator revealed that the inner hydrogen seal oil ring was slightly deflected from its normal position. This condition would cause a higher than normal seal oil flow and would create the previously observed difficulty in maintaining hydrogen purity in the scavenged gas. The ring was machined and reinstalled.

Control rod drive No. 8 was removed from the reactor in preparation for installation of the oscillator rod drive (see Sect. II.A.2.a). Gauging and alignment measurements were taken to determine actual clearances and grid-to-reactor cover alignments so that necessary machining can be done on the oscillator assembly prior to installation. The oscillator drive is on the site and installation is scheduled to commence the first week in October.

a. Experimental Irradiations. The status of all experimental irradiations in the grid at the end of September remained the same as at the end of August (see Progress Report for August 1966, ANL-7249, p. 13),

except that subassembly XO13 has been removed from the reactor and transferred to the storage basket after completing its scheduled irradiation.

Twenty-two mixed oxide capsules were received from NUMEC and are undergoing nondestructive testing inspection. These comprise groups B and C of the NUMEC fuel-evaluation program and are scheduled for insertion into the reactor.

Restricted flow calibrations for the Mark B, 19-pin irradiation subassembly have been completed.

b. Rotating Plug Seals. Improved access was provided to the outer annulus (air side) of the large rotating plug seal trough by enlarging the "window" heater hole and penetrating the gas seal above the trough. An access hole had been drilled to the outer annulus of the small plug trough in August.

The first operation performed through the new access holes was vacuum cleaning to remove as much drossy or oxide-like material as possible from the surface of the alloy. Approximately 26 lb of material was removed from the small plug trough by this method, approximately 50 lb from the large plug trough.

After the vacuum-cleaning operations, exploratory probing of the alloy in the outer annuli of the troughs disclosed the presence of moderately compacted deposits of oxide-like material extending several inches down in the trough and, except for a few discontinuities, apparently extending around the trough circumference. It was found that this material could be removed by "coring" with a half-inch-diameter tube. Accordingly, the method was used to remove as much material as practicable.

Next, a "wire-brushing" technique was found to be effective in removing oxide-like material from the troughs. This technique simply involves inserting a round steel-bristled brush, about 3/4 in. in diameter, into the trough and rotating and oscillating it in the molten alloy. The oxide-like material is worked into the bristles and largely remains there when the brush is withdrawn through the access hole. This material can then be tapped out of the brush into a container. It is believed that the coring and brushing techniques have effectively broken up the compacted material in the troughs and have removed a substantial portion of it. However, it is not known yet how much material remains on the alloy surface or dispersed in the upper portion of the alloy.

Approximately 68 lb of material was removed from the small plug trough by the coring and brushing operations; about the same amount from the large plug trough.

Following the cleaning operations, the alloy levels in the troughs have been measured to be 8 in. in the small plug trough and $6\frac{3}{4}$ in. in the large plug trough. It will be necessary to add new alloy to restore the specified levels for operation, which are 9 and $8\frac{1}{4}$ in., respectively.

The material removed contains an indeterminate amount of metallic alloy--both as the unoxidized metallic component of the "dross" and as small bits of alloy removed with the oxide-like material during cleaning operations. Therefore, the weights quoted above should not be construed as actual oxides of the alloy components, even though the bulk of the material has oxide-like characteristics.

Two selected samples of nodular oxide-like material were analyzed chemically for bismuth and sodium content. Results are as follows:

Sample No. 1		Sample No. 2	
"Oxide" pieces selected from core samples of compacted material, showing more light-colored material than Sample 2.		Gray compacted "oxide" from core samples of compacted material.	
Bi	42.8 w/o	Bi	42.3 w/o
Na	5.5 w/o	Na	4.5 w/o

The sodium oxide (Na_2O) content of Samples 1 and 2, equivalent to the analyzed sodium values, are 7.5 and 6.1%, respectively. These are comparable to the sodium oxide contents of samples reported previously (see Progress Report for July 1965, ANL-7082, p. 2, and Progress Report for September 1965, ANL-7105, p. 2).

Some pieces of initially gray oxide in the compacted material removed from the troughs by "coring" turned white after a few hours of exposure to air. This may reflect a sodium content considerably greater than those tabulated above which are more representative of the composite material.

The bismuth content of these samples is lower than the content of the eutectic alloy (which is 57 w/o Bi) because of the presence of significant amounts of sodium and probably because of preferential oxidation of tin resulting in a larger percentage of tin in the "oxide" material than in the alloy.

Further work is required to define the effects of sodium upon the properties of the alloy and its oxidation products.

c. Determination of Carbon in EBR-II Secondary Sodium. Twenty analyses on four samples of secondary sodium, by the oxyacidic flux analytical method (see Progress Report for July 1966, ANL-7245, p. 20), gave

an average carbon value of 14.7 ppm with a standard deviation of ±1.8 ppm. Samples of varying size were used during this series of analyses to permit extrapolation of the data to obtain an estimate of the blank value in the presence of sodium. Extrapolation of a curve representing the least-squares fit of the data indicates that a zero blank in the presence of sodium is not inconsistent with the observed data.

The results of carbon recovery tests in the presence of sodium, shown in Table I, indicate that gettering of CO_2 by sodium oxides is obviated in the presence of the acidic flux. Carbon was added to the reaction bottle as potassium acid phthalate; then a sample of reactor secondary system sodium was introduced. A more rigorous test in which standard samples of sodium with a known carbon content are analyzed by the oxyacidic flux method is desirable, and will be performed when such standard samples can be prepared reliably.

TABLE I. Carbon Recovery Tests

Run No.	Weight Sodium Sample (g)	Weight Carbon Present* (μg)	Amount Carbon Added (μg)	Total Carbon Present (μg)	Carbon Found (μg)	Percent Recovery
1	0.7954	11.6	160.3	171.9	172.5	100.3
2	0.8026	11.8	160.3	172.1	173.5	100.8
3	0.6143	9.0	160.3	169.3	164.5	97.1

*Calculated on the basis of 14.7 ppm carbon in sodium.

2. Reactor Improvements

a. Oscillator System Mark II. The third, and final, series of high-speed test runs of oscillator rod and drive were successfully completed (see Progress Report for August 1966, ANL-7249, pp. 10-11).

At the conclusion of the third series, the oscillator drive system was disassembled and inspected. The appearance of all the bearings, including the oscillator rod bearing, was good; careful inspection did not disclose any measurable wear. The two lower bearings have been operated for 781,000 cycles since they were replaced after the first series of test runs, and the three upper bearings as well as the oscillator rod bearings have received a total of 1,085,000 cycles through the entire series of test runs. In view of the length of operation and satisfactory bearing condition, the tests were terminated and the oscillator drive system was crated and shipped to the EBR-II site in Idaho.

The first oscillator rod containing two capsules of boron carbide was completed and dynamically balanced in time to be shipped with the drive system.

The second oscillator rod containing one capsule of boron carbide is in final assembly and will be shipped to Idaho as soon as inspection and dynamic balance tests are completed. This oscillator rod will not be used until the first rod experiments have been completed.

b. Irradiation Subassembly Mark B-7. Irradiation experiments on structural materials will be performed using the Mark B-7 type of irradiation subassembly which will be inserted into the EBR-II reactor core at a location where it will be exposed to high heat generation. The most desirable region would be in the second row of core subassemblies.

The required heat-generation calculations, flow-orificing tests, thermal analysis, and stress calculations have been completed. The Mark B-7 type (see Fig. 4) provides a cluster of seven irradiation specimen tubes, tightly packed, without spiral spacing wires, each with an inside diameter of 0.750 in. and an overall length of $57\frac{7}{8}$ in.

It was calculated that a heat generation of 11.5 to 15.4 kW per subassembly can be expected. This heat generation is small compared to that of a fuel subassembly in the same region of the core, so that a major portion of the coolant temperature increase through the subassembly will be due to the heat transfer from adjacent fuel subassemblies. This method of heating is necessary as it is not practical to reduce the flow by orificing to less than 2 gpm, which would be required for equivalent heat generation in the irradiation specimens. The desired flow value was determined by establishing the calculated mixed coolant outlet temperature at less than 100°F below that of adjacent fuel subassemblies and considering the minimum value of heat generation of the B-7 irradiation subassemblies. Flow tests on a mockup of the Mark B-7 irradiation subassembly experimentally established the proper orificing for this flow.

No filler strips are employed in the larger flow areas along the inside perimeter of the hexagonal enclosure, as thermal analysis has shown that the most favorable temperature distribution occurs with high coolant flow in the edge channels. The coolant temperature rise in the center and edge flow channels are approximately equal in the core region with the established flow value. Even in the remote possibility that flow through the subassembly should be completely obstructed, natural-convection cooling will be adequate to prevent structural damage. The calculated maximum temperature difference is 104°F, occurring at the top of the irradiation tubes which, if applied across a single metal wall, would produce an acceptable thermal stress of 13,000 psi. The plenum volume above the irradiation tubes provides a mixing of the coolant prior to exit from the subassembly.

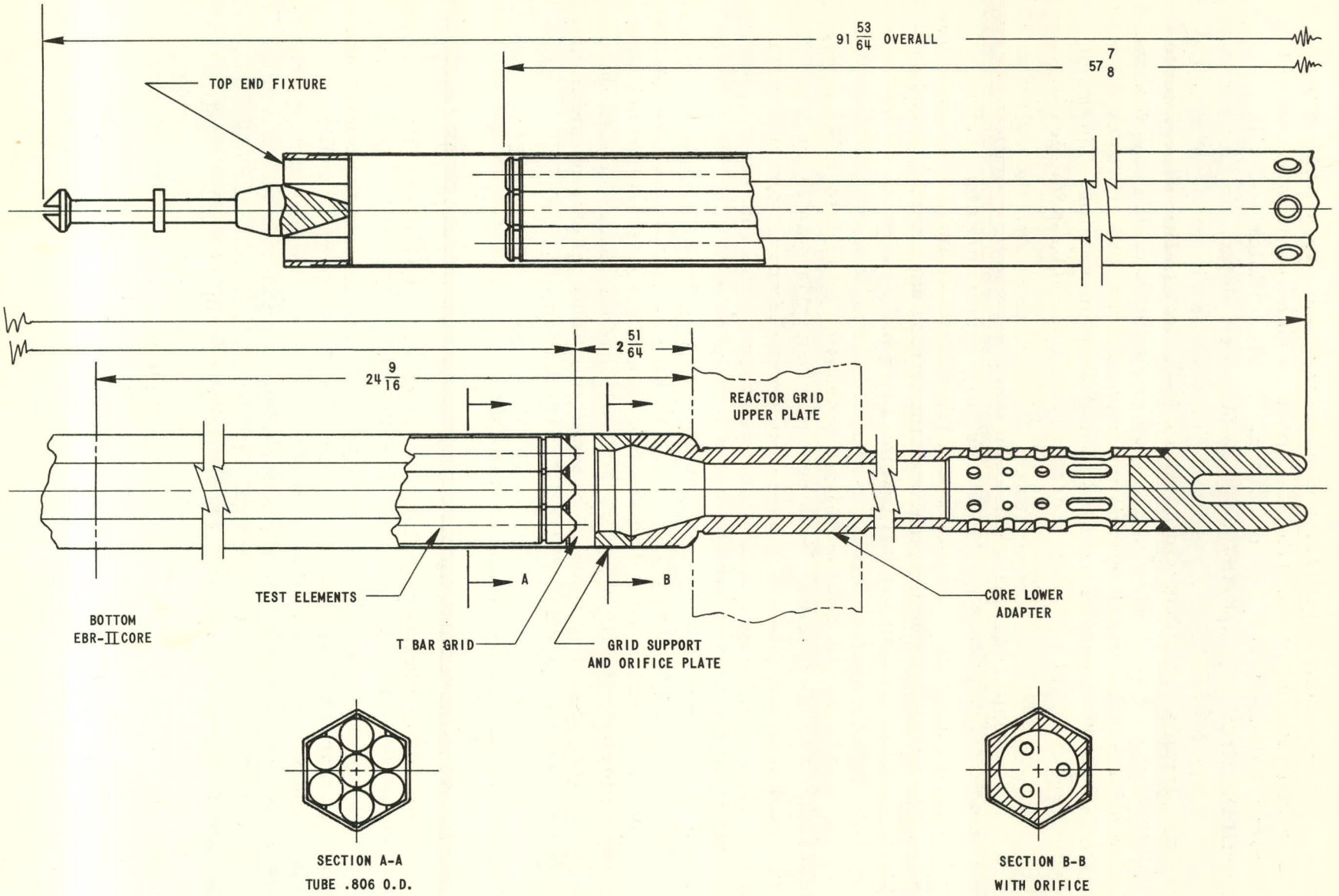

Fig. 4. EBR-II Irradiation Subassembly Mark B-7

c. Irradiation Subassembly Mark C. The assembly and detail drawings of the Mark C-19 and Mark C-37 have been completed and are now in final checking.

The Mark C-19 subassembly provides a cluster of 19 irradiation specimen tubes, 0.290 in. in OD by 0.250 in. in ID, which are spaced by a spiral wrapping of 0.080-in.-dia wire around each tube. The Mark C-37 subassembly provides 37 specimen tubes, of 0.220-in. OD and 0.188-in. ID, spaced by a spiral wrapping of 0.051-in.-dia wire on each tube.

3. Fuel Development

Tube-burst tests at 500°C have been made on a postirradiation annealed Type 304L stainless steel fuel jacket. A similar jacket with the same irradiation history was tested without annealing.

The fuel jackets, E2 and E9, were from subassembly C113, which had been in the EBR-II in reactor position 4B3 for 3665 MWd. The maximum fluence (nvt, fast neutrons) was about 1.2×10^{22} at the reactor midplane; the minimum was about 5×10^{21} at the top of the fuel rod. Temperatures along the lengths of the fuel rods in the subassembly increased from 371°C at the bottom to about 517°C at the top.

The fuel was removed from the jackets and each jacket was cut into five sections of approximately the same length (3.5 in.). The five sections from E9 were annealed in argon at 900°C for one hour prior to testing. Tangential rupture strengths were calculated from bursting pressures, and elongations were calculated from diameter changes.

Rupture strengths are given in Table II. The results for the as-irradiated specimens are compared with values from an "average" curve plotted from data accumulated from previous tests on material with a similar irradiation history. The strength of the E2 jacket increased continuously on going from the top to the bottom. The "average" curve data indicate the presence of a plateau along the lower half of the jackets, with perhaps a slight tendency for a decrease in strength at the very bottom.

TABLE II. Rupture Strength at 500°C

Specimen Location	Tangential Rupture Strength (psi)		
	Irradiated	Irradiated ("average curve")	Irradiated and Annealed
1--top	66,600	66,000	53,300
2	74,500	79,000	52,400
3	83,400	83,000	52,600
4	88,300	83,000	52,900
5--bottom	90,300	82,000	52,400

All the annealed tube sections from E9 had about the same rupture strength regardless of position along the jacket. Unirradiated jacket specimens in the annealed condition and tested at 500°C gave rupture strengths of 47,800 and 48,500 psi. The annealed irradiated specimens are obviously stronger than the original tube stock. Longer annealing times and/or higher temperatures will be tried to test their influence.

Ductility as indicated by elongation values are given in Table III. The as-irradiated specimens gave very low values of elongation. Data from previous tests gave a range of 0 to 5.1% (average, 0.2%) compared to 0 to 6.2% (average, 0.4%) for specimens from E2. After annealing the irradiated specimens (E9) and burst testing, the elongation values were 8.0 to 21.5% (average, 13.2%). Unirradiated annealed specimens gave values ranging from 8.0 to 13.6%, averaging 9.7%. The irradiated and annealed specimens seem to be more ductile than unirradiated annealed specimens at 500°C.

TABLE III. Percent Elongation from Burst Tests at 500°C

Specimen Location	Percent Circumferential Elongation			
	Irradiated		Irradiated and Annealed	
	Range	Average	Range	Average
1--top	0-0.6	0.2	10.3-21.5	14.5
2	0-6.2	1.3	12.6-21.4	14.0
3	0-1.6	0.4	10.5-14.8	12.5
4	0-0.3	0.1	9.2-21.4	14.4
5--bottom	0-0.4	0.2	8.0-13.7	10.9

The reduction of strength by annealing of the irradiated stainless steel is probably due to annealing out of defect clusters. It remains to be seen whether residual defects are the cause of the remaining increase in strength over the unirradiated annealed material. It is surprising that the ductility of the irradiated specimens after annealing is apparently greater than the unirradiated annealed material at 500°C. Examination of the microstructures of these materials may aid our understanding of the phenomenon.

4. Reactor Physics Analysis

Data from the fission-rate distribution obtained during Runs 20-A and 20-B (see Progress Report for August 1966, ANL-7249, pp. 15-17) have been compared to a calculated distribution from a two-dimensional characterization of the core by means of the CANDID code. Although these results appear to be in better agreement with the measured values, they do not resolve the apparent discrepancy between calculation and experiment. When new flux wire subassemblies are available, the experimental data will be

repeated. Meanwhile, the scattered results from the measured burnup on surveillance subassemblies will be examined in an attempt to correlate these data with the calculated power distribution.

5. Fuel Cycle Facility (FCF)

a. Surveillance of Mark-IA Fuel. Measurements of sodium level in Mark-IA fuel elements after irradiation in EBR-II continue to show differences in fuel performance which may be related to the type of operations used in their fabrication.

Examination of 41 elements, representing 6 casting batches, from subassembly C-196 (irradiated in position 3B1 to a maximum burnup of 1.11 a/o, and an average burnup of 0.93 a/o) revealed increases of fuel volume for the various casting batches ranging from 9.2 to 11.5%. Five of the six ingots used in these casting batches were prepared by melt refining fuel removed from irradiated subassemblies; the sixth, for which the highest fuel volume increase was observed, was prepared by consolidation of heels left from previous casting batches. This behavior confirmed data reported previously for subassembly C-197 which contained elements from substantially the same casting batches.

Examination of 55 elements, representing 6 additional casting batches, from subassembly C-217 (irradiated in position 4D2 to a maximum burnup of 1.06 a/o, and an average burnup of 0.84 a/o) also showed differences in fuel performance. Seventeen elements from 3 casting batches, which were prepared using ingots from melt refining fuel removed from irradiated subassemblies, showed average volume increases of 8.3%, whereas 34 elements from 2 batches cast from ingots prepared from consolidating roughly equal amounts of heels and sheared pin ends showed an average volume increase of 4.9%. Further, 4 elements from a batch cast from an ingot prepared primarily from rejected castings showed an average volume increase of 6.6%. Causes for variations in performance among different casting batches are being sought by analyses for minor constituents (C, Si, Fe, Al, Th, etc.) and studies of microstructure.

b. Plutonium in the Radial Blanket. The plutonium content of 14 samples of depleted uranium contained in three rods from radial blanket subassembly A-711 (irradiated in position 6E2 for 5050 MWd of reactor operation) varied from 119 to 2039 μg/g U as shown in Table IV.

TABLE IV. Plutonium in Radial Blanket Rods from Subassembly A-711
5050 MWd--Position 6E2

Level of Sample within Rod Expressed as % Distance from Lower End	Pu (μg/g U) in Rod Nearest Core	Pu (μg/g U) in Central Rod	Pu (μg/g U) in Rod Farthest from Core	Level of Sample within Rod Expressed as % Distance from Lower End	Pu (μg/g U) in Rod Nearest Core	Pu (μg/g U) in Central Rod	Pu (μg/g U) in Rod Farthest from Core
0.98	241	205	197	0.25	859	790	875*
0.74	1269	1052	908*	0.0	168	141	119
0.49	-	2039	1843*				

*Level uncertain.

c. Production Summary for September 1966

Subassemblies received:	16		
Subassemblies dismantled:	13		
Subassemblies fabricated:	11		
Subassemblies transferred to reactor:	10		
Pins decanned:	1230		
Melt refining:	7	Irradiated	8 Recycle
Pour yield (average):	92.7		91.7
Injection-casting runs:	14		
Pin processing:			
Accepts:	1273		
Rejects:	126		
Pins welded:	1439		
Leak testing:			
Accepts:	1333		
Rejects:	84		
Bond testing (completed runs):			
Accepts:	1456		
Rejects:	275		
Surveillance:	C-196, C-217, S-609, C-182, C-210, C-188, C-190, C-199, C-218, C-225		

D. Physics Development

1. ZPR-3[1]

The critical mass of Assembly 48 has been measured, and a series of corrections has been applied to the experimental value to determine the critical parameter of a more idealized configuration (see Progress Report for June 1966, ANL-7230, pp. 5-6). Principal corrections are as follows:

(1) A temperature correction was determined as a result of seven identical runs over the course of several weeks with slightly varying core temperatures. Based on two selected thermocouples representing the interior of the core, this correction amounts to -2.3 Ih/°C.

[1] In the Progress Report for April 1966, ANL-7204, a typographical error was made in Table IV on p. 6. The material composition for Pu^{239} and Pu^{241} in the "old fuel" core region should be changed from 0.7572 to 0.6572.

(2) The worth of core material substituted for blanket near the radial boundary was determined as a function of radius. Nine such determinations were made, and a least-squares fit to the temperature-corrected data provided information for evaluating an edge-smoothing correction [see (3) next].

(3) The deviations from a true circular outline at the edge were plotted on a large scale and divided into small annular increments. The increments were measured with a planimeter and their worth estimated using the average of their radii.

(4) Safety rods in this core are loaded with supplemental fuel to provide the necessary safety margin. The worth of this fuel was evaluated as a function of rod radial location. This was the largest correction applied to the critical mass.

With these adjustments, the critical mass of the heterogeneous composition reported in ANL-7230 is 272 ± 2 kg Pu^{239}. The uncertainty is largely a result of the scatter in values of edge core worth as a function of radius, and the application of this worth to the large correction for the safety rod. A further small correction may be made still later when interface effects are evaluated.

Although not required for determination of the critical mass, a control-rod calibration in terms of conventional reactivity units is desirable for reporting small sample worths. Such calibrations have been made by period measurements and by inverse kinetics analysis.

Reactivity measurements of various small samples continued. To increase the accuracy of measurement, a procedure was devised for inserting small samples to the center of the reactor without introducing other intervening perturbations. Since the traverse tube for insertion of such samples must be small, the samples themselves are necessarily quite small. This means that the method is particularly useful for high-cross-section materials for which smallness of sample is required to avoid self-shielding or self-multiplication effects. Accuracies of about 10^{-7} in reactivity measurements have been attained, and still further gains may be possible with improved servomechanisms for measuring reactivity changes.

A more detailed and extensive report of the experimental results on Assembly 48 will be presented at the International Conference on Fast Critical Experiments and Their Analysis at Argonne, October 10-13, 1966, and will also be reported in the next monthly report.

2. ZPPR

In the construction phase, thirteen piling holes have been finished, the foundation for the outside equipment building has been poured, and excavation for the service wing is approximately 90 percent complete.

Procurement of reactor components is continuing. The present status of the reactor components is as follows:

a. Bed and Tables: The ball screw assembly and bed have been completed and checked out. The transmission has also been completed. The bearings have been installed on the movable table and it has been placed on a planer to finish the top surface. Test equipment is being prepared to check out the assembled bed and tables for functional requirements at the vendor's plant.

b. Matrix Drawers: Two ANL representatives visited the vendor, Mechanical Products Mfg. Co., Seattle, Washington, to check progress and correct the weld cracking of the drawer fronts. During September the vendor shipped 451 front drawers and 420 back drawers. All back drawers were acceptable. One hundred eightly-four front drawers were rejected because of an unacceptable tab dimension. Removal of 4 to 5 mils from the back edge of the tab is required for the drawers to be acceptable. At present, a total of 348 front drawers and 710 back drawers have been accepted and are stored at ANL-Idaho. Approximately 400 drawers are ready for shipment from the vendor. All remaining pieces have been bent. Additional perforated pieces were required because of the number of rejects.

c. Matrix Tubes: All matrix tubes have been received and accepted.

d. Nuclear Instrumentation: The ZPPR nuclear instrumentation has been completed and checked out. The as-built drawings are now being prepared.

e. Area Gamma Monitors: The area gamma monitors are completed and checked out.

f. Poison Safety Rod Drives: The vendor is fabricating the first drive, which will be checked by ANL prior to work on the remaining rod drives.

g. Reactor Knees: The vendor, Macauley Foundry Company of Berkeley, California, is making cores and patterns. The machining of the knees will be done by the Oakland Machine Works, Oakland, California.

h. Personnel Shields: Because of difficulty in obtaining bids from vendors on this item, the due date of the bids has been extended to September 30.

i. Matrix Alignment: Preliminary drawings are being reviewed by a prospective vendor to determine the feasibility of a single large alignment plate.

j. Source Drives: The vendor, Teleflex, Inc., North Wales, Pennsylvania, has started work on the source drives.

k. Rod-drive Mounting Plates: The rod-drive mounting plates are being fabricated by Greenlee Foundries, Inc., Chicago, Illinois. Completion is scheduled for January 1967.

l. Matrix Tie-down: The Rupert Iron Works, Rupert, Idaho, has started fabrication.

m. Beta-Gamma Air Particulate Monitors: Three beta-gamma air particulate monitors are due from the Nuclear Measurements Corp., Indianapolis, Indiana, in November.

n. Particulate Stack Monitor: The particulate stack monitor takes air samples before and after the high-efficiency filters of the mound-area ventilation system for alpha particulates and beta-gamma particulates. The order for this unit was placed with Nuclear Measurements Corp., Indianapolis, Indiana.

o. Loading Platform: The support bracket assembly, the ramp assembly, and the pit bumper assembly are being fabricated by the Rupert Iron Works, Rupert, Idaho. A purchase order for the pit conveyor assemblies has been given to the Horsley Company, Ogden, Utah. The platform assembly order was placed with McGee and Hogan Machine Works, Salt Lake City, Utah.

p. Drawer Springs: 4600 drawer springs were ordered from Custom Stamping and Manufacturer Co., Portland, Oregon.

q. Reactor Frame: The reactor frame is the superstructure which holds the rod-drive mounting plates, the back ends of the rod drives, and the cooling-system ducting in place on the reactor halves. An order was placed with the Gate City Steel Company, Pocatello, Idaho.

r. Reactor Plenum Assemblies: The outside structures of the plenums were ordered from Bingham Mechanical and Metal Products, Idaho Falls, Idaho. The manifold for the reactor consists of neoprene plugs

which are expanded in the ends of the matrix tubes to block off undesired air flow. The orders for these plugs and accessories were placed with the Kirkhill Rubber Company, Brea, California, and Mechanical Products and Manufacturing Co., Seattle, Washington.

s. Fuel Control and Safety Rod Drawers and Ball Joint Assemblies: The order for these assemblies was placed with Hulbert Brothers, Salt Lake City, Utah.

t. Poison Safety Blades and Sheath: The due date on the bid packages for these items was extended to October 5 upon request of one of the vendors. These bids had been sent out previously but were not accepted due to the previous stoppage of procurement.

u. Control Consoles and Cabinets: The order for the consoles and cabinets was placed with Amco Engineering Company, Chicago, Illinois. They are to be shipped on October 1.

v. Boron Fabrication: The drawings for fabrication of the boron carbide plates for the poison safety rods are being prepared. Calculations on rod worth indicate that it would be helpful to obtain a high boron-10 content in the poison safety rods rather than pack highly enriched powder into the void of the safety blades.

C. Other Reactor Physics

1. Burnup Measurements for Fast Reactors

A program for the development of analytical methods for the determination of burnup of fast reactor fuels and for the measurement of fast fission yields is being carried out. The initial objective of this program was the development of burnup methods for EBR-II. However, this objective has been broadened to include fast reactors in general.[2]

A burnup method which has general applicability to fast reactors must meet the following criteria: (1) the fission yield of the monitor should be independent of the fissioning nuclide and the energy of the fissioning neutrons; (2) the method should be based on a nuclide (or nuclides) that does not migrate in the fuel; (3) the burnup monitor should either be stable or have a sufficiently long half-life to make decay corrections minimal; (4) the precision and accuracy of the method should be such that the relative error at the 1% burnup level is no more than 1%. A burnup method which uses the rare earth group of fission products as the monitor is expected to meet the first three of the above criteria.

None of the available analytical methods for rare earths provide the sensitivity, accuracy, and/or freedom from potential interferences (e.g., uranium, plutonium, and other fission products) to meet the fourth criterion. However, the possibility exists that a refinement of one of these methods can be combined with a suitable preliminary separation from interferences to achieve the desired result. A rare earth titration with ethylenediaminetetraacetic acid (EDTA)[3] has been modified by incorporation of photometric endpoint detection. The method now provides the required sensitivity and accuracy. The separations being tested are (1) precipitation of the rare earths on calcium fluoride to remove the bulk of the uranium and (2) anion exchange to separate the rare earth group from the other interferences.

The entire procedure has been tested with lanthanum as a stand-in for the rare earth group of fission products. The results obtained at the 500-μg level have a relative standard deviation of $\pm 0.9\%$ with no significant bias. Future testing will involve evaluation of the procedure with (1) a simulated mixture of rare earth fission products and (2) a high-burnup fuel sample.

---

[2] Chemical Engineering Division Semiannual Report, July-December 1965, ANL-7125, p. 241.

[3] Fritz, J. S., Oliver, R. T., and Pietrzyk, D. J., Anal. Chem. 30, 1111 (1958).

D. Component Development

1. Sodium Technology--Engineering Development

a. Physicochemical Mechanics of Metals. A series of measurements of the electrical resistivity of specimens of Type 304 stainless steel tubing was made after their exposure to sodium, sodium vapor, air, and vacuum, both before and after an application of a modified Strauss test. The temperature was varied and the time duration of the exposure was held constant at seven days. The results are shown in Table V. The electrical resistivity of the "as received" tubing was found to be unaffected by the application of the modified Strauss test alone. The modified Strauss test consisted in all cases of boiling the specimen 15 min in a solution of: 30 g $CuSO_4$, 55 ml H_2SO_4, and 870 ml distilled H_2O.

TABLE V. Electrical Resistivity (microhm-cm at room temperature) of Type 304 Stainless Steel Tubing

	Exposed for 7 days in							
	Liquid Sodium		Sodium Vapors		Vacuum at 5-10 μ		Air Furnace	
Temperature of Exposure (°F)	Before Strauss Test	After Strauss Test	Before Strauss Test	After Strauss Test	Before Strauss Test	After Strauss Test	Before Strauss Test	After Strauss Test
As Received	80	80						
900	73	68	-	-	-	-	-	-
1000	59.7	105	59.5	66.7	-	-	-	-
1100	65.6	126	62.2	68.6				
1200	68	201	65	65	65	65	73	73
1300	74	78	64.7	112/210 (est)	-	-	-	-

The data indicate that sensitivity to the modified Strauss test caused by sodium is much more adverse than either air or vacuum and that sodium vapor has little effect up to 1200°F. Sodium exposure increases resistivity, indicating deterioration of grain boundaries, up to 1200°F. Of importance is a marked decrease in resistivity between the 1200 and 1300°F Strauss-tested specimens, indicating a decrease in grain boundary deterioration. The physical nature of this effect is shown in Fig. 5. Voids clearly indicated at 1200°F, after Strauss test and etching the sample, completely or nearly completely disappear in the specimen exposed to 1300°F sodium followed by Strauss testing and etching.

b. Core Component Test Loop (CCTL). A minimum effort is being expended to bring the facility to a state of readiness for initial sodium filling. To date the tests performed on the loop have included preliminary vacuum, pressure, and temperature tests. No attempt has been made to operate the centrifugal pump, heat-exchanger blower, or purification system.

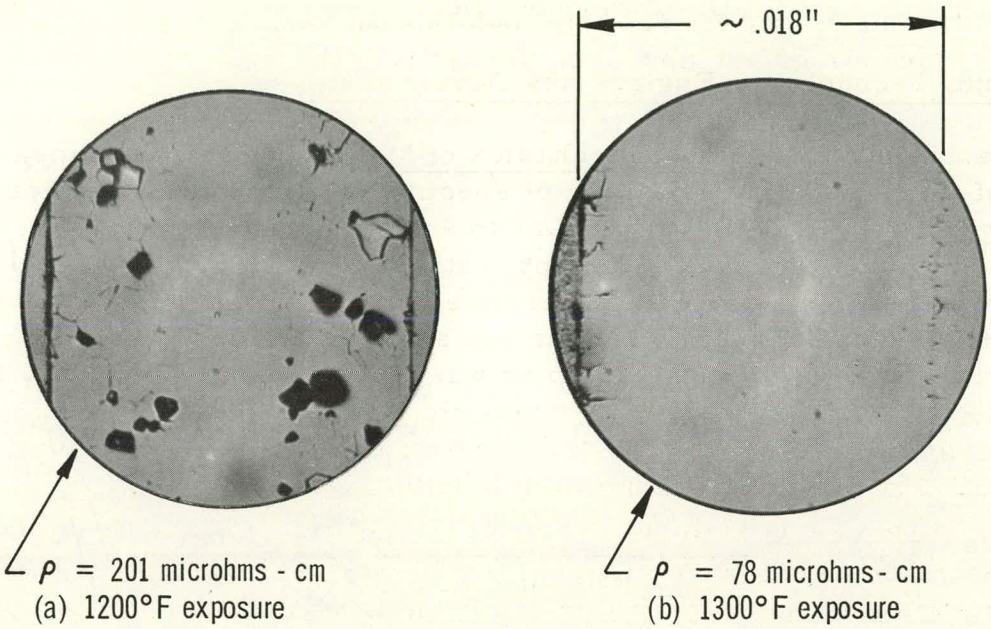

Fig. 5. Strauss-solution Effects on Type 304 Stainless Steel after Sodium Treatment for 7 days

Initial tests were performed to determine if any gross leaks existed in the system. The most highly suspect areas were at the pump-shaft seal, the safety pressure release, and at the large flange gaskets. No large leaks were found.

c. Sodium Analytical Loop. A new Sodium Analytical Loop, designed to permit careful control of oxide impurities on a relatively small volume of sodium, is being erected. It will also permit uniform circulation of sodium to various analytical apparatus. All lines are routed and ready for final welding. Work on the loop and associated facilities is approximately 40% complete. All of the main sodium components will be connected to the loop with "Conoseal" tube joints.

The manually operated sodium plugging valve has been modified to accommodate an air operator for automatic monitoring of the plugging temperature. The line sampler and dip sampler vacuum distillation heating process will be accomplished using a 2.5-kW high-frequency induction-heating generator which has a two-station manual transfer switch.

d. Component and Materials Evaluation Loop (CAMEL). The Dymec data-acquisition system was checked to determine the proper location and continuity through the thermocouples located over the loop. A difficulty was experienced with the tape punch which resulted in an intermittent omission of one data character, subsequently traced to a defective capacitor in one of the printed-circuit boards. This unit was replaced. The switch-control terminal has been wired, and the capability of the

data-acquisition system to read through this unit was checked. Final terminal connections are now being made from the switch control unit to the data-acquisition system.

The programmable X-Y plotter was modified by a factory representative to allow plotting of a continuous run of data points on the tape against a step advance on the X axis. This capability was not previously available. The modification extends the usefulness of the data plotter.

The remaining addition needed on the loop is the installation of heater control variacs. These units have been on order for an extended period of time.

e. Universal Materials Test Specimen Development. A tubular test capsule that would approach uniform strain in the walls when gaseous pressure was applied to the inside has been developed. This test capsule will permit a simplified method of testing reactor materials under conditions of stress and irradiation.

A sketch of the revised design for the "Biaxially Stressed" specimen (see Progress Report for April 1966, ANL-7204) was prepared and sent to interested parties with descriptive memorandum. The main features of this revised design are: (1) the inside radii of the cylindrical portion and the hemispherical ends are identical, and (2) the thickness of the hemispherical ends is reduced to $(1 - \nu/2 - \nu)$ x, the thickness of the cylindrical portion. These changes produce essentially uniform strain throughout the specimen when under pressure, such that the geometry remains similar, i.e., the cylindrical portion remains cylindrical and the ends remain hemispherical. Volume change calculations are thereby greatly simplified. Sheets showing pressure-temperature-volume relations for this modified design were prepared and attached to the descriptive memorandum.

f. High-temperature Instrument Development

(i) Resistivity of Refractory Oxide Insulators. The "apparent" resistivity of helium and a vacuum were measured for two reasons: (1) as an aid to predicting experimental errors during the measurement of the resistivity of refractory oxide insulators, and (2) to help evaluate the effectiveness of using gas gaps as part of the electrical-insulator region of a thermocouple. The experiment was performed using a coaxial probe with a 0.120-in.-OD tantalum center electrode placed inside a tantalum tube with a 0.208-in. ID. The probe was inserted into a reasonably uniform furnace hot zone, 6 in. in length. Data were taken with a helium pressure of 30 in. of water and also with a vacuum of 2×10^{-6} mm Hg in the furnace

and probe. The tantalum electrodes were in the recrystallized state. The resistivity values with the more positive voltage applied to the tube were measured with a transistor curve tracer and represent the slope of the voltage-current curves in the region of 0 to 100 mV.

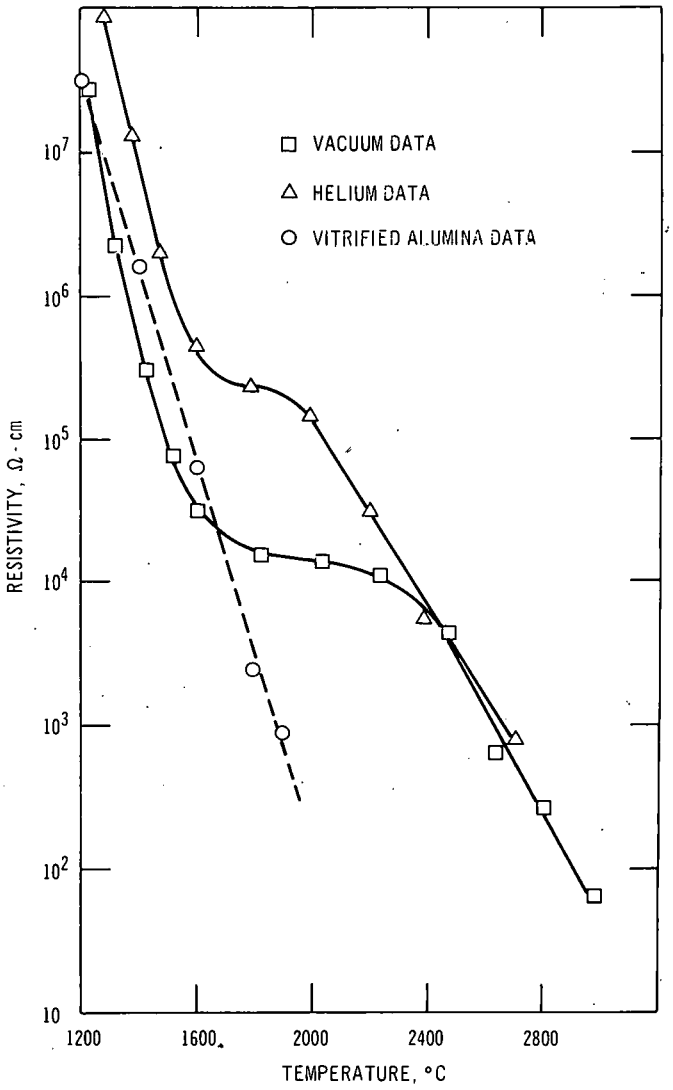

Fig. 6. Apparent Resistivity of Helium and Vacuum When Using Tantalum Electrodes

The resistivity values obtained are shown in Fig. 6 along with measured values of the resistivity of vitrified alumina (see Progress Report for July 1966, ANL-7245, pp. 42-43). It was expected that the apparent resistivity of helium would be higher than that of a vacuum since the helium atoms (if the helium were not ionized) would impede the flow of the emitted electrons. This was found to be true. The apparent resistivities of both helium and a vacuum are considerably higher than the resistivities of refractory oxide insulators at temperatures above 1700°C. The apparent resistivities of helium and a vacuum are, on an absolute basis, quite low at temperatures in excess of 2600°C.

These data are very dependent on the electrode materials, test-voltage polarity, and geometry, and must not be broadly applied. They are presented here only to demonstrate their general magnitude.

(ii) Wide-range Neutron-flux Monitoring. As mentioned previously (see Progress Report for July 1966, ANL-7245, p. 42), the mean square charge per alpha pulse must be determined to be able to predict the signal contribution due to these unwanted pulses.

The rms alpha voltage at the output of a preamplifier was measured when a chamber without any interconnecting cable and with two

different cable lengths and, hence, different cable capacities, were used. The mean square charge per pulse was then determined from:

$$\overline{q_\alpha^2} = \frac{2(E_{rms\alpha})^2 C_0}{N_\alpha R_o K_4},$$

where

$\overline{q_\alpha^2}$ is the mean square charge per pulse;

$E_{rms\alpha}$ is the measured voltage;

C_0 is the total lumped chamber and cable capacity;

N_α is the alpha pulse rate;

R_0 is the input resistance of the preamplifier;

K_4 is a factor depending upon the preamplifier characteristics.

The values of $\overline{q_\alpha^2}$ obtained from the measurements were 3.6, 4.3, and 4.6 x 10^{-30} coulombs square per pulse. A mean square value of 4 x 10^{-30} coulombs square per pulse will therefore be considered as the accepted value of $\overline{q_\alpha^2}$.

2. Sodium Technology--Liquid Sodium Coolant Chemistry

a. Behavior of Carbon in Sodium

(i) Segregation of Carbon in Sodium. Various mechanisms can be postulated for the observed segregation of carbon in sodium toward container walls, e.g., fused silica and stainless steel tubing (see Progress Report for August 1966, ANL-7249, p. 36). An obvious mechanism is the adsorption of carbon from liquid sodium by the container surface itself. A simple test of this possibility was made with respect to Pyrex glass.

Liquid sodium was made to drain (at ~33 ml/min) through 3-mm-dia Pyrex beads packed in a Pyrex column heated to 120°C. The sodium did not fill the column but, instead, flowed in a narrow channel through the beads. The surface-to-volume ratio of this channel was estimated to be ~36 cm^2/ml, about nine times that of the fused silica tubing used in the earlier experiments. Analyses of the effluent sodium, which was collected in several fractions, showed no significant difference in total carbon content from that of the original sodium. This result suggests that adsorption on container surfaces, such as Pyrex glass, is not a primary mechanism for the previously observed segregation of carbon in sodium.

(ii) Dispersion of Carbon in Liquid Sodium. Previous experience has shown that as much as 50% of the carbon in reactor-grade sodium (containing ~30 ppm carbon) is present as particulate matter capable of passing through a 5 μ-porosity filter. To obtain more information about the particulate behavior of carbon in sodium, attempts are being made to prepare dispersions of C^{14}-labeled amorphous carbon in liquid sodium.

Sintered agglomerates of C^{14}-labeled amorphous carbon were added to sodium in a stainless steel crucible, and the mixture was stirred at temperatures between 200 and 425°C for extended periods of time. However, radiocarbon particulates smaller than 5 μ were not formed, possibly due to the relatively large particulate size of the starting material and/or poor wetting of the carbon by the sodium.

Efforts are now being made to generate very finely divided C^{14}-labeled carbon in liquid sodium by decomposition of $Na_2C^{14}O_3$ at elevated temperatures. In an initial experiment, 7 g of inactive Na_2CO_3 was heated with 200 g of sodium at ~670°C and stirred for several days. Although carbon was formed, it was found to be agglomerated at the bottom of the crucible. By modifying the method of introducing the Na_2CO_3--introduction of very small amounts below the surface of the hot sodium--it is hoped that stable dispersions of C^{14}-labeled carbon will result.

E. Fuel Development

1. Metallic Fuels

a. Irradiation of Uranium-Plutonium Alloys. A total of 20 full-length (14 in.) metal fuel rods are undergoing irradiation in the EBR-II reactor. Eighteen of these rods are U-Pu-Zr alloys clad in either V-20 w/o Ti, Type 304 stainless steel, Type 316 stainless steel, Hastelloy-X, or Hastelloy-X-280 tubing. These rods are operating at maximum jacket temperatures of 630°C and at present have reached a calculated maximum 3.8 a/o burnup. Two additional rods are fueled with U-Pu-Ti alloy and are clad in V-20 Ti alloy tubing. The rods are being irradiated at maximum jacket temperatures of 540°C and have attained a maximum burnup of 3.9 a/o. Additional details on the design of the fuel rods and the irradiation conditions are summarized in Table VI. Additional burnup was not accumulated because of shutdown of the reactor.

Postirradiation examination of 19 experimental U-Pu-Fs alloy rods irradiated in subassembly XA01 in EBR-II has been initiated. The fuel pins are 0.144-in.-dia rods jacketed in either Nb-1 w/o Zr, Hastelloy-X, or Nb-4 w/o V. All jackets had an ID of 0.156 in., except one Hastelloy-X tube lined with tungsten which measured 0.158 in. in ID. The jacket wall thicknesses varied between 0.009 and 0.015 in. These rods were irradiated at maximum jacket temperatures of 472°C for a calculated 0.56 a/o burnup.

TABLE VI. Status of Metal Fuel Irradiations in Progress

Test Reactor	Capsule or S/A No.	Specimen Number	Design Parameters: Fuel Composition (w/o)	Design Parameters: Effective Density (%)	Design Parameters: Cladding Composition	Design Parameters: Cladding OD (in.)	Design Parameters: Cladding Thickness (in.)	Operating Conditions: Power Density (kW/cc)[a]	Operating Conditions: Max Cladding Temp (°C)	Operating Conditions: Burnup to Date: a/o (U + Pu)	Operating Conditions: Burnup to Date: fiss/cc x 10^{-20}[a]
CP-5	CP-45	1N15	U-19 Pu-14 Zr	66	V-20 w/o Ti	0.208	0.015	2.6	640	10.2	22.1
EBR-II	XG06	ND23	U-15 Pu-10 Zr	66	V-20 w/o Ti	0.209	0.016	1.7	540	3.8	9.1
EBR-II	XG05	ND24	U-15 Pu-10 Zr	66	V-20 w/o Ti	0.209	0.016	1.7	535	3.6	8.6
EBR-II	XA07	ND28	U-15 Pu-9 Zr	75	304 SS	0.208	0.021	2.0	630	3.7	10.3
EBR-II	XA07	ND41	U-15 Pu-9 Zr	75	304 SS	0.208	0.021	2.0	625	3.6	10.0
EBR-II	XA07	ND32	U-15 Pu-9 Zr	75	316 SS	0.196	0.015	2.0	605	3.5	9.8
EBR-II	XA07	ND43	U-15 Pu-9 Zr	75	Hastelloy-X	0.196	0.015	2.0	615	3.6	10.0
EBR-II	XA07	ND25	U-14 Pu-12 Zr	76	304 SS	0.208	0.021	1.9	600	3.2	8.2
EBR-II	XA07	ND27	U-14 Pu-12 Zr	76	304 SS	0.208	0.021	1.9	605	3.3	8.4
EBR-II	XA07	ND26	U-14 Pu-12 Zr	76	316 SS	0.196	0.015	1.8	590	3.1	7.9
EBR-II	XA07	ND29	U-14 Pu-12 Zr	76	316 SS	0.196	0.015	1.8	595	3.3	8.4
EBR-II	XA07	ND30	U-14 Pu-12 Zr	76	316 SS	0.196	0.015	1.9	615	3.6	9.2
EBR-II	XA07	ND31	U-14 Pu-12 Zr	76	316 SS	0.196	0.015	1.9	610	3.5	8.9
EBR-II	XA07	ND33	U-14 Pu-12 Zr	76	Hastelloy-X	0.196	0.015	1.9	605	3.4	8.7
EBR-II	XA07	ND34	U-14 Pu-12 Zr	76	Hastelloy-X	0.196	0.015	1.9	610	3.5	8.9
EBR-II	XA07	ND35	U-14 Pu-12 Zr	76	Hastelloy-X	0.196	0.015	1.9	615	3.6	9.2
EBR-II	XA07	ND37	U-14 Pu-12 Zr	66	Hastelloy-X-280	0.208	0.015	1.8	610	3.6	9.0
EBR-II	XA07	ND39	U-14 Pu-12 Zr	66	Hastelloy-X-280	0.208	0.015	1.8	610	3.5	8.7
EBR-II	XA07	ND44	U-14 Pu-12 Zr	66	Hastelloy-X-280	0.208	0.015	1.8	600	3.4	8.5
CP-5	CP-44	1N14	U-15 Pu-10 Ti	69	V-20 w/o Ti	0.203	0.015	2.4	560	9.0	20.7
EBR-II	XG05	NC17	U-15 Pu-10 Ti	63	V-20 w/o Ti	0.209	0.016	1.6	540	3.7	8.1
EBR-II	XG06	NC23	U-15 Pu-10 Ti	63	V-20 w/o Ti	0.209	0.016	1.6	540	3.9	8.6
CP-5	CP-41	4N10	U-10 Pu-10 Fz	77	V-20 w/o Ti	0.196	0.016	1.9	550	7.8	22.9
CP-5	CP-41	5N11	U-10 Pu-10 Fz	79	V-20 w/o Ti	0.193	0.016	2.0	550	7.8	23.4
CP-5	CP-41	6N12	U-10 Pu-10 Fz	84	V-20 w/o Ti	0.189	0.016	2.1	550	7.8	24.9
CP-5	CP-41	1N7	U-15 Pu-10 Fz	77	V-20 w/o Ti	0.196	0.016	1.9	550	7.8	22.9
CP-5	CP-41	2N8	U-15 Pu-10 Fz	79	V-20 w/o Ti	0.193	0.016	2.0	550	7.8	23.4
CP-5	CP-41	3N9	U-15 Pu-10 Fz	84	V-20 w/o Ti	0.189	0.016	2.1	550	7.8	24.9
CP-5	CP-50	1N16	Th-20 U	75	V-20 w/o Ti	0.196	0.015	1.9	610	9.0	4.3
CP-5	CP-50	4N19	Th-20 U	75	V-20 w/o Ti	0.196	0.015	1.9	610	9.0	4.3
CP-5	CP-50	2N17	Th-10 Pu-10 U	75	V-20 w/o Ti	0.196	0.015	2.0	630	10.4	4.8
CP-5	CP-50	5N20	Th-10 Pu-10 U	75	V-20 w/o Ti	0.196	0.015	2.0	630	10.4	4.8
CP-5	CP-50	3N18	Th-10 Pu-20 U	75	V-20 w/o Ti	0.196	0.015	1.9	630	6.0	4.4
CP-5	CP-50	6N21	Th-10 Pu-20 U	75	V-20 w/o Ti	0.196	0.015	1.9	610	6.0	4.4

[a]Based on effective density.

Neutron radiographs of the encapsulated rods showed the fuel to be straight, uniform, and intact. The X radiographs taken of the top end of the capsules showed that an approximate 2-in. section of the jackets on three of the pins had been flattened. This occurred in the gas plenum, which is above the fuel pin. The incident was common to the three Nb-1 w/o Zr jackets, which were in the fully recrystallized condition. The jackets of the same material but in a stress-relieved condition remained unaffected.

It appears that the XA01 subassembly was lowered into the hot reactor sodium before the sodium in the capsule had fully melted. Volume changes resulting from melting of sodium in the lower part of the capsule applied against a solid plug of sodium at the top may have subjected the jacketing about the plenum of the fuel rod to a high hydrostatic pressure that collapsed the tubing. All the rods are being measured for dimensional and volume changes before continuation of the metallographic examination of the fuel.

U-Pu-Fs alloy specimens being irradiated in CP-5 were designed for a study of fuel-density parameters that have a direct bearing on maximum attainable burnup. These specimens reached a maximum

burnup of 7.8 a/o at maximum cladding temperatures of 550°C. The specimens have been removed from the reactor and are awaiting a destructive examination.

2. Oxide and Carbide Fuels

a. Irradiations. The status of mixed oxide, mixed carbide, and stainless steel-PuO_2 cermet specimens under irradiation in EBR-II is shown in Tables VII, VIII, and IX. Additional burnup was not accumulated during the month because of reactor shutdown.

TABLE VII. Status of UC-20 w/o PuC Fuel Irradiations in EBR-II

		Design Parameters				Operating Conditions			
								Burnup to Date	
Capsule or S/A No.	Specimen Number	Effective Density (%)	Cladding Composition	Cladding OD (in.)	Cladding Thickness (in.)	Power Density (kW/cc)[a]	Max Cladding Temp (°C)	a/o (U + Pu)	fiss/cc x 10^{-20}[a]
XG05	SMV-2	84	304 SS	0.297	0.020	2.1	645	3.8	10.4
XG05	HMV-5	80	Hastelloy-X	0.297	0.015	2.2	670	3.9	10.2
XG05	NMV-11	84	Nb-1 w/o Zr	0.281	0.012	2.1	645	3.9	10.8
XO08	NMP-2	82	Nb-1 w/o Zr	0.281	0.012	1.6	545	2.2	5.8
XO08	NMV-4	80	Nb-1 w/o Zr	0.281	0.012	2.4	635	3.1	8.2
XO08	NMV-7	80	Nb-1 w/o Zr	0.281	0.012	2.1	605	2.8	7.5
XO08	NMV-12	86	Nb-1 w/o Zr	0.281	0.012	2.4	635	3.1	8.7
XO08	HMV-1	80	Hastelloy-X	0.297	0.015	2.1	640	2.8	7.3
XO08	HMV-4	80	Hastelloy-X	0.297	0.015	2.3	670	3.0	8.1
XO08	HWMP-1	82	Hastelloy-X + W	0.297	0.020	1.6	555	2.1	5.6
XO08	HWMV-1	83	Hastelloy-X + W	0.297	0.020	2.4	685	3.1	8.5
XO09	SMV-1	82	316 SS	0.306	0.024	1.6	570	2.3	6.3
XO09	SMP-1	80	316 SS	0.306	0.024	2.1	640	1.8	4.7
XO09	VMV-1	86	Vanadium	0.301	0.022	2.5	640	2.7	7.6

[a]Based on effective density.

TABLE VIII. Status of UO_2-20 w/o PuO_2 Fuel Irradiations in EBR-II

		Design Parameters				Operating Conditions			
								Burnup to Date	
Capsule or S/A No.	Specimen Number	Effective Density (%)	Cladding Composition	Cladding OD (in.)	Cladding Thickness (in.)	Power Density kW/cc[a]	Max Cladding Temp (°C)	a/o (U + Pu)	fiss/cc x 10^{-20}[a]
XO09	SOV-5	82	304 SS	0.297	0.020	1.7	555	2.3	4.8
XO09	SOV-6	82	304 SS	0.297	0.020	1.7	565	2.5	5.1
XO11	SOV-3	83	304 SS	0.296	0.019	1.9	610	1.8	3.8
XO11	HOV-4	80	Hastelloy-X	0.295	0.014	1.8	600	1.8	3.6
XO11	TVOV-1	77	V-20 w/o Ti	0.297	0.020	1.7	575	1.8	3.4
XO11	SOV-7	85	304 SS	0.296	0.019	2.0	630	1.8	3.7
XO11	SOV-1	80	304 SS	0.296	0.019	1.7	590	1.8	3.5
XO11	HOV-10	86	Hastelloy-X	0.295	0.014	1.9	615	1.7	3.7
XO11	HOV-15	80	Hastelloy-X	0.295	0.014	1.7	590	1.7	3.4

[a]Based on effective density.

TABLE IX. Status of Cermet Fuel Irradiations in EBR-II

		Design Parameters					Operating Conditions			
									Burnup to Date	
Capsule or S/A No.	Specimen Number	Fuel Composition (w/o)	Effective Density (%)	Cladding Composition	Cladding OD (in.)	Cladding Thickness (in.)	Power Density (kW/cc)[a]	Max Cladding Temp (°C)	a/o (U + Pu)	fiss/cc x 10^{-20}[a]
XO11	5P-9	SS-40 PuO_2	98	304 SS	0.301	0.015	0.88	495	2.5	1.9
XO11	5P-12	SS-27 PuO_2	99	304 SS	0.294	0.015	0.59	450	2.5	1.2
XO11	5U-14	SS-27 UO_2	98	304 SS	0.298	0.013	0.45	435	1.9	0.98

[a]Based on effective density.

b. Synthesis. In the fluidized-bed preparation of UC and (U, Pu)C by reaction of the metals with methane-hydrogen mixtures, the extent of reaction is limited to formation of the monocarbide by controlling the hydrogen-to-methane ratio in the fluidizing gas (see Progress Report for November 1965, ANL-7122, p. 65). Excess carburization is prevented by maintaining the methane concentrations at less than the equilibrium value for the reaction:

$$2(U, Pu)C + CH_4 \rightleftarrows (U, Pu)_2C_3 + 2H_2.$$

Thermobalance studies are being conducted to determine a more precise value for the equilibrium methane concentration than can be obtained by calculations based on currently available free energy data.

Previous thermobalance experiments with uranium-20 w/o plutonium alloy samples had indicated that at 770°C the equilibrium methane concentration was approximately 0.75 v/o methane (see Progress Report for February 1966, ANL-7176, p. 68). However, after making improvements in the equipment, data have been obtained that indicate the equilibrium methane concentration is lower. The data for one such experiment at 750°C are given in Fig. 7. The curve shows that with an initial methane concentration of 0.43 v/o, the weight gain continued to increase with a slope of 0.3 mg/hr after the theoretical weight gain for stoichiometric monocarbide was achieved. When the methane flow was stopped and hydrogen alone was passed over the sample, the weight immediately decreased and continued to decrease until the weight gain for stoichiometric monocarbide was reached. This would indicate that the weight increase beyond the stoichiometric value was due to the formation of the sesquicarbide, which in turn decomposed to the monocarbide in the hydrogen atmosphere. When methane was again introduced into the gas stream, the weight immediately began to increase. With a gas concentration of 0.25 v/o CH_4, the weight increased at a rate of 0.11 mg/hr. When the methane contribution to the gas flow was again terminated, the weight decreased once again.

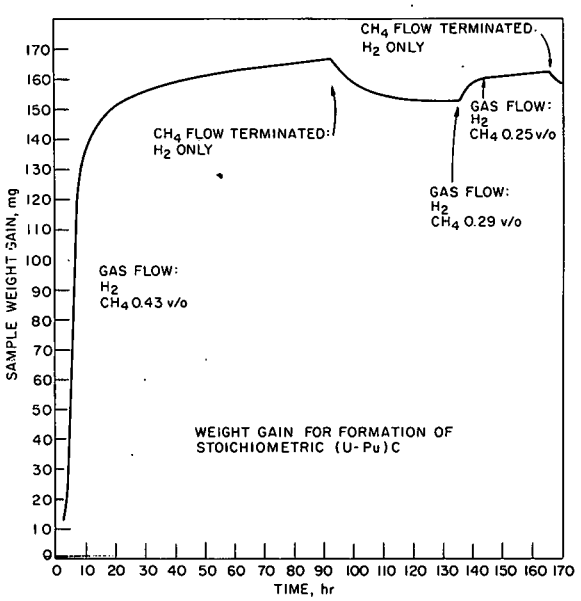

Fig. 7. Thermobalance Experiment: U-20 w/o Pu Alloy Reacted with H_2-CH_4 Mixtures at 750°C

A preliminary evaluation of this experiment indicates that the equilibrium methane concentration for the system (U, 20 w/o Pu)C,

$(U, 20\ w/o\ Pu)_2C_3$, CH_4 and H_2 is less than 0.25 v/o CH_4 at 750°C and one atmosphere pressure. This would yield a $\Delta G°$ value of less than -6.4 kcal/mole of $(U, 20\ w/o\ Pu)_2C_3$ at 750°C for the reaction

$$2(U, 20\ w/o\ Pu)C + C \rightarrow (U, 20\ w/o\ Pu)_2C_3.$$

The equilibrium methane concentration observed in this experiment was lower than that observed in the previous experiments; this lower equilibrium concentration of methane may be due to greater success in excluding oxygen and water vapor from the system. The fact that the reaction curve leveled out at the calculated weight gain for (U, Pu)C after 125 hr of operation is evidence of the purity of the gas.

3. Fuel Cladding and Structure

a. Vanadium-base Alloy Tubing. Considerable effort has been devoted to improving the secondary fabrication operations for producing high-quality tubing of V-15 w/o Ti-7.5 w/o Cr alloy (see Progress Report for February 1966, ANL-7176, pp. 26-27). Whereas the tube-reducing operation was earlier used for only a 58% area reduction (extruded tube-blank size of 0.800-in. OD by 0.100-in. wall reduced to 0.640-in. OD by 0.050-in. wall), additional roll sets will now permit a reduction to a size of approximately 0.375-in. OD by 0.020-in. wall, for a total area reduction of approximately 90%. The tube is mandrel drawn and finally plug drawn to the final size (typically of 0.290-in. OD and 0.015-in. wall) by means of conventional carbide tooling. Not only does the tube-reducing operation significantly reduce the number of processing steps from extruded tube-blank to finished tubing, but it circumvents many of the worrisome problems of drawing, such as uniform deformation, lubrication, and pointing losses.

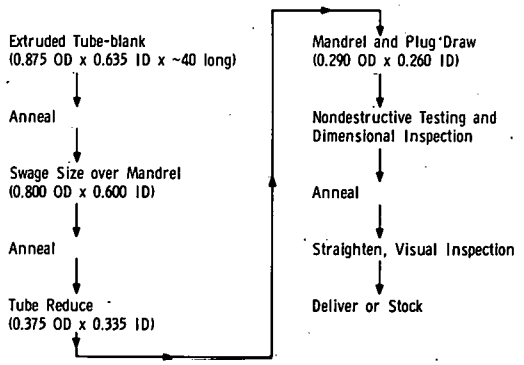

Fig. 8. Fabrication Flow Chart for Vanadium-base Alloy Tubing (all dimensions in inches)

A sufficient quantity of vanadium-base alloy tubing has now been processed by this method to establish firmly the simplified flow chart outlined in Fig. 8. Yields of >90% (weight of starting tube-blank to finished drawn tubing) are typical.

b. Development of Refractory-metal Alloys for Service in Oxygen-contaminated Sodium. Samples of V-5 w/o Cr alloy have been exposed for 23 days to 650°C sodium flowing at 6.1 m/sec and containing 8 to 9 ppm oxygen by weight. The average weight gain was only 0.02 mg/cm^2, compared with 0.55 mg/cm^2 for V-20 w/o Ti exposed this length of time. At higher (>12 ppm) oxygen concentration in oxygen-refreshed static systems, this alloy showed no significant difference in corrosion resistance as compared with V-20 w/o Ti.

Testing of levitation-melted V-Cr-Al alloys in the static oxygen-refreshed system (see Progress Report for July 1966, ANL-7245, p. 11) has continued. The results are summarized in Table X. It is apparent that corrosion resistance is greatly improved with increases in the chromium or aluminum content. However, fabricational problems have not been solved.

TABLE X. Corrosion of Vanadium Alloys in Sodium at 650°C Containing 15-18 ppm Oxygen

Alloy (w/o)	Weight Loss (mg/cm^2) at Indicated Time (days)				
	7.0	21.0	44.3	58.1	72.1
V-25 Cr-10 Al	1.29	3.61	7.0	10.0	14.6
V-20 Cr-10 Al	2.40	4.30	11.9	17.1	22.7
V-20 Cr-15 Al	0.46	1.09	3.32	4.78	5.55
V-20 Ti (Annealed Sheet)*	9.70	22.3	22.3	64.7	74.7

*900°C--vacuum--one hour.

4. Fuel Reprocessing

a. Processes for Fast Reactor Fuels. The process flowsheet that is currently being investigated is shown in Fig. 9. The process utilizes liquid metal-molten salt extractions and salt transport separations[4] for the

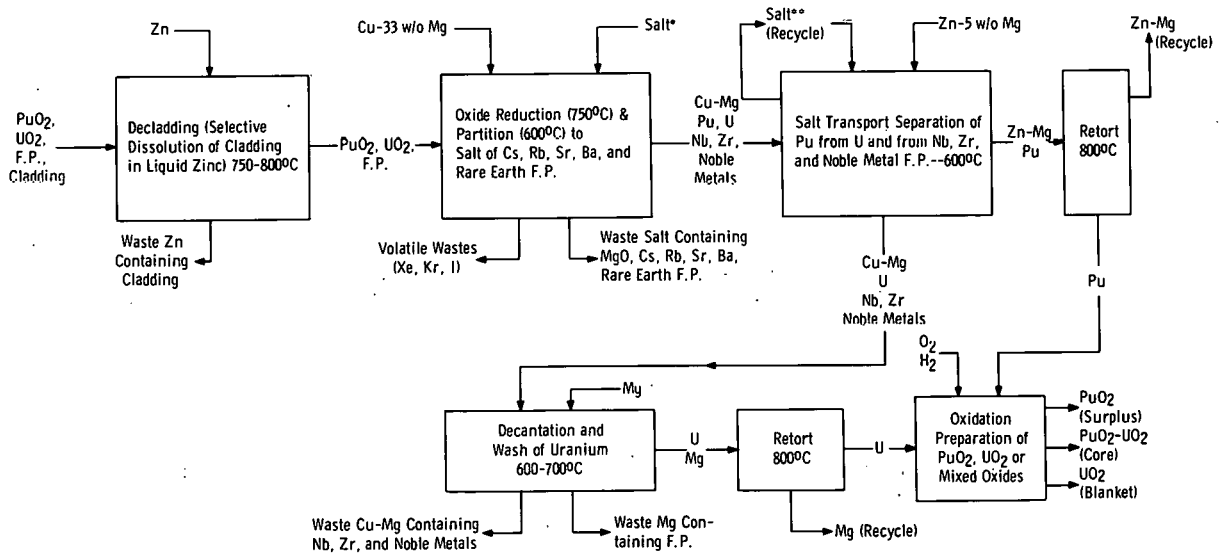

*For example, a 42.5 m/o NaCl-42.5 m/o $CaCl_2$-15 m/o $MgCl_2$.
**For example, a 50 m/o $MgCl_2$-30 m/o NaCl-20 m/o KCl salt.

Fig. 9. Reference Pyrochemical Process Flowsheet for Fast Breeder Reactor Oxide Core and Blanket Fuel. (Cladding material: stainless steel.)

[4]In the salt transport separations, the fissile and fertile materials are selectively transferred from one liquid metal solution (donor) to another (acceptor) by cycling a molten salt phase which acts as a carrier between the two metal solutions. Noble and refractory metal fission products remain in the donor alloy.

separation of fissile and fertile constituents of the fuel from the fission products. This process consists of the following steps:

(i) A decladding step in which the cladding from fuel or blanket material is selectively dissolved in liquid zinc. The oxide fuel is then separated from the waste zinc solution.

(ii) An oxide reduction-partition step in which the oxide fuel is reduced to metal (uranium and plutonium) by a Cu-33 w/o Mg alloy. Alkali, alkaline earth, and rare earth fission products remain in a molten $MgCl_2$-based halide salt phase which serves as a vehicle for the removal of the solid MgO formed as a by-product of the oxide reduction. The plutonium and uranium together with noble metal and refractory metal fission products remain with the copper-magnesium alloy.

(iii) A salt-transport-separation step in which plutonium is separated from uranium and the noble metal and refractory metal fission products. By cycling a molten $MgCl_2$-based salt carrier between the donor alloy (Cu-33 w/o Mg) and the acceptor alloy (Zn-5 w/o Mg), the plutonium is selectively transferred to the acceptor alloy. The uranium and the fission products remain in the copper-magnesium alloy.

(iv) Plutonium is recovered from the acceptor alloy by retorting the magnesium and zinc.

(v) Uranium, which is insoluble in the copper-magnesium alloy, is recovered by decantation of the liquid alloy, followed by washing with liquid magnesium. The magnesium residue is removed from the uranium by retorting.

(vi) A conversion step in which the uranium and plutonium are converted to the final oxide form.

On the basis of existing solubility and distribution data, salt-transport-separation information, and oxide-reduction results, it is estimated that the process performance for the current reference flowsheet will be approximately as follows:

Plutonium recovery	99+%;
Uranium recovery	~99%;
Overall decontamination factor	10^3 to 10^4.

Laboratory investigations of the current flowsheet are being carried out. A salt-transport-separation experiment (Pu-T-6) using the crucible-in-a-crucible technique (see Progress Report for May 1966, ANL-7219, p. 23) was completed. In this experiment, conducted at 600°C, plutonium was selectively transferred from a liquid Cu-33 w/o Mg donor alloy

containing U-20 w/o Pu through a molten $MgCl_2$-30 m/o NaCl-20 m/o KCl salt to a liquid Zn-10 w/o Mg acceptor alloy. To avoid entrainment of the acceptor alloy with the donor alloy, the contents of both crucibles were individually stirred at a low speed (150 rpm). At the end of the experiment, analytical results indicated that 99.5% of the plutonium charged to the donor alloy had transported to the acceptor alloy and only 1.9% of the originally charged uranium had transferred to the acceptor alloy. The measured final concentrations of plutonium in solution in the donor and acceptor alloys and the transport salt were in agreement with calculated concentrations based on experimentally determined distribution coefficients and solubilities in the metal phase. On the basis of the initial plutonium-to-uranium ratio of 0.25 in the donor and the final ratio of 13.3 in the acceptor alloy, a satisfactory concentration of the blanket plutonium can be achieved with the reference flowsheet.

Contrary to expectation, a significant transfer of magnesium from the donor to the acceptor alloy was observed. However, the transferred magnesium did not interfere with the desired plutonium transfer and would not cause any difficulty in the succeeding steps of the process. A small amount of copper was also transferred from the donor to the acceptor alloy. Copper transfer is undesirable, since it results in copper contamination of the plutonium product after the retorting steps. Work is therefore under way to reduce the transfer of copper from the copper-magnesium alloy to the plutonium acceptor alloy.

In other laboratory work, the distribution coefficients of uranium between molten 50 m/o $MgCl_2$-30 m/o NaCl-20 m/o KCl and Zn-Mg acceptor alloys saturated in uranium at 600, 700, and 800°C were determined. At the same time, determinations were made of the solubilities of uranium in the Zn-Mg alloys at the same temperatures. The amount of solute extracted is a function of the distribution coefficient and of the concentration in the metal phase, which is often set by solubility.

The distribution coefficients, in general, decreased from their value in pure zinc to a minimum value in a Zn-Mg alloy and then increased to their value in pure magnesium. The minimum values for the distribution coefficients (w/o U in salt/w/o U in metal) were as follows:

Temperature (°C)	Magnesium (w/o)	Distribution Coefficient ($\times 10^4$)
600	25	1.3
700	15	2.8
800	11	3.3

The uranium solubilities were generally found to increase from their value in pure zinc to a maximum in the Zn-Mg alloy and then decrease to their value in pure magnesium. The maximum uranium solubilities were as follows:

Temperature (°C)	Magnesium (w/o)	Solubility (w/o U)
600	25	4.4
700	17	10.7
800	11	15.7

These data permit an accurate prediction of the behavior of uranium in Zn-Mg alloys.

Engineering experiments are being conducted to determine systematically the rates of transfer of various solutes (U, Pu, Cu, Mg, Zn, and fission products) in the salt-transport-separation step (see Progress Report for August 1966, ANL-7249, pp. 9-10). The purpose of these tests is to provide information which will make it possible to calculate mass-transfer rates for various batch and continuous versions of the salt-transport-separation step. In an immiscible liquid metal-molten salt system, the mass-transfer rate of a solute is a function of the geometry, mixing conditions, solute mass-transfer coefficient, and difference in solute activities in the bulk salt phase and the metal phase. Volumetric mass transfer coefficients, K(a),[5] in kg/(hr)(liter), have been calculated for plutonium from data obtained in two plutonium extraction experiments. For both experiments, the extractions were conducted in a baffled $2\frac{1}{2}$-in.-ID tantalum vessel with a paddle stirrer ($1\frac{1}{4}$ in. long by 5/8 in. wide) at a stirring speed of 650 rpm. One experiment (UPU-1) involved the simultaneous transfer of plutonium and uranium at 840°C from a liquid Cu-5.5 w/o Mg-5.5 w/o U donor alloy to a molten $MgCl_2$ salt phase. The other experiment (UPU-2) involved the simultaneous transfer of plutonium and cerium at 600°C from Cu-33 w/o Mg to a molten $MgCl_2$-30 m/o NaCl-20 m/o KCl salt (ANL-7249, p. 10). The calculated plutonium volumetric mass transfer coefficients were as follows:

Experiment	K(a) [kg/(hr)(liter)]
UPU-1	0.18
UPU-2	0.27

[5] $K(a) = \frac{r}{C^*_s - C_s}$

where

K = Overall mass-transfer coefficient of solute, kg/(hr)(cm^2)
a = Interfacial area, cm^2/liter of reacting fluids
r = Instantaneous mass-transfer rate of solute, kg/(hr)(liter) of reacting fluids
C^*_s = Equilibrium salt concentration corresponding to metal composition, w/o
C_s = Concentration of solute in salt phase, w/o.

The smaller transfer coefficient shown for the Cu-5.5 w/o Mg-5.5 w/o U alloy system is probably a result of a low diffusion rate for plutonium in the alloy. It has been observed qualitatively that the Cu-5.5 w/o Mg-5.5 w/o U and $MgCl_2$ system is very viscous, whereas the Cu-33 w/o Mg and ternary salt system is relatively fluid.[6] Liquid metal diffusion appears to be the controlling mass-transfer resistance in salt-metal extraction.

A supporting program to investigate containment materials for pyrochemical process solutions is in progress. In recent corrosion work, specimens of molybdenum and TZM alloy, a molybdenum alloy containing titanium (0.5 w/o and zirconium (0.08 w/o), in the form of agitator blades were exposed to Cu-Mg-U/salt or Zn-Mg-U/salt systems. The test conditions and the results are shown in Table XI. In the metal/$MgCl_2$ system tests at 850°C, the molybdenum and TZM showed good corrosion resistance (penetrations of <0.01 mm/200 hr and up to 0.05 mm/133 hr, respectively). In the Zn-Mg-U/$MgCl_2$ system test at 750°C, the TZM evidenced a slight increase in corrosive attack (penetrations of 0.07 mm/195 hr), principally at the ends of the agitator blades. Further testing of TZM in the form of a crucible is planned. In the tests that were carried out at 700°C with Zn-Mg-U/$MgCl_2$-30 m/o NaCl-20 m/o KCl and Cu-Mg-U/ternary salt systems, the molybdenum exhibited a pitting-type corrosion (penetrations up to 0.26 mm/192 hr), which was observed over the entire length of the agitator blade. A comparison of the test results at 750 and 700°C suggests the possibility that the ternary salt may have been responsible for the higher corrosion rates observed. This possibility will be investigated.

TABLE XI. Corrosion of Molybdenum and TZM Alloy in Cu-Mg-U/Salt and Zn-Mg-U/Salt Systems

Coupons were exposed as agitator blades in the test solutions.

Coupon Composition: Molybdenum of low carbon content (0.003 w/o); TZM, a molybdenum alloy containing titanium (0.5 w/o) and zirconium (0.08 w/o).

	System						
	Cu-Mg-U/Salt				Zn-Mg-U/Salt		
Coupon	Mo	TZM	TZM	Mo	TZM	TZM	Mo
Metal Phase (w/o)	89 Cu-9 Mg-2 U	89 Cu-9 Mg-2 U	89 Cu-9 Mg 2 U	66 Cu-33 Mg-1 U	35 Zn-65 Mg-0.1 U	90 Zn-10 Mg-0.3 U	95 Zn-5 Mg-0.1 U
Salt Phase (m/o)	100 $MgCl_2$	100 $MgCl_2$	100 $MgCl_2$	50 $MgCl_2$-30 NaCl-20 KCl	100 $MgCl_2$	100 $MgCl_2$	50 $MgCl_2$-30 NaCl-20 KCl
Time (hr)	200	200	133	192	200	195	192
Temperature (°C)	850	850	850	700	850	750	700
Observed Corrosion Penetration (mm)	<0.01	<0.01	0.05	0.1-0.2	<0.01	0.07	0.23-0.26

b. Waste Disposal. A study is under way of the wastes produced from the various steps in the reference pyrochemical flowsheet and of the techniques for the handling and disposal of these wastes. The composition, fission product heating, and radiation levels of the various wastes produced are being calculated in order to examine their effect on waste disposal techniques.

[6]The diffusion rate varies inversely with the viscosity.

F. Design Concept Analyses and Advanced Systems Evaluation

1. 1000-MWe Study

Argonne National Laboratory has received from Atomics International four copies of the topical report entitled, "1000-MWe FBR Parametric Study of Secondary Sodium-Steam System." This work constitutes part of Phase III of the 1000 MWe follow-on study program and was performed under the technical guidance of ANL.

The report constitutes an initial exploratory effort to narrow the range of turbine-throttle steam conditions warranting further detailed parametric study. Results show that the range of variables attractive for further detailed parametric study are: turbine-throttle steam pressure of 2400 to 3500 psig, and temperatures of 900 to 1000°F, including sodium for steam reheat cycles. The live-steam reheat cycle did not appear attractive based on results of this study. In preparation for making recommendations to the AEC, ANL is reviewing the report for both technical content and applicability to the pending 1000-MWe follow-on studies.

ANL has completed individual preliminary negotiations with all 1000-MWe follow-on study contractors (see Progress Report for August 1966, ANL-7249, p. 37). Atomics International, General Electric, Babcock and Wilcox, and Westinghouse have submitted their revised proposals reflecting their understanding of the program as discussed in the preliminary negotiations. ANL has reviewed the individual proposals and has established the detailed scope.

III. GENERAL REACTOR TECHNOLOGY

A. Applied and Reactor Physics Development

1. Slow-Fast and Fast-Slow Coincidence Methods

A significant time difference exists between the slow and prompt responses delivered by a detector. In coincidence analysis it is necessary to integrate the slow response, for example, to determine energy, while at the same time retaining the timing element afforded by the prompt fast pulse. Two conventional counting methods have been developed to treat this problem. The two methods, the fast-slow and slow-fast techniques, are illustrated in the logic diagrams shown in Fig. 10.

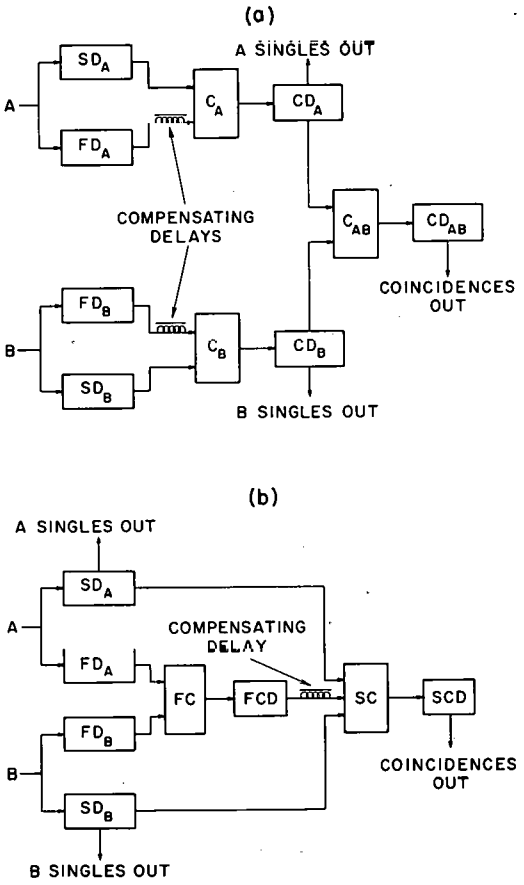

NOTATION

F	"fast," that is, involving bandwidth in the order of 100 MHz
S	"slow," relatively, with bandwidths typically 20 MHz
D	discriminator
C	coincidence unit
A	one of two channels
B	the second of two channels
AB	coincidence channel with inputs A and B
SD	"slow" discriminator
FD	"fast" discriminator
FCD	fast coincidence (post-) discriminator
SCD	slow coincidence (post-) discriminator
FC	"fast" coincidence
SC	"slow" coincidence
CD	coincidence (post-) discriminator

Fig. 10. Block Diagrams of Conventional (a) Slow-Fast and (b) Fast-Slow Methods of Coincidence Counting

Various reasons for favoring one arrangement over the other have been advocated. Clearly the equipment inventory for the fast-slow method is smaller than required for the slow-fast arrangement. On the other hand, it would appear that there are some advantages in precision data collection and in accidental monitoring which favor the slow-fast alignment. For situations in which very low count rates prevail, both methods are

equivalent to a simple twofold coincidence system. A realistic comparison of the utility of these two methods must therefore be made at high accidental count rates.

An analytical comparison of these two systems has been made using the assumption of a constant deadtime. Such a condition can be met in practice by employing an Adjustable Paralysis Discriminator (APD) (see Progress Report for August 1966, ANL-7249, pp. 37-38). Indeed, one of the chief advantages of this discriminator lies in the fact that the correction factors necessary for precision coincidence counting become more readily accessible.

Under these conditions, the ratio of the fast-slow accidentals to the slow-fast accidentals is

$$\frac{A(F - S)}{A(S - F)} = \alpha_A \epsilon_A \alpha_B \epsilon_B (\omega\theta N)^2, \qquad (1)$$

where

$A(F - S)$ fast-slow accidental rate;
$A(S - F)$ slow-fast accidental rate;
α ratio of count rate in fast channel to count rate in corresponding slow channel (A or B);
ϵ efficiency of channel (A or B);
$\omega\theta$ constant "on-time" or pulse-width of APD;
N source disintegration rate.

The number of fast-slow accidentals can be more or less than the number feeding through the slow-fast system, depending to a large extent on the α ratios which reflect not only source-related counts, but also background, noise, and other uncorrelated origins; the value of each α can be anywhere in the range from a little over one to possibly hundreds under severe conditions. If the deadtime effect ($\epsilon\omega\theta N$) of each slow channel is kept small, then the advantage could be in favor of the fast-slow system. For example, a deadtime of 1% would allow the product $\alpha_A\alpha_B$ to be as high as 10^4; this situation applies when channel efficiencies are small. On the other hand, if both deadtime losses and α values become large, then the slow-fast system has noticeable advantages.

2. Evaluation of Cross Sections

The preparation of neutron cross sections of magnesium and titanium for the ENDF/B library has been completed, and cards have been punched in the ENDF/B Format. The cross sections for magnesium were obtained mainly from Traili et al.,[7] and those for titanium from the same source

[7]Tralli, N., et al., Fast Neutron Cross Sections for Titanium, Potassium, Magnesium, Nitrogen, Aluminum, Silicon, Sodium, Oxygen and Manganese, UNC-5002 (Jan 1962).

and modifications from Miller and Parker.[8] Various changes and additions were made. Among these are calculations of $\bar{\mu}_L$, ξ, and γ from the Legendre expansion coefficients, using a double precision FORTRAN program based on methods used in the CHAD code.[9] Here $\bar{\mu}_L$ is the average elastic scattering cosine in the laboratory system, ξ is the average logarithmic energy decrement, and γ is the Greuling-Goertzel parameter.[10] Other additions included the evaluation of nuclear temperatures for continuum inelastic scattering and the (n,2n) reaction, and the inclusion of parameters for the free gas thermal scattering law.

Much of the work has been completed in compiling vanadium cross sections for the ENDF/B library. This is a new evaluation based on both experimental and theoretical work. Experimental values exist for total, capture, (n,p), and (n,α) cross sections over fairly large energy ranges, and for scattering angular distributions up to about 1.8 MeV. There is also some experimental data for inelastic scattering and the (n,2n) reaction. Calculations of inelastic and elastic scattering have been done using the Abacus 2-Nearrex combination.[11-13] The (n,2n) cross sections have been calculated by Pearlstein's method,[14] renormalized to pass through a single experimental point. Angular distributions are being processed with the aid of the SAD code (see Progress Report for February 1966, ANL-7176, p. 47). Educated guesses are being used for some cross sections to fill out the entire energy range of interest.

The plotting program for the MC^2 library has been revised with many improvements. Almost any arbitrary selection of data can now be plotted during one computer run. Legendre expansion coefficients, which have recently been added to the MC^2 library tape from the Elmoe tape, can be plotted.

3. Unitary Models of Nuclear Resonance Reactions

Although most reaction theories are formally flux conserving, the kinds of models and approximations used to specify the S-matrix for resonance reaction processes are often of doubtful unitarity, particularly

---

[8] Miller, S. M., and Parker, K., Neutron Cross Sections of Natural Titanium in the Energy Range 0.001 eV-18 MeV--Incorporation of the United Nuclear Corporation Data in the UKAEA Nuclear Data Library, AWRE 0-77/64 (Oct 1964).

[9] Berland, R. F., CHAD--Code to Handle Angular Data, NAA-SR-11231 (Dec 1965).

[10] Goertzel, G., and Greuling, E., An Approximate Method for Treating Neutron Slowing Down, Nucl. Sci. Eng. 7, 69-72 (Jan 1960).

[11] Auerbach, E. H., et al., Abacus-1: A Program for the Calculation of Nuclear Cross Sections Using the Cloudy Crystal Ball Model, KAPL-3020 (June 1, 1964).

[12] Auerbach, E. H., Abacus-2 (Revised Version) Program Operation and Input Description, BNL-6562 (Nov 1962).

[13] Moldauer, P. A., et al., Nearrex, A Computer Code for Nuclear Reactor Calculations, ANL-6978 (Dec 1964).

[14] Pearlstein, S., Analysis of (n,2n) Cross Sections for Medium and Heavy Mass Nuclei, Nucl. Sci. Eng. 23, 238-250 (Nov 1965). See also BNL-897 (Dec 1964).

in the overlapping resonance region. To investigate the consequences of unitarity in this domain, several classes of simple analytically specified unitary S-matrices are constructed by means of R-matrix models having various periodic arrangements of poles and residues. The resulting reaction amplitudes have a variety of fluctuating resonance spacings and widths, as well as nonresonant direct terms and up to three competing channels.

Relationships between resonance parameters, channel transmission coefficients, average cross sections, and cross-section fluctuations must be considered. It is found that, contrary to common belief, unitarity imposes no restriction on the average ratio of channel width to resonance spacing. In all models investigated having no direct coupling between channels, the transmission coefficients are given by $T_c = 1 - \exp(-2\pi\overline{\Gamma}_c/D)$. Localized structure in the resonance parameters was investigated, and the effects of a single strong R-matrix pole were compared with those of a "giant resonance" distribution of R-matrix pole strength. In this way the shapes of both Robson's analog resonances and Feshbach's doorway state resonances were derived in a different dynamical context. Direct scattering and reaction amplitudes were found to be strongly correlated with resonance amplitudes. Thus, for example, two channels coupled by a direct reaction have correlated resonance width amplitudes, and the pole terms of the resonance reaction amplitude coupling them have a nonzero average. Evidence is found that unitarity imposes correlations among resonance width amplitudes and these in turn affect the relation between average resonance parameters and average cross sections and even more between these and cross-section fluctuations.

4. The ARC System

a. Cross-section Preparation. The original method used to calculate the resolved resonances for MC^2 has been changed. The effective group cross sections are now evaluated by use of a $1/\Sigma_t(E)$ weighting, where $\Sigma_t(E)$ includes the total resonant plus smooth background scattering for all materials in the mixture. Previously, a pseudo-Goldstein-Cohen approach had been used. This earlier method produced results only very slightly different from the new method, but required more storage space in the computer core and running time. The present code is capable of handling 800 resonances as compared to only 500 in the earlier version.

Test runs involving the consistent B1 and consistent P1 flux options, as well as the hydrogen capability, have revealed minor code errors. These are currently under investigation. It is expected that MC^2 will be largely debugged so that it may be used with the ENDF/B cross sections which are forthcoming later this fall.

b. Fast Reactor Accident Analyses. A major effort has been initiated to extend greatly the present capacity for analysis of the behavior of fast reactors over a wide range of accident conditions. All programming is to be in the FORTRAN IV language and for the IBM-360 computer system. This programming development is a part of the ARC system.

Initial plans call for representation of the reactor as a one-dimensional model of either a slab, cylinder, or a sphere. The first two-dimensional model will be in r-z geometry. An indication of the eventual range of computation can be seen from Fig. 11. For the first stage of development, the plan is to create only a few initiating mechanism "modules" and perhaps a simple Core State module in the post-burst area. The concentration of effort will thus be on neutronics, feedback, and disassembly.

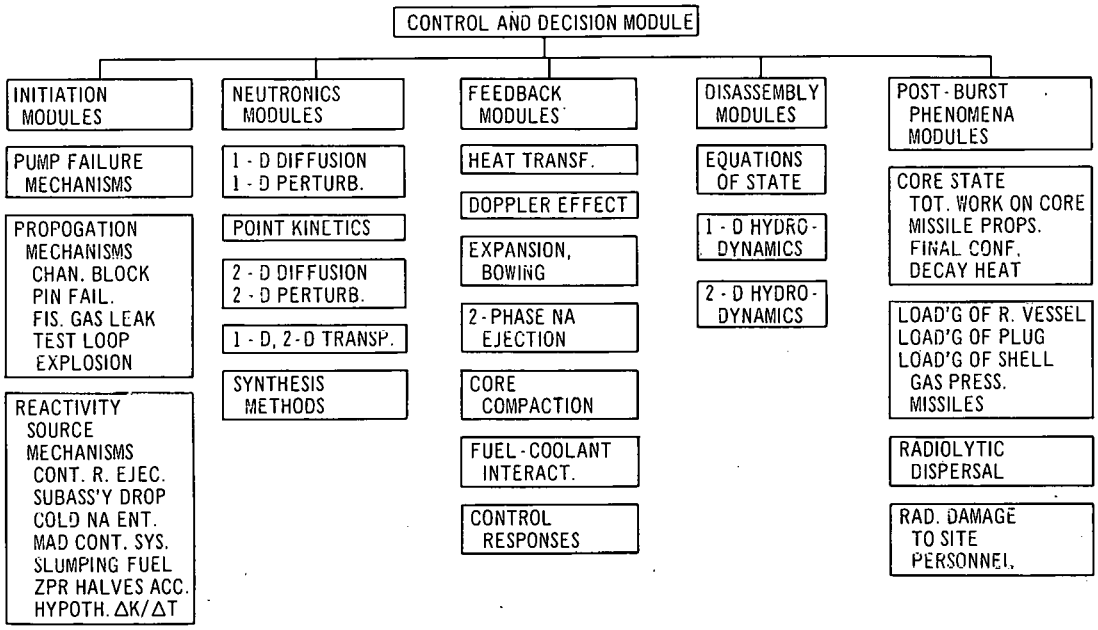

Fig. 11. System for Fast Reactor Accident Analysis

The one-dimensional space- and time-dependent neutronics module will use the method outlined by Ott in a forthcoming note to Nuclear Science and Engineering. This method follows the formulation developed by Henry.[15]

The space-dependent diffusion equation is solved in the quasi-static approximation, that is, the fluxes are calculated in the asymptotic approximation with, however, an accurate representation of the spatial distribution of delayed-neutron sources. A CDC-3600 program (QX-1), which is now in an advanced debugging stage, will provide the basis for programming this module.

In the area of feedback modules, the most advanced developments are in heat transfer, sodium ejection, and Doppler effect calculation. A standard heat-transfer code will be employed in the beginning. The sodium ejection will be treated by an extension of a program developed at ANL.

[15] Henry, A. F., The Application of Reactor Kinetics to the Analysis of Experiments, Nucl. Sci. Eng. 3, 52 (Jan 1958).

The Doppler-broadened capture and fission cross sections in each energy group at any temperature are computed from a three-term equation for $\delta\sigma$, whose coefficients are found by fitting to previously computed values at four temperatures. These calculations are material- and region-dependent.

The hydrodynamics of disassembly will be treated very much as are the hydrodynamics calculations performed in the AX-1 code. The method is described in ANL-5977. A very important difference in the computations in the area of the accident is the treatment of the neutronics, which will now include effects of delayed neutrons and the Doppler effect throughout the burst. The strategy which decides when another neutronics calculation must be performed promises to save considerable computer time with respect to the use of the AX-1 code.

c. Standard Neutronics Modules. A one-dimensional multigroup perturbation-theory module is being developed for use within the ARC system. The module will use essentially the same algorithms as the DEL[16] code but will also include expressions for β_{eff}, ℓ, and α, the delayed-neutron fraction, lifetime, and reciprocal periods, respectively.

Questions have arisen regarding perturbation of boundary conditions caused by changes such as in the diffusion coefficient D or in the moderator cross sections. The two-dimensional perturbation routine in CANDID2D treats these boundary perturbations for changes in D. However, it is now felt that the simpler DEL treatment of leakage effects is rigorously correct while CANDID2D is not strictly correct for problems of interest in reactor physics.

B. Fuels and Cladding*

1. Fabrication and Evaluation

a. Irradiation of High-temperature Materials. A series of irradiations of ceramic fuel materials being developed under the high-temperature materials program are in progress in MTR. A summary is shown in Table XII.

b. Properties of High-temperature Ceramics

(i) (Th-U-Pu)S Properties. Uranium monophosphide and uranium monosulfide are of interest as high-temperature reactor fuels because of their high melting points and apparent high-temperature stability. Their potential usefulness has prompted extensive research on

*Please note that the graphs indicated as Figs. 14 and 15, p. 42, of Progress Report for August 1966, ANL-7249, were interchanged accidentally.

[16] Kvitek, L. C., DEL, A Perturbation Theory Program Written in FORTRAN II for the IBM-704, ANL-7052.

these materials at ANL. As part of the overall program on characterization of the monophosphide and monosulfide of uranium, vaporization rates in vacuum were measured. The effective vapor pressure was then calculated from the Langmuir equation.

TABLE XII. Status of Ceramic Fuel (Clad in Nb-1 w/o Zr) Irradiations in MTR

		Design Parameters				Operating Conditions			
								Burnup to Date	
Capsule or S/A No.	Specimen Number	Fuel Composition (w/o)	Effective Density (%)	Cladding OD (in.)	Cladding Thickness (in.)	Power Density (kW/cc)[a]	Max Cladding Temp (°C)	a/o (U + Pu)	fiss/cc x 10^{-20}[a]
56-11	MV-2	UC-20 PuC	79	0.281	0.012	1.2	470	6.0	15.5
56-8	MV-3	UC-20 PuC	81	0.281	0.012	1.2	715	6.5	17.2
56-8	MV-5	UC-20 PuC	80	0.281	0.012	1.2	705	6.2	16.2
56-11	MV-6	UC-20 PuC	80	0.281	0.012	1.2	480	6.5	17.0
56-13	Z-4	UC-20 PuC	79	0.174	0.015	1.2	665	1.4	3.6
56-13	Z-5	UC-20 PuC	79	0.174	0.015	1.2	585	1.4	3.6
56-13	Z-7	UC-20 PuC	79	0.174	0.015	1.2	570	1.4	3.6
56-13	C-45	PuC	84	0.174	0.009	1.4	700	1.4	3.8
56-8	S-7	US	80	0.281	0.012	1.0	535	4.8	9.3
56-8	S-8	US	89	0.281	0.012	1.0	725	6.0	14.7
56-8	S-9	US	76	0.281	0.012	1.0	750	6.8	12.5
56-8	S-10	US	91	0.281	0.012	1.0	690	6.8	15.0
56-11	S-15	US	82	0.281	0.012	1.0	380	3.9	8.0
56-11	S-16	US	90	0.281	0.012	1.0	510	5.8	12.6
56-11	S-17	US	88	0.281	0.012	1.0	500	4.5	9.6
56-11	S-18	US	77	0.281	0.012	1.0	610	6.3	11.8

[a]Based on effective density.

The data for UP, given in Table XIII, are plotted in Fig. 12 together with the Knudsen cell data of Gingerich and Lee.[17] The Langmuir

TABLE XIII. Evaporation Rate Data for Uranium Monophosphide

Sample Number	Temp (°K)	Weight Loss (mg)	Time (min)	Evaporation Rate (g/cm^2-sec) (10^{-6})	Pressure (atm x 10^{-7})
55	1828	0.39	27	0.28	0.17
43	1848	0.60	18	0.65	0.38
56	1853	0.465	20	0.48	0.28
56	1868	0.85	33	0.53	0.32
55	1868	0.555	22	0.49	0.30
44	1878	0.50	13	0.77	0.46
43	1898	0.74	13	1.10	0.66
56	1898	0.72	13	1.15	0.69
4	1913	1.38	30	0.885	0.53
55	1918	1.34	23	1.14	0.68
56	1943	1.04	13	1.66	1.00
55	1963	2.225	22	1.98	1.20
44	2008	1.97	12	3.29	2.02
3	2018	3.46	17	4.00	2.47
44	2043	3.16	11	5.76	3.57
45	2073	5.48	17	6.31	3.94
43	2078	7.19	14	9.96	6.23
4	2088	11.04	24	8.86	5.55
44	2108	6.39	10	12.82	10.39
45	2123	4.67	8	11.43	7.23
45	2133	6.13	9	13.34	8.45
59	2163	7.17	4	34.45	21.98

[17]Gingerich, K. A., and Lee, P. K., J. Chem. Phys. 40, 3520 (1964).

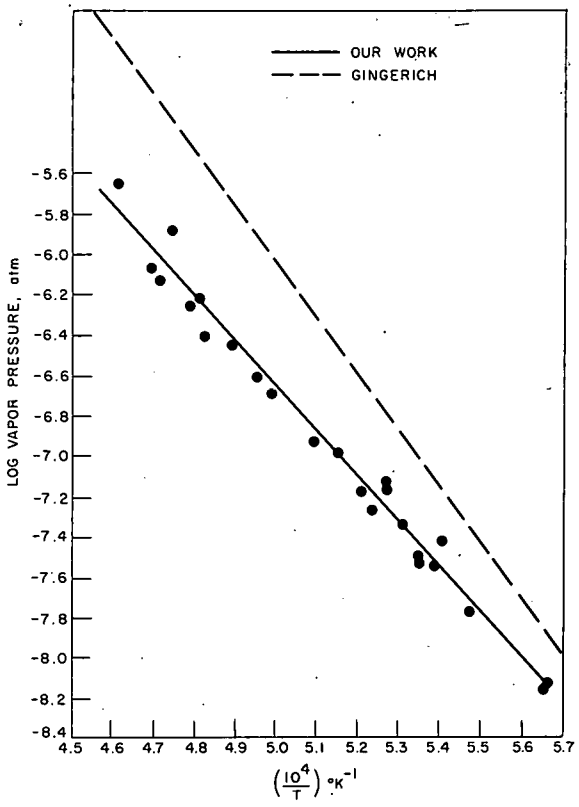

Fig. 12. Effective Vapor Pressure of UP vs. Reciprocal Temperature

data are in fair agreement at low temperatures but the curves tend to diverge at high temperatures. Work is in progress to determine the reason for the differences between the two curves.

Metallographic examination of samples in the as-sintered condition showed the presence of uranium metal dispersed in a UP matrix. After heat treatment at 1860°C, grain growth and diffusion of free uranium to the grain boundaries were observed. There was no apparent change of composition of the UP sample due to preferential evaporation of phosphorus or uranium.

Vaporization data for uranium monosulfide, given in Table XIV, are plotted in Fig. 13 together with the Knudsen cell data of Cater et al.[18] The higher vapor pressure observed in our work could be due to the presence of secondary phases of UOS and/or U_2S_3 in the specimens. Work is in progress to resolve the discrepancy between the two curves.

TABLE XIV. Evaporation Rate Data for Uranium Monosulfide

Sample Number	Temp (°K)	Weight Loss (mg)	Time (min)	Evaporation Rate (g/cm^2-sec) (10^{-6})	Pressure (atm x 10^{-7})
73	1808	0.18	18	0.21	0.13
67	1868	0.49	13	0.83	0.49
67	1903	0.88	20	0.97	0.58
71	1973	1.68	13	2.84	1.73
71	1983	1.86	10	4.09	2.50
71	1998	1.29	6	4.73	2.90
61	2003	3.90	16	5.32	3.27
71	2038	4.31	10	9.47	5.86
61	2068	8.48	12	15.44	10.08
73	2098	3.25	3	23.84	14.97
67	2113	4.30	4	23.64	14.91
67	2143	6.60	4	36.28	23.02

[18]Cater, E. D., Gilles, P. W., and Thorn, R. J., J. Chem. Phys. 35, 608 (1961).

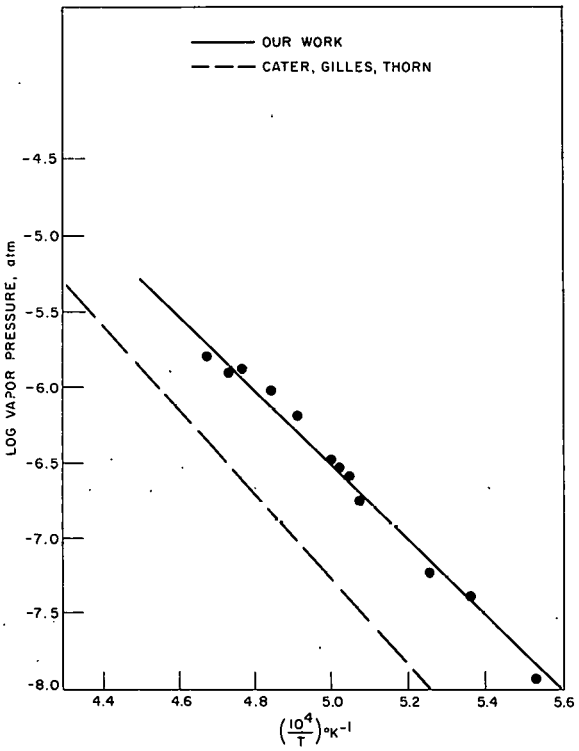

Fig. 13. Effective Vapor Pressure of US vs. Reciprocal Temperature

The vapor-pressure curves for our UP and US specimens are described by the equations

$$\log P_{UP} = 4.46 - \frac{2.22 \times 10^4}{T}$$

(1830 - 2160°K);

$$\log P_{US} = 5.73 - \frac{2.45 \times 10^4}{T}$$

(1800 - 2140°K).

(ii) U-S-O System. In anticipation of preparing compositions on the U-S join, sintered US specimens were fabricated directly from mixtures of UH_3 and US_2, and mixtures of U powder and US_2, without using an intermediate homogenization. Pellets isostatically pressed without binder at 55,000 psi and vacuum-fired at 1850°C for 3 hr achieved 82.5% theoretical density (TD) when made with UH_3 and 85.5% TD when made with U powder. About 4 m/o UOS was present in these sintered specimens. To reduce the amount of UOS present, a more pure starting material will be prepared. The lattice parameter ranged from 5.486 to 5.488 Å for the stoichiometric US mixtures, but jumped to 5.491 Å when an excess of 13 m/o UH_3 was used.

Chemical analyses were received for the series of UOS mixtures that covered the range $UO_{1.05}S_{0.95}$ to $U_{0.93}S_{1.07}$. In general, it was indicated that the oxygen was fairly stable in all the compositions, whereas much of the hyperstoichiometric sulfur was lost at 1650°C. The eutectic reported between UOS and U_3S_5 in the compositions with hyperstoichiometric sulfur was found by areal analysis to contain 28 to 31 m/o UOS.

Two compositions from the U_3O_8-US_2 series, which X-ray powder patterns clearly showed to be mixtures of UO_2 and UOS after a 1200°C vacuum firing, were refired at 1650°C. Polished sections of the resulting materials revealed light yellow particles in a gray matrix. X-ray diffraction showed no lines for UO_2 in either case, and very faint lines for UOS only in the pattern for the sample initially high in UOS. Some of the low-angle lines for the unidentified primary phase (or phases) roughly corresponded to those of UOS, but the high-angle lines differed markedly. The UOS-UO_2 binary system will be more carefully examined using UO_2 and UOS as starting materials.

A study was made in which the progressive reaction of US_2 powders exposed to the humid laboratory atmosphere was followed by weight change and X-ray analysis. The X-ray patterns showed a loss of the high-angle US_2 lines after 20 days, the appearance of a $UO_3 \cdot 2H_2O$ phase (accompanied by a change in color from gray-black to yellow-green) after 120 days, and finally a predominant conversion to a yellow $UO_3 \cdot 8H_2O$ phase after 160 days. The powders gained weight steadily through 120 days and thereafter remained almost constant in weight. The excessive amount of weight gain indicated that the sulfur displaced during the formation of the uranium oxide hydrate must in some manner be retained in the product. Chemical analysis will be used to confirm this.

(iii) Mechanical Properties of Uranium and Plutonium Compounds. Fracture tests have continued on urania specimens at 25°C and at 1500°C with variations in strain rate. These tests will probably complete the studies on UO_2. Additional work on UP and US is planned. Before this work is started, the furnace will be modified for installation in a glovebox in preparation for studies on the behavior of plutonium-bearing ceramic materials.

Studies have shown that at a slow strain rate, a linear increase in stress was observed up to a maximum at 1000°C. Above 1000°C there was a gradual decrease in stress to 1500°C, and then a rapid decrease to 1750°C. At the medium strain rate, the maximum stress was observed at 1125°C with a gradual decrease to 1500°C, and then a rapid decrease to 1900°C. With a fast strain rate the maximum stress was observed at 1250°C. Above this temperature the stress decreased with an increase in temperature up to 1750°C.

The brittle-ductile transition also appeared to be temperature dependent. Slow strain rates indicated a brittle-ductile transition temperature range of 1250 to 1375°C while with fast strain rates a temperature range of 1500 to 1625°C was observed.

(iv) Lithium Corrosion Studies at Elevated Temperatures. No information regarding the inhibition of lithium corrosion of tantalum has been found in the literature. There have been rather few recent studies of the lithium corrosion of tantalum at high temperatures.

As previously reported (see Progress Report for May 1966, ANL-7219, pp. 37-38), the addition of a small amount of silicon to lithium exerted a significant influence in retarding corrosion of tantalum at 1200°C. Recently, duplicate tests made under strictly controlled conditions showed that a tantalum capsule containing uninhibited lithium suffered cracking penetrations to a maximum depth of 140 μ, whereas there was no detectable corrosion of tantalum exposed in silicon-containing lithium (1.56 a/o Si). The test period was seven days at a temperature of 1200 ± 25°C.

More recently, microhardness measurements taken from transverse sections of the exposed tantalum samples revealed that there is a surface layer formed as a result of continuous contact of tantalum with silicon-containing lithium. In the absence of silicon in lithium, no such layer was discernible.

Further evidence of silicon deposition on tantalum is revealed by the results of spectrochemical analysis. A concentration of 0.1 to 0.01% of silicon was found on the surfaces of tantalum samples exposed to silicon-containing lithium. No silicon was detected on tantalum samples that had contacted lithium alone.

The initial results indicate that this inhibition phenomenon may be of a diffusion-barrier type. Metallographic and chemical analyses now in progress may lead to a better understanding and evaluation of this phenomenon.

2. Radiation Damage to Structural Materials

a. Fast-neutron Irradiation of Jacket Materials. The tensile, creep, creep-rupture, and tube-rupture properties of Type 304 stainless steel, Hastellow-X, Inconel-625, V-20 w/o Ti, and V-15 w/o Ti-7.5 w/o Cr are being evaluated as a function of fast neutron irradiation in the exposure range from 1×10^{21} to 1×10^{23} n/cm^2 and at elevated temperature in the range from 500 to 750°C. Eighteen capsules containing 162 tensile-type specimens, which were irradiated to a maximum total neutron exposure of 6.5×10^{21} n/cm^2 at a temperature of 650°C, were removed from EBR-II subassembly XO13 during this report period. Twenty-six capsules containing 60 tube-rupture specimens and 296 tensile-type specimens are being irradiated in EBR-II subassemblies XA07, XA08, XO09, and XO10 at temperatures between 500 and 670°C. No change in status occurred during this report period, and the specimens have accumulated at this time maximum total neutron exposures ranging from 7.5×10^{21} to 3×10^{22} n/cm^2. The status and identification of the capsules are given in Table XV.

3. Techniques of Fabrication and Testing

a. Determination of Elastic Moduli of High-temperature Materials by Ultrasonics. Calculations of the sound velocities and elastic moduli of a rod of V-15 w/o Ti-7.5 w/o Cr have been completed, and have been corrected for thermal expansion (see Progress Report for February 1966, ANL-7176, p. 30). Figure 14 shows the Young's modulus, shear modulus, and Poisson's ratio for this rod, as well as the corresponding values for a V-20 w/o Ti rod. Since both of these rods were machined to fit the low-temperature vacuum furnace, measurements could not be made at temperatures above 1150°C.

TABLE XV. Status of Cladding-materials Irradiations in EBR-II

S/A No.	Capsule Number	Design Parameters: Cladding Composition	Type of Specimen	No. of Specimens	Specimen Environment	Operating Conditions: Max Specified Temp (°C)	Exposure to Date (n/cm^2)
XA07	AS-9	V-20w/oTi	Tensile	16	Argon-helium	590	3.0×10^{22}
XA07	AS-10	Hastelloy-X	Tensile	16	Argon-helium	590	2.7×10^{22}
XA07	AS-11	304 SS	Tensile	16	Argon-helium	590	2.9×10^{22}
XA08	AS-1	V-20w/oTi	Tube-burst	12	Argon-helium	540	2.4×10^{22}
XA08	AS-2	V-20w/oTi	Tube-burst	12	Argon-helium	540	2.4×10^{22}
XA08	AS-3	Hastelloy-X	Tube-burst	12	Argon-helium	540	2.5×10^{22}
XA08	AS-4	Hastelloy-X	Tube-burst	12	Argon-helium	540	2.5×10^{22}
XA08	AS-5	304 SS	Tube-burst	12	Argon-helium	540	2.5×10^{22}
XA08	AS-6	V-20w/oTi	Tensile	16	Argon-helium	580	2.6×10^{22}
XA08	AS-7	Hastelloy-X	Tensile	16	Argon-helium	580	2.4×10^{22}
XA08	AS-8	304 SS	Tensile	16	Argon-helium	580	2.4×10^{22}
XA08	AS-12	V-20w/oTi	Tensile	16	Argon-helium	580	2.3×10^{22}
X009	AS-14	V-20w/oTi	Tensile	13	Argon-helium	670	2.1×10^{22}
X009	AS-15	V-20w/oTi	Tensile	13	Argon-helium	670	2.0×10^{22}
X009	AS-27	304 SS Hastelloy-X	Tensile	13	Argon-helium	670	2.2×10^{22}
X010	AS-16	V-20w/oTi	Tensile	13	Argon-helium	500	7.9×10^{21}
X010	AS-17	V-20w/oTi	Tensile	13	Argon-helium	500	8.6×10^{21}
X010	AS-18	V-20w/oTi	Tensile	13	Argon-helium	500	7.5×10^{21}
X010	AS-19	V-20w/oTi	Tensile	13	Argon-helium	500	7.9×10^{21}
X010	AS-20	V-20w/oTi	Tensile	13	Argon-helium	500	8.8×10^{21}
X010	AS-21	V-20w/oTi	Tensile	13	Argon-helium	500	10.4×10^{21}
X010	AS-22	Hastelloy-X	Tensile	13	Argon-helium	500	9.1×10^{21}
X010	AS-23	304 SS	Tensile	13	Argon-helium	500	10.4×10^{21}
X010	AS-24	304 SS	Tensile	13	Argon-helium	500	8.8×10^{21}
X010	AS-25	304 SS	Tensile	13	Argon-helium	500	8.4×10^{21}
X010	AS-26	304 SS	Tensile	15	Argon-helium	500	8.5×10^{21}
X013	AS-34	Hastelloy-X	Tensile	9	Sodium	650	7.0×10^{21}
X013	AS-35	V-20w/oTi	Tensile	9	Sodium	650	6.5×10^{21}
X013	AS-36	V-20w/oTi	Tensile	9	Sodium	650	6.3×10^{21}
X013	AS-37	Hastelloy-X	Tensile	9	Sodium	650	7.0×10^{21}
X013	AS-38	V-20w/oTi	Tensile	9	Sodium	650	7.3×10^{21}
X013	AS-39	V-20w/oTi	Tensile	9	Sodium	650	7.0×10^{21}
X013	AS-40	V-20w/oTi	Tensile	9	Sodium	650	7.3×10^{21}
X013	AS-41	V-20w/oTi	Tensile	9	Sodium	650	6.5×10^{21}
X013	AS-42	V-15w/oTi-7.5Cr	Tensile	9	Sodium	650	6.5×10^{21}
X013	AS-43	V-15w/oTi-7.5Cr	Tensile	9	Sodium	650	6.8×10^{21}
X013	AS-44	V-15w/oTi-7.5Cr	Tensile	9	Sodium	650	6.8×10^{21}
X013	AS-45	V-15w/oTi-7.5Cr	Tensile	9	Sodium	650	6.5×10^{21}
X013	AS-46	Hastelloy-X	Tensile	9	Sodium	650	7.3×10^{21}
X013	AS-47	304 SS	Tensile	9	Sodium	650	7.5×10^{21}
X013	AS-48	304 SS	Tensile	9	Sodium	650	7.3×10^{21}
X013	AS-49	304 SS	Tensile	9	Sodium	650	7.3×10^{21}
X013	AS-54	V-15w/oTi-7.5Cr	Tensile	9	Sodium	650	6.8×10^{21}
X013	AS-55	V-15w/oTi-7.5Cr	Tensile	9	Sodium	650	7.0×10^{21}

b. Ultrasonic Instrument and Transducer Development. Two 5-Mc, focused, ultrasonic transducer probes were fabricated in order to evaluate polystyrene and Ciba 502 epoxy resin as lens materials. Both probes contained 0.64-cm-dia, lead zirconate-titanate piezoelectric elements and Fiberglas-loaded epoxy backings. Plano-concave lenses, with a radius of curvature of 0.64 cm, were attached to the probes.

A Schlieren system was used to examine the beam patterns. The focal lengths in water are between 1.27 and 1.92 cm. Since the velocity of longitudinal waves is slightly higher in epoxy resins, the probe with the Ciba 502 lens has the shorter focal length. Intensities of the beams from the two probes are comparable.

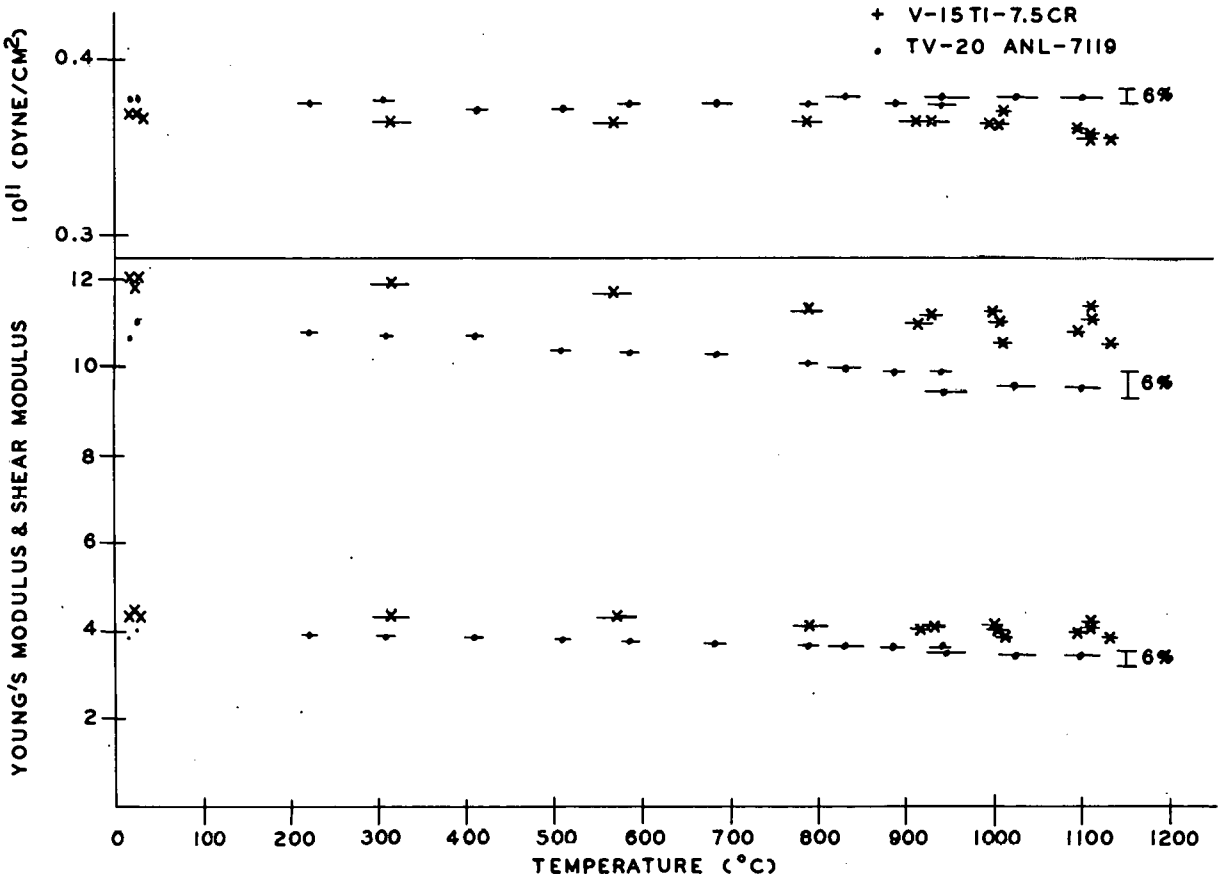

Fig. 14. Young's Modulus, Shear Modulus, and Poisson's Ratio for V-15 Ti-7.5 Cr (w/o) and for V-20 w/o Ti, as Measured by an Ultrasonic Pulse Echo Technique

c. Development of a Neutron-image-intensification System. Low-neutron-level tests have recently been completed at the Juggernaut reactor in order to determine the low-threshold neutron intensities that are observable on a television presentation. The equipment used included the neutron image intensifier, and closed-circuit television systems with vidicon and image orthicon cameras. The image orthicon (camera tube was a Type 7198) system used was an older (circa 1950) system and does not completely represent what might be accomplished with newer image orthicon systems. Nevertheless, tests with this system did give improvement by a factor of 100X in low-level detection, as anticipated.

Previous low-level tests with the vidicon system had indicated that thermal-neutron intensities as low as 10^5 n/cm^2-sec could be observed on television. The newer tests with a vidicon system showed the influence of the improved neutron image intensifier tube;[19] neutron intensities as low as 2×10^4 n/cm^2-sec were observed with the vidicon television system.

The image orthicon tests (with a 5-cm, f/0.95 lens) proved that television brightening could be observed for neutron intensities as low as

[19] Dolon, P., Berger, H., and Niklas, W. F., An Improved Neutron Image Intensifier Tube, Thirteenth Nuclear Science Symposium, Boston, October 19-21, 1966, to be published in Proceedings.

200 n/cm^2-sec. The television image of a cadmium test object (~2 x 4 cm) was detectable for neutron intensities as low as 1000 n/cm^2-sec.

The general impression given by these tests was that, for neutron intensities about 2 x 10^5 n/cm^2-sec or higher, either television system would provide useful information. For lower neutron intensities the improved low-light-level sensitivity of the image orthicon system would be a definite advantage.

One additional threshold test completed involved the image orthicon system and a neutron scintillator [a Li-6 F, ZnS(Ag) mixture, commercially available for neutron radiographic use from Nuclear Enterprises, Ltd. (Type NE 421)]. Television images with this system could be observed for neutron intensities as low as 4 x 10^6 n/cm^2-sec.

A comparison of this threshold level for the scintillator and the threshold value for the neutron image intensifier would indicate that the neutron image intensifier was providing a brightness gain of 2 x 10^4. This figure is reasonably in line with brightness gains available from X-ray image intensifier tubes.

4. Engineering Properties of Reactor Materials

a. Thermal Properties of U-15 w/o Pu-10 w/o Zr Alloy. The heat content of U-15 w/o Pu-10 w/o Zr alloy was measured to support reactor kinetics calculations. The heat content increases monotonically from about 10 cal/g at 300°C to about 55 cal/g at 1150°C as shown in Fig. 15. The heat content of uranium up to its melting point is below that of the alloy by an average of 2 cal/g. The solid-state heats of transformation of the alloy and the total ($\alpha \rightarrow \beta$ and $\beta \rightarrow \gamma$) heats of transformation for uranium are nearly equal, 8 cal/g compared to 7.9 cal/g for the uranium solid-state transformations.

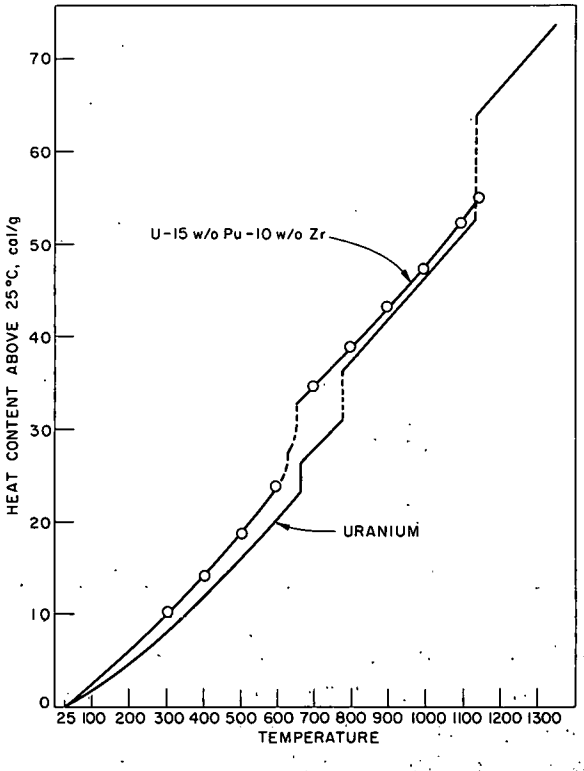

Fig. 15. Heat Content above 25°C of U-15 w/o Pu-10 w/o Zr Alloy

Parabolic equations representing the data were derived for the regions outside the transformations. The equations were differentiated to obtain equations representing the specific heat C_p. The observed heat content and calculated heat content and specific heat for indicated temperatures are shown in Table XVI.

The equations and their temperatures of validity are:

$$\Delta H_{25}(25\text{-}600°C) = -0.9 + 0.0310T + 0.0000155T^2 \text{ cal/g};$$
$$(650\text{-}1150°C) = 14.2 + 0.0185T + 0.0000152T^2 \text{ cal/g};$$
$$C_p(25\text{-}600°C) = 0.0310 + 0.000310T \text{ cal/g/°C};$$
$$(650\text{-}1150°C) = 0.0185 + 0.000304T \text{ cal/g/°C}.$$

The maximum deviation between the observed and calculated heat content values is substantially less than 1%.

TABLE XVI. Thermal Properties of U-15 w/o Pu-10 w/o Zr

Temp (°C)	ΔH_{25}(cal/g) Calc	ΔH_{25}(cal/g) Obs	C_p(cal/g/°C) Calc
25	-0.1		0.031
100	2.4		0.034
200	5.9		0.037
300	9.8		0.040
306.5		10.2	
400	13.9		0.043
402.4		14.1	
500	18.3		0.047
505.3		18.7	
599.6		23.9	
600	23.3		0.050
650	32.6		0.038
696.1		34.7	
700	34.7		0.040
798.1		38.9	
800	38.7		0.043
897.0		43.3	
900	43.2		0.046
997.0		47.4	
1000	47.9		0.049
1097.0		52.4	
1100	53.0		0.052
1140.3		55.1	
1150	55.6		0.054

The transformation in the U-15 w/o Pu-10 w/o Zr alloy proceeds essentially to completion during the rapid cooling rate attained by the specimen in the drop calorimeter. The cooling rate is estimated at about 100°C/min through the transformation range, 597 to 660°C. Unsteady-state

measurements of the transformations are available. The differential thermal analysis results of both uranium and the alloy against thorium were analyzed and the latent heat of transformations of the alloy determined. The 8.5-cal/g value found by this method agrees within the error limits with the 8 cal/g found by drop calorimetry.

b. Creep Behavior of Type 318 Stainless Steel at 650°C. The creep behavior of columbium (niobium)-stabilized Type 318 stainless steel[20] was determined in vacuum at 650°C for stress levels of 15, 20, and 30 kg-mm^{-2}. The rod tensile specimens were machined from 2.54 cm OD by 3.2-mm-wall tubing in the as-received condition and after exposure to steam at 0.42 kg-mm^{-2} pressure and 650°C for 350 days. The as-received tubing conformed to ASTM Specification A-269 for unfired pressure vessels with regard to heat treatment and surface finish. The strain-versus-time curves for this material before and after exposure to steam are given in Fig. 16A, B, and C. Specimens in the as-received condition ruptured at the indicated strains whereas creep tests on the exposed specimens are continuing. The indicated increase in ductility and decrease in creep strength after exposure are attributed to decarburization by the steam. The creep behavior of Type 318 stainless steel at 650°C and 15 kg-mm^{-2} stress is compared with that of Type 316 stainless steel in Fig. 15D.[21] The variation of the minimum strain rate with stress for the as-received and exposed Type 318 stainless steel is shown in Fig. 17.

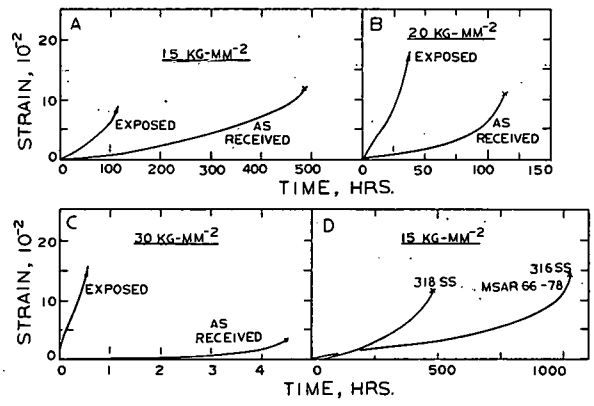

Fig. 16

Creep of Type 318 Stainless Steel at 650°C and Indicated Stress Level. (A, B, and C)--comparison of creep before and after exposure to steam at 0.42 kg-mm^2 pressure and 650°C for 350 days. (D)--comparison of Type 318 and 316 in creep at 650°C and 15 kg-mm^2 stress.

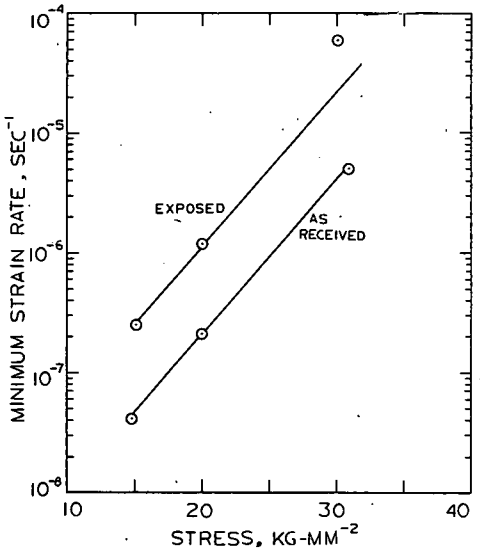

Fig. 17

Semilogarthmic Plot of Minimum Strain Rate vs. Stress for Type 318 Stainless Steel Tested at 650°C before and after Exposure to Steam at 0.42 kg-mm^{-2} Pressure and 650°C for 350 days.

[20]Type 318 stainless steel is similar to Type 316 stainless steel plus a niobium content equal to nine times the carbon content.

[21]Effect of High Temperature Sodium on Austenitic and Ferritic Steels, MSA Report 66-78 (May 1966).

5. Chemistry of Fuel Materials

a. Container Materials for Plutonia Systems. A comprehensive program is now under way to determine high-temperature thermodynamic properties of the condensed plutonium-oxygen and plutonium-uranium-oxygen systems. This work will be carried out by mass-spectrometric and transpiration techniques, and will be supported by a study of selected areas of the phase diagrams of these systems.

The question of what container or crucible material to use is of primary importance because of its possible influence on the equilibria being examined. Refractory metals were considered to be the leading candidate materials for the plutonia studies. Previous work with the uranium-oxygen system demonstrated that refractory metals possess desirable properties for the high-temperature work contemplated. For example, temperature gradients are minimized, the conductivity of metals enables direct heating of crucibles by induction and by electron bombardment (as in our mass spectrometer), and fabrication of parts is facilitated (such as condenser tubes for transpiration experiments). Estimates of the stability to oxidation of the refractory metals rhenium, tungsten, tantalum, and molybdenum indicated that the two higher melting metals, rhenium and tungsten, would be the most satisfactory. The fragmentary thermodynamic data available also indicated that tungsten, which was used quite successfully in the urania studies, might be less suitable than rhenium: the considerably higher oxygen pressures expected over plutonia-containing systems could cause oxidation of the tungsten to volatile oxides, accompanied by reduction of the plutonia. Some simple experiments were made to determine the relative stabilities of rhenium and tungsten.

b. Relative Stabilities of Rhenium and Tungsten to Oxidation. Urania of composition $UO_{2.095}$ (the use of hyperstoichiometric urania simulates the oxygen pressures that could prevail if plutonia were present) was heated in a Bendix TOF mass spectrometer to about 1800°C under three sets of conditions:

(i) tungsten effusion cell containing mixed $UO_{2.095}$ and rhenium powders;

(ii) rhenium effusion cell containing mixed $UO_{2.095}$ and tungsten powders;

(iii) rhenium effusion cell containing $UO_{2.095}$ powder.

In experiments (i) and (ii), only tungsten-containing vapor species were observed, which signifies the greater stability of rhenium to oxidation. Beginning at 1150°C, the effusing species were those normally found[22,23]

[22] Ackermann, R. J., and Rauh, E. G., J. Phys. Chem. 67, 2596 (1963).

[23] Battles, J. E., Technical Documentary Report No. ML-TDR-64-272 (Aug 1964).

during vaporization of solid WO_2 and WO_3, namely, the parent vapor species $W_2O_6^+$, $W_3O_9^+$, and $W_4O_{12}^+$, and their associated fragments. In experiment (iii) the effusing species, beginning at 980°C, were ReO_2^+, ReO_3^+, $Re_2O_5^+$, $Re_2O_6^+$, and $Re_2O_7^+$.

The results of experiment (iii) indicate that even rhenium crucibles will probably react with plutonia-containing phases to form volatile rhenium oxides. Hence, quantitative information concerning the equilibria among rhenium oxide species becomes relevant in order to know whether the extent of the reaction is tolerable. However, such information is virtually nonexistent. This has prompted a limited study of vapor equilibria in the rhenium-oxygen system while the equipment for the plutonia studies is being constructed and assembled. Accordingly, the vaporization of rhenium dioxide (ReO_2), which gives rise to numerous oxide species, is being examined mass spectrometrically. The results obtained thus far are discussed below.

c. Vapor Species over ReO_2. Rhenium dioxide was heated to about 850°C in a platinum effusion cell in the Bendix TOF mass spectrometer. The effusing species that were observed for an ionizing electron energy of 25 eV were ReO_2^+, ReO_3^+, $Re_2O_5^+$, $Re_2O_6^+$, and $Re_2O_7^+$. The appearance potentials for these ions, corrected on the basis of the value 12.83 eV[24] for the appearance potential of H_2O^+, are listed in Table XVII. For an ionizing electron energy of 17 eV, the only species observed were $Re_2O_7^+$, ReO_3^+, and $Re_2O_6^+$, with relative ion intensities of 90:10:1. At the conclusion of the experiment, X-ray diffraction analysis showed the solid residue in the crucible to be mainly rhenium metal. This result, together with the observation that the vapor phase was predominantly Re_2O_7, strongly suggests that at 850°C the reaction proceeds mainly according to the equation

$$7\ ReO_2(c) \rightarrow 2\ Re_2O_7(g) + 3\ Re(c).$$

TABLE XVII. Approximate Appearance Potentials of Species Vaporizing from Solid ReO_2 at 850°C

	eV(a)		eV(a)
$Re_2O_7^+$	13.1	ReO_3^+	15.6
$Re_2O_6^+$	16.3	ReO_2^+	~19
$Re_2O_5^+$	~20		

(a)A correction of -1.0 eV has been applied to the observed appearance potentials.

[24]Field, F. H., and Franklin, J. L., Electron Impact Phenomena, Academic Press, Inc., New York (1957).

C. Engineering Development

1. Heat Transfer, Fluid Flow, and Mechanics of Materials

a. Boiling Liquid Metal Technology

(i) Niobium-1% Zirconium Loop. The loop sodium has been dumped and a number of modifications to the loop and vacuum chamber are underway, in preparation for operation at higher temperature.

(ii) Electron-bombardment Heater Experiment. This experiment is designed to gain experience with electron-bombardment heating and to investigate mechanical and geometric factors involved in the construction of a high heat flux heater. The present design incorporates a sodium pool boiler with a sixteen inch heated length. Although the information obtained from this experiment is being used primarily in the design of a high temperature, high heat flux electron-bombardment heater, basic information pertinent to the pool boiling of sodium, from a vertical cylinder may also be gleaned.

Approximately 500 hr of testing with the 0.030-in.-dia uncarburized thoriated-tungsten filament have been achieved. Heat fluxes ranging up to 350,000 Btu/hr-ft^2 have been supplied to the anode during both steady state and transient testing with peak sodium temperatures to 1500°F. This includes an emission current range to 5.2 A and a cathode to anode voltage of 7700 V.

Present testing utilizes a 0.030-in.-dia tungsten filament. Approximately 150 hr of testing with the tungsten filament have been achieved with heat fluxes ranging up to 300,000 Btu/hr-ft^2. This experiment is approaching limiting design conditions and will be modified to provide higher heat fluxes for short periods of time. These tests and an evaluation of the EBH study by Eimac Corporation will provide the basis of the final EBH design for use in the 2100°F Nb-1% Zr loop.

b. General Heat Transfer

(i) Heat Transfer in Double-pipe Heat Exchangers

(α) Countercurrent Turbulent Liquid-metal Flow. Experimentation continued with the first mercury-to-mercury concentric tube heat exchanger. Experiments with constant flowrates (see Progress Report for August 1966, ANL-7249, p. 56) revealed a dependence of overall heat transfer coefficient and heat exchanger efficiency on inlet temperature difference. This dependence indicates that certain idealities upon which the analysis is based, such as negligible axial conduction and thermal convection, were not satisfied in the test apparatus. The present experiments are designed to determine the cause of the dependence on inlet temperature difference.

Additional experiments were performed at higher flowrates than before, but overall heat transfer coefficients and heat exchanger efficiencies were still dependent on inlet temperature differences. Since the flowrates were high enough to prevent significant thermal convection and axial conduction within the fluid, these non-idealities have been eliminated as likely causes. A sample of the data obtained is shown in Table XVIII. Fully developed overall heat transfer coefficients are shown as Nusselt numbers based on tube-side properties. Note that both Nusselt number and efficiency increase with increasing inlet temperature difference, which suggests an unaccounted-for mechanism in heat exchange between the fluids.

TABLE XVIII. Typical Counter-flow Heat Exchanger Experimental Results Showing Dependencies on Inlet Temperature Difference, ΔT

Run No.	Pe_1	Pe_2	ΔT	H	Nu_1^0	ϵ
41	310	202	15.4	2.73	2.34	0.749
49	303	200	48.9	2.73	4.30	0.771
56	284	198	102.7	2.85	5.59	0.811
35	1267	105	9.1	0.348	4.14	0.660
25	1266	103	12.1	0.343	4.61	0.668
26	1237	104	30.2	0.353	5.40	0.699
27	1194	101	59.1	0.350	6.15	0.733
62	1242	302	26.6	1.01	4.64	0.364
66	1170	292	68.2	1.02	6.27	0.386
73	1119	286	94.8	1.03	7.12	0.397

Pe_1 -- Peclet number in tube

Pe_2 -- Peclet number in annulus

ΔT -- Inlet temperature difference

H -- Flowrate ratio (Annulus Flowrate/Tube Flowrate)

Nu_1^0 -- Fully developed overall Nusselt number based on tube side

ϵ -- Heat exchanger efficiency

A second test section has been designed and is being fabricated. The primary consideration in the design of this test section is to limit further the possibility of extraneous heat transfer between the fluids at the ends of the heat exchanger.

(β) Cocurrent Laminar Flow. A paper describing the solution of the cocurrent laminar-flow, double-pipe heat exchanger problem by Hybrid Computer has been prepared.[25]

[25]Bryant, L. T., Amiot, L. W., and Stein, R. P., A Hybrid Computer Solution of the Co-Current Flow Heat Exchanger Sturm-Liouville Problem, AFIPS Conference Proceedings, 1966 Fall Joint Computer Conference, San Francisco, Nov. 1966 (In Press).

(γ) Nonsymmetrical Geometries. The double-pipe heat exchangers considered to date have had mathematically simple symmetrical duct shapes such that only two orthogonal space coordinates, one of which denotes axial distance, are required for detailed analyses. The concentric tube exchanger is the most familiar example. The important shell-and-tube configuration does not have mathematically symmetrical duct shapes in the sense just described. As a result, detailed analyses are much more difficult. There are indications, however, that when the spacing between tubes in a shell-and-tube configuration is sufficiently large, analyses can be based on a simple concentric tube model.[26] With this simplification, all previous analyses can be made applicable to unbaffled single-pass shell-and-tube heat exchangers.

An attempt was made during this past month to design an experiment using sodium to test this extension of the double-pipe heat exchanger research. It was found that, for spacings sufficiently large to justify the use of the symmetrical duct model and also of interest to current fast reactor heat exchanger designs, the predictions of traditional methods of analysis and the new methods developed at Argonne gave about the same results. Experiments with more "tightly packed" tube bundles and with eccentric annuli are also being designed. The latter is of fundamental interest since current ideas suggest that overall heat transfer rates in liquid metal, concentric tube heat exchangers would be significantly reduced if the annular space were eccentric. There do not appear to be any liquid-metal heat exchanger experiments reported in the readily available literature which study the effect of eccentricity on overall heat transfer rates.

(ii) Heat Transfer in Liquid-metal-cooled Reactor Channels. Investigations of the effect of axial heat conduction within the liquid metal in heated channels continued. The case of a heated parallel-plane channel with long unheated inlet and outlet ducts of the same shape and size was further explored (see Progress Report for June 1966, ANL-7230, p. 42). The influence of nonuniform heat-flux distributions was studied by considering flux distributions represented by

$$q(y)/q_{av} = A\, e^{By} \sin \pi y,$$

where

$y = \ell/L$;

ℓ = channel position measured from inlet of heated section;

L = length of heated section;

$A = (B^2 + \pi^2)/[\pi(1 + e^B)]$;

[26] Dwyer, O. E., and Tu, P. S., Chem. Eng. Prog. Symp. Ser., 56, 183 (1960).

$B = -\pi \cot \pi y_m$;

y_m = position of maximum flux $(0 < y_m < 1)$.

For $y_m = 0.5$, $B = 0$, and $A = \pi/2$, the above represents the simple "unchopped" cosine distribution. For other values of y_m, the ratio of maximum to average flux is given by

$$q_{max}/q_{av} = (B^2+\pi^2)^{1/2} \; e^{By_m}/(1+e^B).$$

Investigations of this equation have indicated that axial conduction within the liquid metal can be neglected except for combinations of the following conditions: (1) Peclet numbers less than 10, (2) very small channel lengths, and (3) flux distributions for which y_m is near the duct inlet or outlet.

Further studies of the uniform flux case were carried out by students of the 1966 AMU-ANL Summer Engineering Practice School. A report is in preparation.

D. Chemistry and Chemical Separations

1. Fluoride Volatility Processes

a. Recovery of Uranium and Plutonium from Low-enrichment Fuels: Laboratory Support Work

(i) Fluorination of UO_2-PuO_2-Fission Product Pellets. Development studies are being performed in a 2-in.-dia fluid-bed reactor to determine optimum conditions for fluorinating UO_2-PuO_2 pellets containing fission products. Previous work has shown that uranium and plutonium can be fluorinated from an alumina fluid bed containing fission products, including cesium, by a process based on the selective volatilization of uranium as UF_6 by reaction with BrF_5, followed by the volatilization of plutonium as PuF_6 with fluorine (see Progress Report for July 1966, ANL-7245, pp. 45-46).

A recent experiment (Purse-9) was performed to determine the behavior of neptunium, as well as uranium and plutonium, during reaction with bromine pentafluoride and the subsequent recycle-fluorination with fluorine. Results of laboratory-scale experiments (see Progress Report for July 1966, ANL-7245, p. 46) have shown that NpF_4 is converted to volatile NpF_6 by reaction with BrF_5 at 300 to 450°C. In Purse-9, 650 g UO_2-PuO_2-fission product pellets, 0.6 g CsF, and 0.15 g RbF were added to 1100 g of refractory alumina particles to form a fluidized-packed bed. The CsF and RbF were added to the alumina bed to simulate more closely

the fission product distribution expected from irradiated fuel. In addition, 0.52 g NpO_2 was added to the alumina bed; this quantity was governed by the ability to analyze low concentrations of neptunium in alumina bed samples. The oxide pellets were oxidized for 4 hr at 450°C using 20 v/o oxygen in nitrogen to produce a powdered mixture of U_3O_8 and PuO_2. Fluorination of the powdered oxides with BrF_5 was carried out for 2.1 hr at 300°C with 9 v/o BrF_5 in nitrogen. This step was followed by recycle-fluorination with 90 v/o fluorine for 3 hr at 300°C, 5 hr while the temperature of the reactor was increased from 300 to 550°C at 10°C/12 min, and 3 hr at 550°C.

The addition of RbF and CsF to the fluid bed did not affect the fluorination of uranium and plutonium from the alumina bed. The final bed contained 0.003 w/o uranium and 0.005 w/o plutonium, indicating a removal of more than 99.9% of the uranium and 98% of the plutonium from the bed.

The concentration of neptunium in the fluid bed increased during the first hour of fluorination with BrF_5 owing to the rapid depletion of U_3O_8 by reaction to form UF_6. At the end of the BrF_5 step, 0.2 g of NpO_2 remained in the bed, indicating that approximately one-half of the neptunium had volatilized. The final alumina bed after recycle-fluorination with fluorine contained about 0.002 w/o neptunium corresponding to the removal during both fluorination steps of 95% of the neptunium charged to the system. These results indicate that neptunium can be volatilized by fluoride-volatility techniques and that the product appears in both the UF_6 and PuF_6 streams. Work is planned to derive a method whereby neptunium will qunatitatively accompany the UF_6 stream for subsequent separation.

(ii) Corrosion of Materials. The uranium hexafluoride produced by fluoride-volatility techniques may be purified by fractional distillation. To assure high recovery of uranium during distillation, it may be necessary that a high-boiling liquid such as SbF_5 be added to or accumulated in the still. An experiment was performed to measure the rates of corrosion of nickel-200, Monel, and Duranickel-301 coupons in equimolar solutions of UF_6 and SbF_5 at 105°C. Samples of the test metals were exposed to liquid, vapor, and the liquid-vapor interface. No intergranular corrosion was observed in any sample. The rate of corrosion of all coupons in any of the test environments was not greater than 0.006 mil/hr, and it appears that the three alloys would be satisfactory candidates for materials of construction.

b. Recovery of Uranium and Plutonium from Low-enrichment Fuels: Engineering Work

(i) Process Development Studies for Uranium Dioxide Fuels. Previous work to establish processing conditions for the fluorination of UO_2 fuel with BrF_5 has been carried out in a $1\frac{1}{2}$-in.-dia fluid-bed reactor

(see Progress Reports for May 1966, ANL-7219, p. 52 and for December 1965, ANL-7132, p. 47). Engineering-scale studies are under way in a 3-in.-dia fluid-bed reactor. A single experiment (run BRF5-2) was performed to determine (1) the feasibility of fluorinating a deep bed of U_3O_8 fines produced by oxidation of fragmented UO_2 pellets, (2) the rate of UF_6 production throughout the fluorination step, and (3) the utilization efficiency of the BrF_5. In this experiment, 4.4 kg of fragmented UO_2 pellets (-0.5 +0.132 in. particles) and 5.8 kg of prefluorinated -100 mesh sintered alumina were charged to the fluid-bed reactor. Approximately 3.7 kg of +8 mesh sintered alumina was used as a support bed for the oxide fuel. The UO_2 was oxidized to U_3O_8 powder by passing a gas stream containing 20 v/o oxygen in nitrogen at a velocity of 1.5 ft/sec through the bed at 450°C for 11 hr. The U_3O_8 fines were fluorinated to UF_6 by reaction with 12 v/o BrF_5 in nitrogen for 3 hr at 250 to 275°C. The fluidizing gas velocity during fluorination was 0.8 ft/sec. No external heat was supplied to the reactor during fluorination and the reactor was cooled by natural convection. The total qunatity of BrF_5 fed to the reactor was 1.7 times the stoichiometric amount to convert all the uranium to UF_6 (5.9 kg).

Oxidation of the UO_2 charge proceeded without difficulty and resulted in the formation of a 4.5-ft deep bed of U_3O_8 fines and alumina. All equipment operated satisfactorily throughout the fluorination step. No temperature excursions occurred during fluorination.

The average rate of UF_6 production was 86 lb UF_6/(hr)(sq ft reactor cross section). Since the bulk of the uranium was fluorinated during the first two hours, rates approaching 130 lb UF_6/(hr)(sq ft reactor cross section) were probably achieved in that period. This value of UF_6 production rate is significantly higher than that achieved by the two-zone oxidation-fluorination of UO_2-PuO_2 pellets (66 lb UF_6/(hr)(sq ft): see Progress Report for November 1965, ANL-7122, pp. 63-65) and by the fluorination of U_3O_8 with fluorine (88 lb UF_6/(hr)(sq ft): see Progress Report for March 1966, ANL-7193, pp. 76-77). Since high temperatures must be avoided during the fluorination of uranium compounds to assure the absence of bed caking, the rate of UF_6 production is primarily limited by the rate of heat removal from the reaction zone; this problem is more pronounced in systems involving the use of fluorine gas as the fluorinating agent.

The utilization of BrF_5 during the initial period of fluorination was also probably higher than the average utilization of approximately 60% sustained over the 3 hr of fluorination.

More accurate data on the rate of UF_6 production and BrF_5 utilization will be presented when chemical analyses of bed samples taken throughout the course of the fluorination are completed.

(ii) Fluid-bed Studies with Irradiated Fuels. A series of experiments are under way in a $1\frac{1}{2}$-in.-dia fluid-bed reactor to determine the distribution of fission products during the processing of highly irradiated UO_2 by the oxygen-bromine pentafluoride-fluorine process. The primary objective of these experiments is to determine the contaminants in the PuF_6 product, so that decontamination schemes can be developed. An experiment (BRF-1) has been completed using a 108-g charge of irradiated UO_2 (30,000 MWd/ton, 1-year cooled, declad). The processing sequence consisted of fuel oxidation at 450°C, uranium volatilization with BrF_5 at 300°C, and plutonium volatilization with fluorine at 300 to 550°C. Although complete analytical results are not available, some observations regarding this run can be made. Krypton-85 was released during oxidation of the fuel and fluorination of uranium by BrF_5. None was released during fluorination of plutonium with fluorine. About 27% of the krypton was released in the oxidation step, and the remainder in the BrF_5 step. The preponderant gamma-active isotope present with the uranium product was ruthenium-106, while both ruthenium-106 and niobium-95 were present in the plutonium product.

IV. ADVANCED SYSTEMS RESEARCH AND DEVELOPMENT

A. Other Direct Conversion

1. Liquid-metal Liquid Generator

a. Effects of Interfacial Transport Processes on Film Condensation. Machining of a test section for the air-water studies is complete. Instrumentation is being installed in the test section and piping of the air-water loop begun. The first data will be taken during the next month. Also, analysis of the physical processes using integral techniques is continuing.

b. Condensing Injector. During the past several months, repeated attempts to operate the condensing injector with the Freon loop were unsuccessful. In addition to many equipment malfunctions, the basic problem seemed to be a choking phenomena indicating lack of sufficient condensation of the high-speed vapor. Because of the thermodynamic properties of Freon 11, the final state after expansion of saturated vapor to some low pressure is likely to be in the superheat region. This could seriously lower the condensation which occurs in the mixing section of the injector. A modification of the test setup allowed the use of local plant steam and top water in a once-through system. Injector startup was immediately possible with steam and water, and a back pressure greater than the upstream pressure of either fluid was readily obtained. A complete set of runs will be made with the steam-water system and trends in the data will be indicated in the next reporting period.

B. Argonne Advanced Research Reactor (AARR)

1. General Design

The final project review of the Title I report has been completed.

A preliminary meeting was held between AARR project and AEC-DRL personnel to review comments and questions on the preliminary safety analysis report (PSAR). A supplement to the PSAR is being prepared to answer the questions and to update the design description portion of the report.

2. Mark-I Core Development

a. Heat Transfer

(i) Calculations of Static Pressure Loading. Preliminary calculations have been made to determine static pressure loadings between nominal and off-nominal channels in the AARR core. The first set of calculations have been completed with the following assumptions:

(a) A constant off-nominal channel spacing exists along the entire length, thus changing the pressure drop versus flow characteristic.

(b) The relative number of off-nominal compared with nominal channels (0.040 in.) is very small, so that core pressure drop versus flow is controlled by nominal channels.

(c) The leading edges of fuel plates are either square or well-rounded.

A second set of calculations has been started in which the assumptions are identical to the above except for (a). Instead, a given off-nominal channel spacing exists only locally (over a small region) so as not to affect the off-nominal channel pressure drop versus flow characteristic.

Results to date show that local static pressure drops across channels can easily exceed 50 psi with square leading edges under certain conditions. These maxima can be reduced by a factor of 2 by rounding the channel inlets. In the first set of calculations it was also found that the higher pressure (in the two nominal channels) is always found in the narrow channel. Thus, this type of off-nominal channel can be construed to be self-correcting due to pressure difference alone, i.e., a wide channel tends to get narrower, etc.

In the second set of calculations, the higher pressure in two adjacent channels is found, instead, in the wide channel. In this case the off-nominal channel is definitely not self-correcting, and an off-nominal spacing tends to be self-propagating. It also appears that the second off-nominal channel would be closer to the type of abnormal geometry expected in practice, i.e., bulging, ripples, etc.

(ii) Calculations of Flow Coastdown. Preliminary results have been obtained on flow versus time following a two-pump tripout in AARR. The calculations involved estimates of the system pressure drop versus flow characteristic, water inertia of the loop, rotary shaft inertia (pump plus motor), and operating characteristics of the pump. The primary-system piping layout chosen for calculational purposes corresponded to the Burns and Roe piping layouts of 5/19/66 for Title I, and the pump(s) analyzed was Byron-Jackson Centrifugal, 20 x 20 x 21-DVS, with an operating speed, flow, and head of 1780 rpm, 1500 gpm, and 380 ft, respectively.

An isometric drawing of the AARR primary system layout has been completed showing, to scale, the relative locations of reactor vessel, primary piping, heat exchangers, and primary pumps.

It was found that the dominating parameter affecting flow response to tripout is the rotary shaft inertia, in spite of the long mean path length of the primary loop. The pump half-time was found to be 2.3 sec, while the loop (water) half-time was found to be only 0.45 sec. This means that the water inertia is relatively unimportant and that flow-rate after pump (motor) tripout depends essentially upon pump speed alone. Figure 18 shows flow response for two cases of two-pump tripout without a pony motor:

(1) no flywheel, total shaft inertia = 1900 lb_m-ft^2;

(2) relatively small flywheel, total inertia = 3000 lb_m-ft^2.

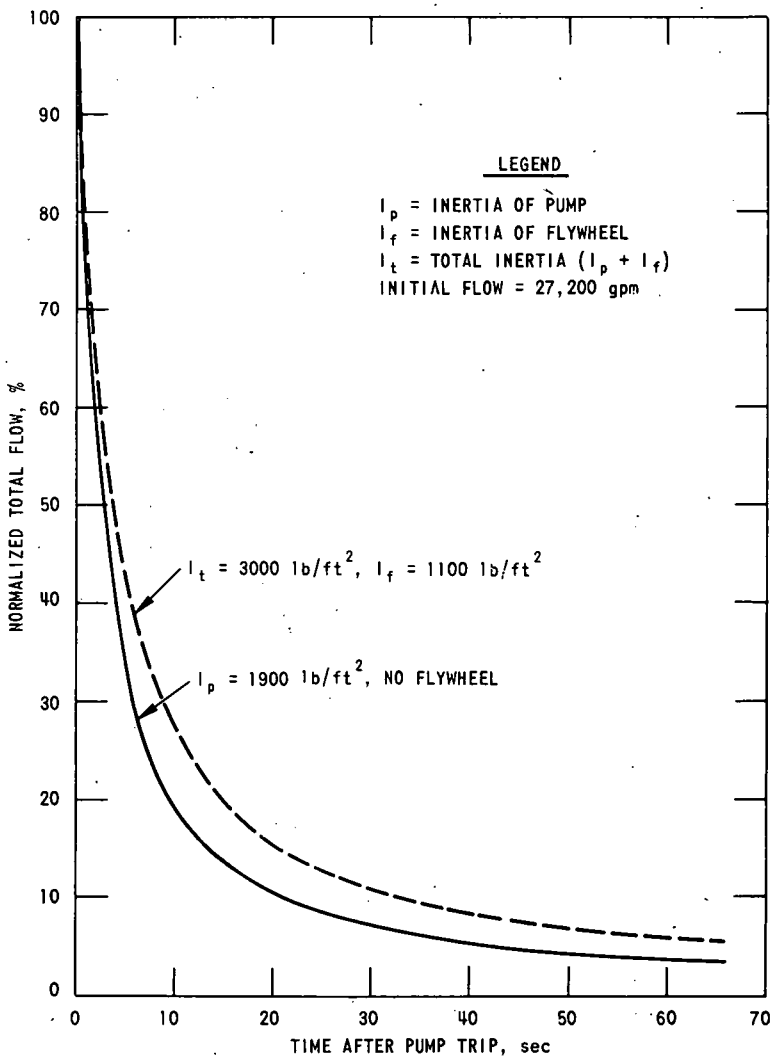

Fig. 18. AARR Flow Coastdown for Two-pump Tripout; No Pony Motor

As indicated in Fig. 18, without flywheel, the flowrate is down to 50% of initial value in 2.3 sec and to 25% flow in 7.0 sec. With a flywheel (e.g., made of steel, having diameter of about 2.2 ft and a length of 1 ft) the flowrate is down to 50% in 3.8 sec and to 25% in 11.3 sec.

(iii) Steady-state Tests. In the steady-state heat transfer program the effects of channel spacing, flow, inlet water temperature, pressure and power upon pressure differential along the channel, void distribution, and critical heat flux are measured with electrically heated, rectangular test sections that simulate the flat-plate geometrical arrangement of the AARR core.

Tests on the section with a 0.050-in.-wide coolant channel are in progress. Test results in Fig. 19 show variation of total pressure drop across the section as a function of flowrate for a number of power settings. These tests were run with a large pressure drop across an upstream valve between the accumulator and the test-section inlet; thus the flowrate was essentially independent of the pressure drop.

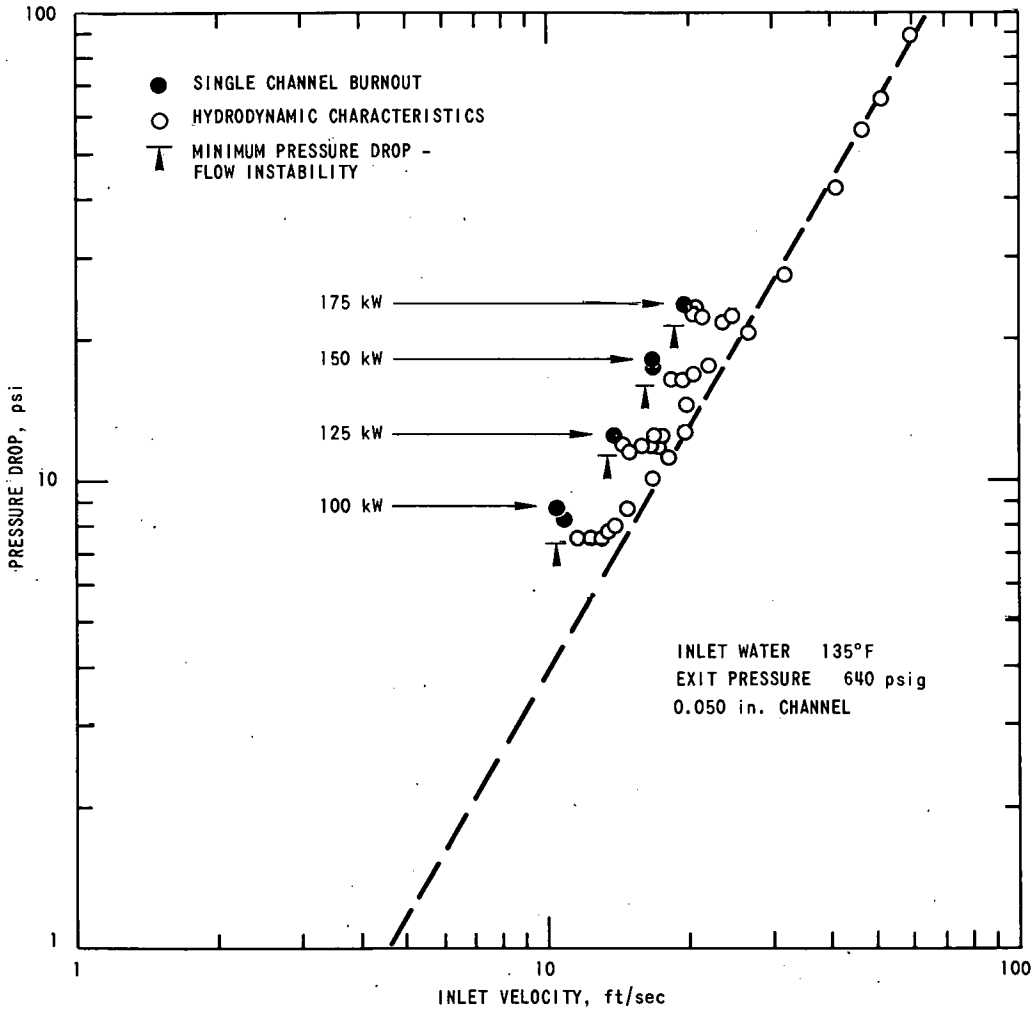

Fig. 19. Pressure Drop-Velocity Characteristics for Various Power Levels in a 0.050-in. AARR Test Section

In a system with alternate flow paths in parallel with the test section, the flowrate will be determined by the available pressure drop

across the section. If the alternate parallel flow path is of much larger cross-sectional area than the test section, the pressure drop is primarily determined by the flow characteristics of the parallel path. Test results shown in Fig. 19 indicate where such a parallel system should lose flow and overheat.

Figure 20 shows a cross plot of the data with power versus minimum pressure drop. This curve should indicate the maximum safe power in a parallel-flow system operating with the pressure drop shown on the abscissa.

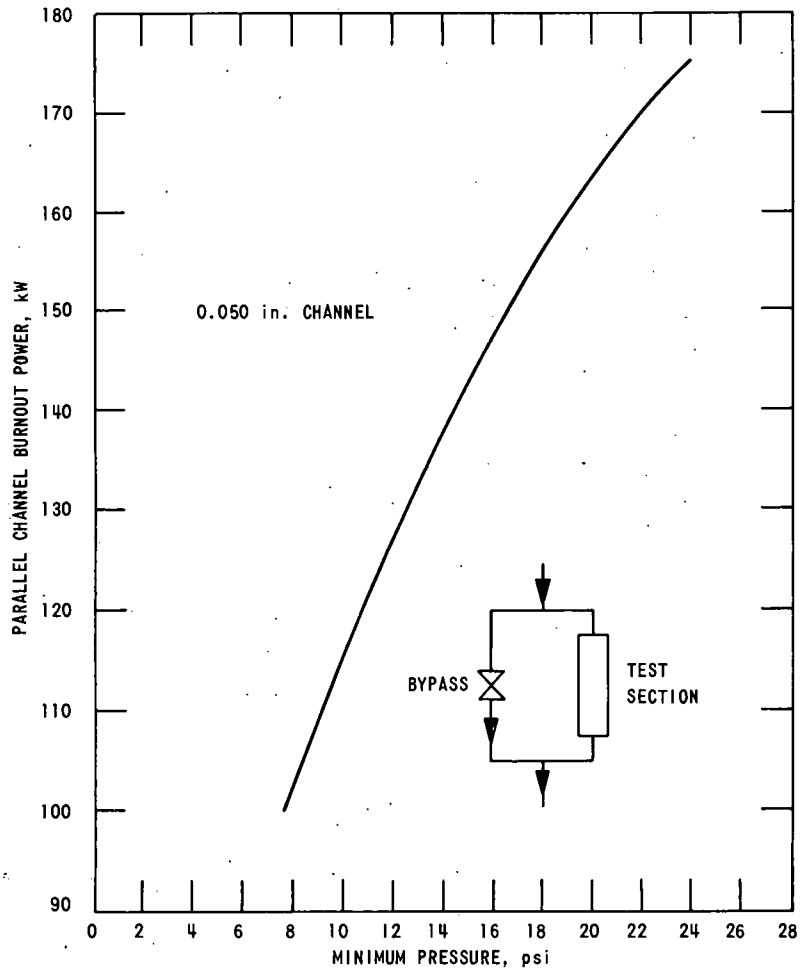

Fig. 20. Estimated Conditions of Flow Instability

Tests are currently being performed with a large parallel-bypass channel. The information from these parallel tests will furnish check points of the predictions for maximum power shown in Fig. 20.

A test-section power level of 100 kW is equivalent to an average heat flux of about 1.4×10^6 B/hr-ft^2. There is an axial heat flux increase above the average heat flux at the hot spot of the test section and therefore higher local heat fluxes exist. The data have not been analyzed in detail to list this variation.

(iv) Transient Tests. The transient heat-transfer tests will evaluate the effect of short-term power transients upon heat transfer, fluid flow, and critical heat flux. Procurement and assembly of the void-measuring package continue.

A one-dimensional perturbation analysis of the effect of wall movement on the flow of a nonviscid compressible fluid through a duct of almost constant area was programmed for the CDC-3600. Results of this very simplified model showed a maximum fractional pressure increase of less than 3% for a power jump of 5/1 from 100 MW. This would correspond to ~20 psi. However, the simplifications underlying this model are not necessarily conservative. A more realistic analysis is currently under study.

(v) Shutdown-emergency Cooling Tests. Fabrication and construction of the Inclined-single-channel Natural Convection Test Loop have been completed. This loop is intended to provide heat-transfer data for assessing the safety of spent cores. Natural convection in the vertical direction and between vertical and horizontal will be studied. Instrumentation of the loop still remains to be completed.

The test loop is shown in Fig. 21. The 0.040 x $1\frac{1}{8}$-in. rectangular channel has a heated length of 18 in. and can be rotated to any desired angle between horizontal and vertical. Loop construction limits pressure to near atmospheric. Available a.c. power will supply heat fluxes up to 125,000 B/hr-ft^2, well above expected requirements.

Measurements of test variables will include power, inlet and outlet water temperatures, twelve outside surface temperatures along both sides of the heated channel, and pressure fluctuations occurring in the channel.

b. Fuel Stress and Hydraulics

(i) Thermally Induced Deflections of Fuel Plates. Among the many mechanisms for fuel-plate deflection leading to channel closure, the case of a flat, thin plate subjected to a uniform temperature change while restrained along the longitudinal boundaries was considered. Since knowledge of the temperature distribution is not necessary at this stage, an energy analysis was used and curves plotted to describe the lateral deformation for various uniform temperature increases in the plate only. The analysis was made with and without a center spacer wire attached to the plate. This is one of the first steps in a more complete dynamic analysis in which a kinetic energy term will be included in the effort to describe plate deformation and stability under combined thermal and hydraulic loading.

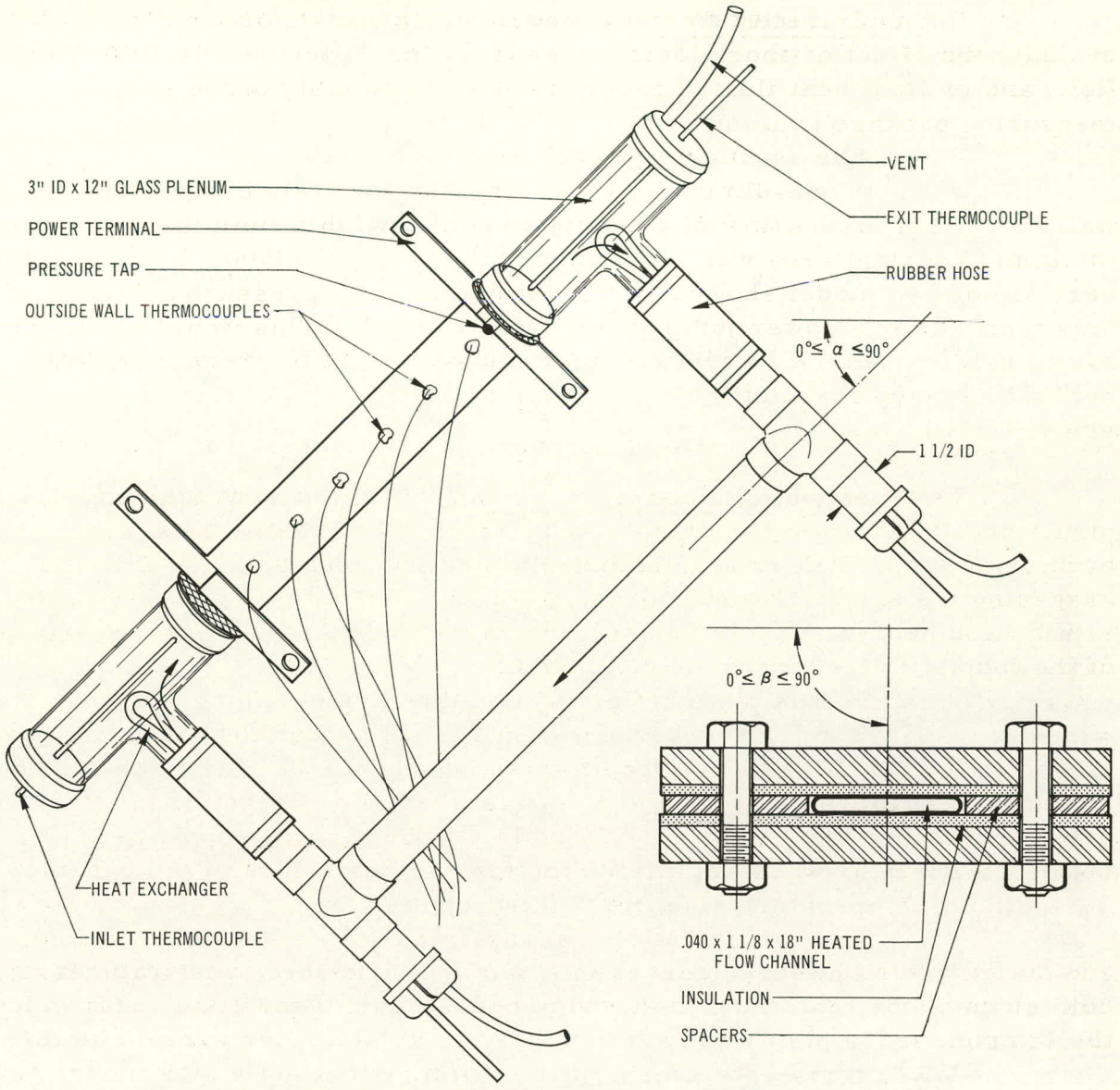

Fig. 21. AARR Inclined-channel Pool-boiling Apparatus

The energy approach used is based on that of Williams.[28] The potential-energy contributions stem from a) middle surface membrane strain energy, b) bending strain energy, and c) the energy contributions from deformation under thermal strain. The differential equations describing the problem are then obtained from equating the first variations of the total energy function to zero. There are two equations that describe the in-plane displacement v and the normal displacement w. The outcome of integrating one of these equations once and substituting the results into the other equation conveniently decouples the equations as well as effectively

[28] Williams, M. L., Large Deflection Analysis for a Plate Strip Subjected to Normal Pressure and Heating, J. Appl. Mech. 77, 458-464 (1955).

removing the nonlinearity so that a linear fourth-order differential equation for the normal deflection w occurs, which is the deflection function being sought.

The assumed physical conditions are:

a) The fuel plates are infinitely long.

b) There is no differential pressure loading on the plate faces.

c) The edges $y = \pm b/2$ are clamped, where b is plate width.

d) The material properties are temperature-independent.

e) The temperature is uniform throughout the entire plate.

If the dimensionless plate deflection is

$$\bar{w} = w(\eta)/b,$$

where $w(\eta)$ is the true plate deflection and the variable along the plate width is

$$\eta = y/(b/2),$$

then the deflection $\bar{w}$ can be calculated for various values of the parameter T_0 (uniform temperature rise) for a fixed ratio of b/η.

The three curves (see Fig. 22) at higher temperatures exhibit the antisymmetrical deflection modes for half the plate width which would occur if the plates are supported by an axial spacer wire. The three curves at lower temperature exhibit the symmetrical deflection modes for half the plate width which are the most probable deflection pattern for unsupported plates. The antisymmetrical modes cannot be excluded in this case, however. Note the horizontal line representing the nominal channel spacing of 0.040 in. and the half spacing of 0.020 in. Although the computations have not yet been completed, preliminary extrapolation indicates that the value of T_0 which would produce a maximum deflection of 0.020 in. for the antisymmetrical core with the spacer wire is approximately 150-160°F.

To demonstrate the influence of the spacer wire on this part of the total problem, use of the same approximate extrapolations for the symmetrical case without the spacer wire leads to a value for T_0 of approximately 70-80°F to produce the maximum 0.020-in. deflection. This maximum deflection however now occurs at the centerline of the plate rather than in the two positions such that $2y/b = 0.4$. It is to be emphasized that

the boundary conditions are those of clamped edges for this example. Actual cases will have to be worked out for design purposes to include many additional features, such as the design temperature distribution and a better estimate of the boundary conditions.

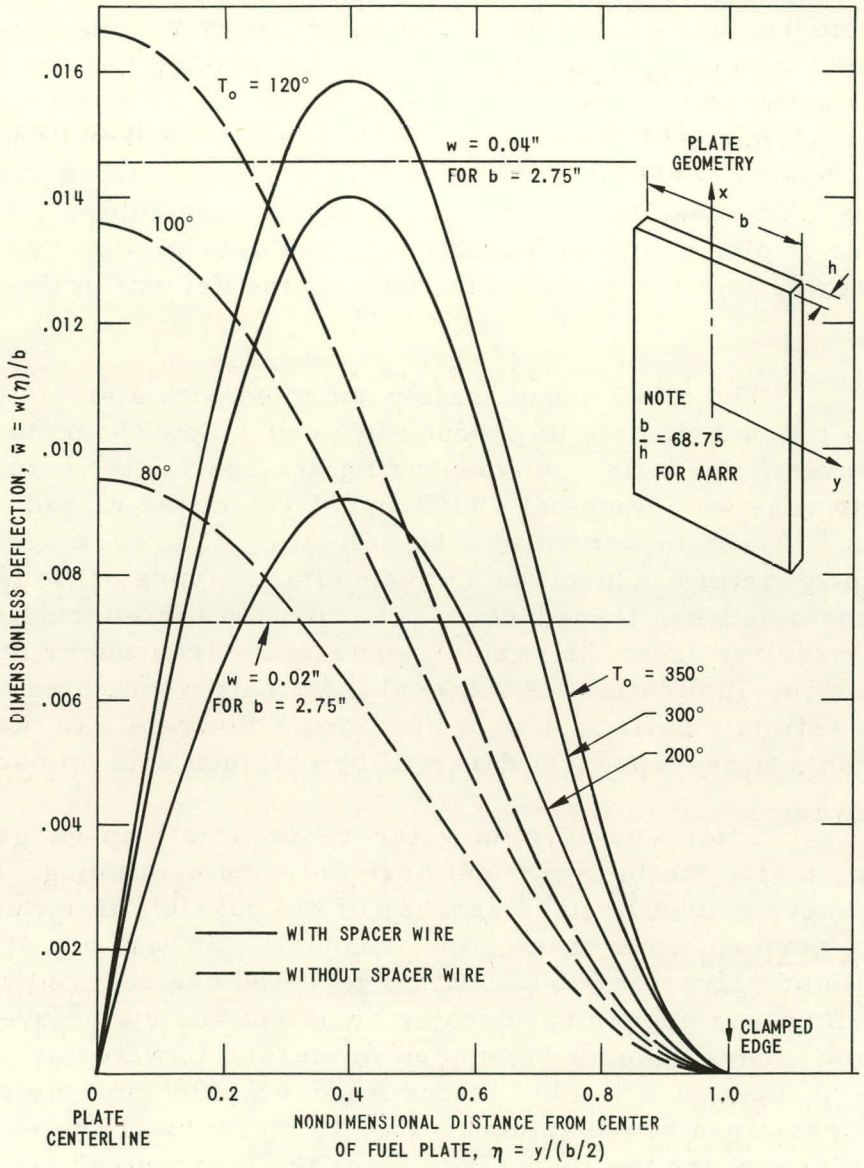

Fig. 22. Thermal Deflections of AARR Fuel Plates at Uniform Temperature T_0

In subsequent work one should determine channel closure by integrating under the appropriate deflection curves. The problem is that the changes of flow area thus produced will tend to produce pressure differences across the plate in such a direction as to amplify the thermally induced "closure." This problem typifies the need to continue to investigate such coupling aspects of structural problems as contrasted to analyses tending to treat each feature separately.

(ii) Fuel-plate Deflection in Flow Loop. Two classes of tests have been initiated for which the first rough results have been obtained. One class is to evaluate a model designed to incur plastic plate deformation under the hydraulic loads applied in the flow loop. Such knowledge of deformation patterns or plate groupings can be used for assumed mode solutions to the hydromechanics problems. Although smaller residual deformations were obtained than desired in the first run, the method has the potential to indicate the patterns and their changes as a function of flowrate. This method may permit a continuation with the problem analysis pending development of transducers to be used in final improved versions of confirming experiments. The results so far indicate that an assembly containing an even number of plates will have a lateral plate deformation that is uniformly periodic over sets of two plates (alternate plates deform in the same direction).

The other set of tests performed with a single plate (1.832 x 7 x 0.040 in.) mounted so as to produce two equal flow channels was primarily to investigate deflection-measuring devices for the outer channels. Steady-state runs were made at 100°F and at velocities ranging from 15 to 70 ft/sec in 5-ft/sec increments. The deflection data were obtained through the use of proprietary inductance and capacitance types of transducers. The agreement between transducers was poor, but the internal consistency of the data acquired from the variable-inductance transducer indicated good potential for our application. Additional information indicates that it is possible to estimate deflection as a function of flowrate. In the next series of experiments time-dependent data will be obtained with an oscillograph.

Efforts to develop water-resistant strain-gauges to study plate motion inside the fuel-element assembly are continuing. Heavily insulated gauges cannot be used because of the possible introduction of undesirable perturbations in the small channels. So far, one strain gauge covered with one layer of 3.2-mil Mylar tape and one covered with a 6-mil layer of Teflon tape appear to be water resistant and stable over long periods of time. These gauges have been immersed in water at temperatures alternating between 20 and 100°C since August 5, 1966 and the resistance to ground has remained above an acceptable 10 megohms. The effect of leakage at the place where the lead wires leave the "protected" region is being investigated.

c. Fuel Material Fabrication Development

(i) Fabrication. The work completed by Battelle Memorial Institute (see Progress Report for June 1966, ANL-7230, pp. 51-52) on fabrication of low-UO_2-concentration cermet fuel plates, boron-bearing burnable-poison additions to cermet fuel plates, and UO_2 fuel-material evaluation, inspection, and classification, has been evaluated and incorporated into the vendor's qualification-program fuel specifications and the

preliminary Mark-I-core fuel specifications. The BMI work has shown that restrictions in temperature, atmosphere, or mechanical working are required in order to enhance the fabrication of satisfactory fuel.

The burnable-poison-addition back-up study by ORNL has indicated that 4 w/o and 6 w/o B_2O_3 additions to SiO_2 yields a boron-bearing glass particle that experiences very little distortion when fabricated into the UO_2-SS cermet fuel plates. The softening temperature for these low-boria addition silicates is above 1400°C. Fabrication of 8 and 10 w/o boria additions is to be studied in an attempt to obtain an optimum balance between maximum boron loading and nominal distortion, so that a minimum amount of glass will have to be added to the cermet. The 4 w/o B_2O_3-SiO_2-UO_2-SS cermet irradiated in the ETR in the Phase II effort contained ~6 vol % glass in the cermet. This should be reduced to 3 to 4 vol % in order to minimize the cermet dilution effect on the tensile strength.

The use of the borosilicates instead of the reference Nb-coated ZrB_2 is attractive from the point of being able to retain completely helium from the $B^{10}(n,\alpha)Li^7$ reaction without experiencing any appreciable volume change, and also to eliminate the need for the maximum temperature limit of 1175°C imposed by the Ni-Nb eutectic reaction (and subsequent reactions that produce loss of boron) that is imposed when Nb-coated-ZrB_2 is used.

(ii) Irradiation Studies. The last of the AARR Phase-II irradiation test specimens (see Progress Reports for May 1966, ANL-7219, p. 66, and for June 1966, ANL-7230, p. 52) have been removed from the ETR-G12 loop. The type of specimens tested and their respective irradiation test performances are as follows:

Sample	Description	Calculated Peak Heat Flux (Btu/hr-ft^2)	Calculated Peak Burnup (% U^{235} Fissions)	Calculated Peak nvt* in Steel (x 10^{-21})
P-900	SS-347 plates with wire spacer brazed to surface;	0	0	~2
P-900		0	0	~1.2
P-909		0	0	~2
P-910		0	0	~1.2
B-927	37 w/o UO_2-SS with 1.06 w/o Nb-coated ZrB_2.	2.9×10^6	40.3	
B-928		2.9×10^6	40.3	
B-929		2.9×10^6	40.3	
B-936	37 w/o UO_2-SS with 1.7 w/o Nb-ZrB_2	2.6×10^6	48.5	
B-938	37 w/o UO_2-SS with 1 w/o Bn-ZrB_2	2.6×10^6	48.9	
B-939	37 w/o UO_2-SS with 0.6 w/o B-Si-glass	2.6×10^6	48.9	
SA-934	37 w/o UO_2-SS	1.3×10^6	42	
SA-932	37 w/o UO_2-SS	1.3×10^6	42	
SA-954	40 w/o UO_2-SS	1.3×10^6	42	

*Total based on effective fission flux.

Postirradiation evaluation by Idaho Nuclear Corp. of these samples has been started. Nondestructive measurements and metallographic analysis are in process. The complete program for evaluation of the behavior of these materials will include isotopic burnup analysis and gamma scanning to determine the fission profile; blister-anneal tests and metallography to determine the lower limits of fuel stability; tensile tests, microhardness tests, and microprobe measurements to determine the changes in mechanical and physical properties that are of greatest interest to the fuel design.

Visual examination of both the flat plates and the three-plate microassembly have revealed no perceptible distortion. Crud deposits appear to be extremely thin even after 75 operating days at heat fluxes above 1×10^6 Btu/hr-ft^2.

(iii) Blister-anneal Tests. The irradiation-stability blister-anneal tests of the nineteen-tube-and-plate Advanced Army Fuel test specimens at ORNL (see Progress Report for June 1966, ANL-7230, p. 55) have been evaluated. These fuel specimens were made with various types of UO_2 and stainless steel which were compacted and formed by isostatic compaction. Metallographic examination showed considerable variation in homogeneity between the dispersions made with heavily coated UO_2 and those made by loose powder blending of the stainless steel matrix powders and spherical or angular UO_2. There was no evidence of stringering or fragmentation of the UO_2 in the isostatically compacted cermets. Even though the cross section through the fuel specimens showed that there was considerable difference in the concentration and uniformity of the UO_2 dispersion, the blister-anneal tests revealed no strong correlation between resistance to blister failure and the type of dispersion. The blister tests did show that for these samples the temperature at which the blister formed was almost entirely independent of the fuel concentration and type of dispersion.

Figure 23 shows the results of the ORNL blister-anneal tests, including two points from the ETR-G12-AARR sample tests and the usual curves for predicting instability. The values for fission density have been corrected for the self-shielding effect and are as much as 35% higher than the average fission density across the thickness of the plate below the blister. Almost all of the blisters occurred at a depth of approximately one particle diameter below the clad-cermet interface.

Although the blister-anneal test data fit the curves derived from data from earlier in-pile studies, the correlation may be more accidental than factual. The early in-pile data were obtained from samples whose temperatures during capsule irradiations can be seriously questioned. In many cases the temperatures in areas where blisters formed were suspected of being several hundred degrees higher than indicated on the basis of extrapolation from coolant temperature alone. Thus, these curves appear to be of use for qualitative appraisal of performance only.

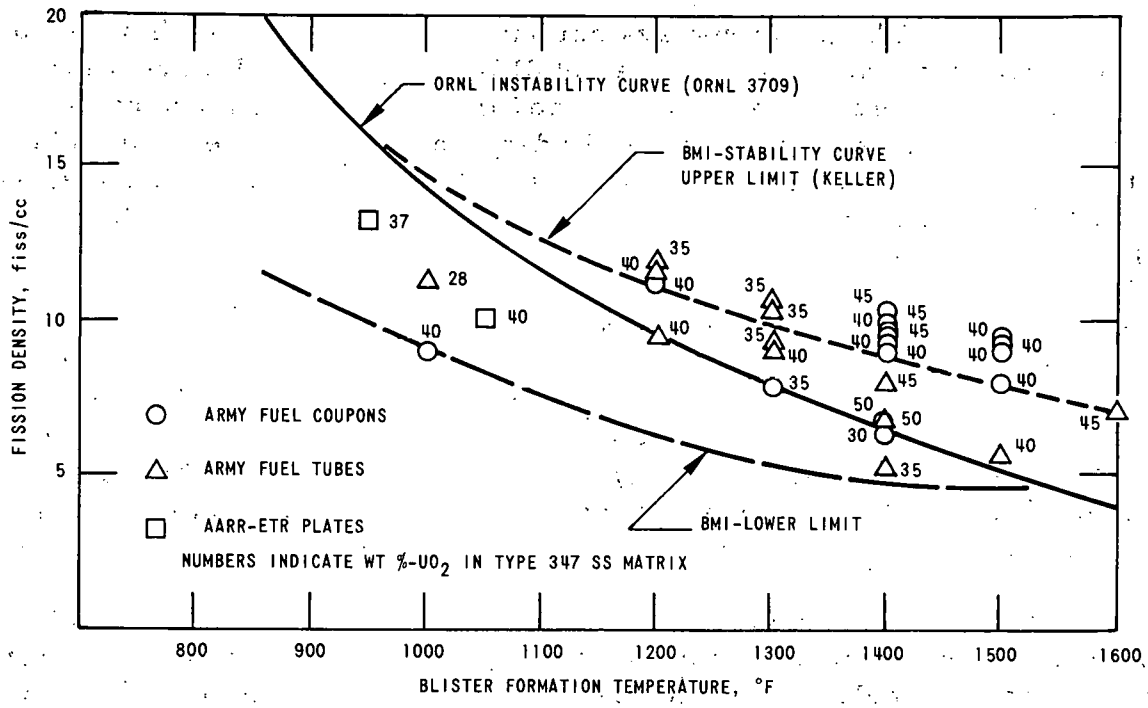

Fig. 23. Blister-anneal Test Data

There is also a strong indication that the postirradiation blister-anneal tests performed with the AARR and Advanced Army Fuel samples give instability burnup-temperature relationships that are considerably lower than would have occurred had the blisters been allowed to form in the reactor. The reason for this is that the hot-cell furnace cannot approach the time-temperature-fission-product-induced stress buildup situation that takes place during irradiation. Thus far no attempt has been made to adjust the hot-cell test data in order to compensate for the combined effect of stress relieving and creep phenomenon that would occur during the gradual approach to the excessive-stress-temperature conditions in the matrix during operation in the reactor.

(iv) Quality Control and Inspection. A gamma-ray transmission technique for measuring fuel-loading homogeneity in fuel plates was investigated by Illinois Institute of Technology Research Institute, and a prototype scanning and recording system was assembled. This system was used to examine fuel plates having nominal loadings of 31, 37, and 40 w/o depleted UO_2.

An uncollimated 1.1-mCi Co^{57} source was used to obtain maximum intensity over an area of ~0.08 in.^{2}. The detector was a NaI crystal mounted on a photo tube. The tube signal was monitored by a microammeter and analyzed by a Harwell Quantizer which, by means of current generators, provides a quantized halftone recording via an Alden facsimile recorder.

The prototype system has demonstrated that this method can be used to examine stainless steel-UO_2 fuel plates. However, for a production-type setup it is recommended that a collimated source of at least 100 mCi be used and a specially designed scanning mechanism be obtained which would reduce the inspection time to ~10 min per plate. Calibration of the equipment with accurate standards would have to be undertaken prior to use.

d. Control Rod Development

(i) Elastic Moduli of Control Blade Material. The samples tested were made by Sylcor and consisted of a sintered core of 32 w/o Eu_2O_3, 15 w/o TiO_2, and 53 w/o Type 302B stainless steel. This core was hot rolled by the "picture frame" technique with cladding plates of Type 347 stainless steel.

The experiments were performed statically and dynamically. The conclusions from the dynamic or resonance test should not be construed as a dynamic modulus but rather as a dynamically determined static or relaxed modulus. Should it become necessary, the transition region between the static and dynamic (relaxed and unrelaxed) moduli will be investigated, initially in terms of a standard linear viscoelastic model. In this region the standard model displays frequency- or strain-rate-dependent moduli.

The statically performed test was made with an Instron tensile tester with which a tensile load was applied at a displacement rate of 0.02 in./min. The strain-gauge output was graphed, providing curves of load versus strain from which Young's modulus and Poisson's ratio were determined.

A tensile stress of 12,700 psi initiated yielding of the sandwich structure, and a tensile stress of 9,000 psi initiated yielding of the unclad core material.

Dynamically performed tests were used to determine the shear and Young's moduli by a resonance method outlined by Spinner and Valore.[29] The specimens were milled to the shape of a rectangular prism (approximately 0.075 x 0.75 x 2.6 in.) and suspended by two cotton threads attached at diagonal corners with the flat side in the horizontal plane. The end of one thread was attached to an exciter, the other to a detector. The natural frequencies of a free-free beam in flexural vibration as well as torsional vibration were noted and recorded. The first two modes of flexural or bending vibration and the first two modes of torsional vibration

[29]Spinner, S., and Valore, Jr., R., Comparison of Theoretical and Experimental Relations between the Shear Modulus and Torsional Resonance Frequencies for Bars of Rectangular Cross Section, J. Res. Natl. Bur. Standards 60, 459 (1958).

were determined. The second modes were within ±2% of those expected from the first-mode frequency. The frequencies of the first-mode resonance were used to calculate moduli values from the equations for vibration of a free-free beam. Tests with solid stainless steel specimens provided values of moduli in agreement with published data. The results of the Eu_2O_3 core material were consistent and should be correct as reported in Table XIX.

TABLE XIX. Test Results

	Core Material	Sandwich Structure	Type 347 SS (Tested for equipment checkout)
Young's Modulus, psi x 10^{-6}			
Tensile	E_T = 18.7	E_T = 21.3	E_T = 27.6
Resonance	E_R = 18.9		E_R = 28.1
Shear Modulus, psi x 10^{-6}			
Resonance	G_R = 7.5		G_R = 10.86
Poisson's Ratio			
Tensile	ν_T = 0.18 (±20%)	ν_T = 0.20 (±30%)	ν_T = 0.287
Resonance	ν_R = 0.26		ν_R = 0.294

Note: Poisson's Ratio (Resonant) was calculated by assuming an isotropic material for which

$$\nu_R = \left(\frac{E_R}{2G_R}\right) - 1.$$

(ii) Control Rod Hydraulic Test. A system operational test was performed on the GPHL (General Purpose Hydraulic Loop) with a dummy control rod test section in place to check out the loop, to familiarize operating personnel with the performance of the loop, and to observe visually the behavior of the control rod under various flow conditions. At the time of this test the installation of instrumentation for the flow test section had not been completed.

The stainless steel dummy control rod measured 0.20 x 6.000 x 47½ in. The upper end of the rod is provided with two 0.020-in. raised buttons on each side of the rod thickness, which prevent total lateral movement of the rod against the wall of the flow channel in the test section. The lower end of the rod is rigidly connected to the test section and positioned centrally within the flow channel of the test section. The behavior of the control rod was observed through the viewing ports in the test vessel.

At a flow velocity of 30 fps through the test section, it was observed that movement of the control rod was very slight, with a frequency of ~5 cps. At 40 fps the control rod was forced off center toward the side of the test-section channel wall. Very little daylight was observed between the control rod side button and the test-section channel wall. At 50 fps, the control rod button was firmly forced against the test-section channel wall. At 60 fps, slight bowing and vibration occurred about midpoint of the length of the control rod. At 70 fps, the control rod returned to its normal central position within the channel of the test section. A slight cyclic vibration was observed.

e. Core Structure Development. Additional experiments were conducted to supplement the preliminary stress studies of the AARR core support grid plate (see Progress Report for February 1966, ANL-7176, pp. 76-78). The slots accommodating the control blades of the reactor were investigated for changes in width upon load application to the grid plate. A strain-gauge-instrumented probe built and calibrated for this purpose permitted the measurement of dimensional changes of 1×10^{-4} in.

Experiments performed at various locations in four typical control-blade slots gave width changes that were generally of about the same magnitude at the top and bottom surfaces of the plate but opposite in direction, indicating deformation of the plate about a neutral plane roughly midway between the surfaces. The maximum closure (or opening) of any slot was less than 0.001 in. for the simulated 25-lb/in. pressure load applied. Extrapolating to 125 lb/in.^{2} pressure drop across the core, the slots would be expected to narrow down by less than 0.005 in., presuming continuing elastic behavior of the support plate.

3. Component Development

a. Reactor Vessel. Detailed calculations of the stresses in a carbon steel reactor vessel for the most recent nozzle configuration are summarized in Fig. 24 (compare with Inconel vessel, Progress Report for June 1966, ANL-7230, p. 56). The computed stress profile was for an SA-302B shell and is also applicable to an SA-212B shell. The combined shell stresses in and near the belt-line region are approximately one-half of the yield strength of either steel. At the shell discontinuities, the maximum stress is roughly two-thirds of the yield strength of the steel. In general, the carbon steel shell designs contain a higher factor of safety for elastic overstress than do the austenitic materials at the same ultimate tensile strength levels.

b. Thermal Analysis of Beam Tube. An extension of the stress analysis of the beam-tube adapters (see Progress Report for July 1966, ANL-7245, pp. 56-58) is being made in order to show the effects of various loads and beam-tube-assembly procedures on clearances between the through-tubes and the reflector.

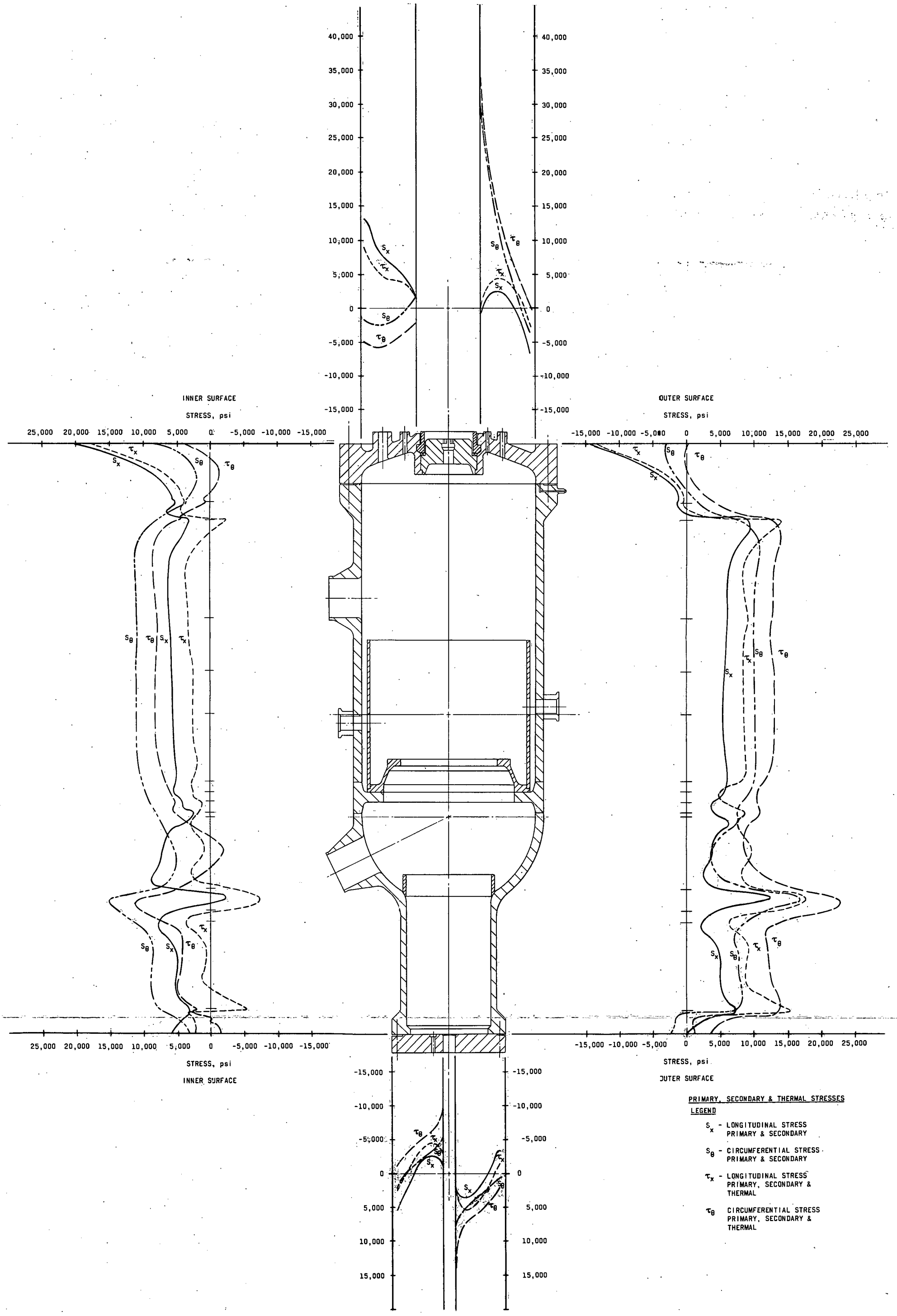

Fig. 24. Primary, Secondary, and Thermal Stresses for AARR Reactor Vessel (Carbon Steel Material)

The adapters, which extend outward from the vessel beam-tube nozzles and secure the ends of the through-tubes, are subject to vertical loads and bending moments. These forces cause the adapters to bend slightly downward from the nozzle centerline. The adapters transmit the bending and the downward displacement to the ends of the through-tube. As a result, a slight upward bowing and a shifting of the tube relative to the reflector may occur. The magnitude of the deflection of the tube from the nozzle centerline was calculated for three positions along the tube for adapter loading conditions I, II, and III as explained in ANL-7245. The positions are: A, outer face of the reflector shroud toward the floating end of the through-tube; B, midway between nozzle faces; C, face of the reflector shroud toward the fixed end of the tube. The results shown in Table XX are for the full length adapter.

TABLE XX. Summary of Through-tube Deflection Calculations

Case	Vessel Condition	Deflection* at Tube Supports (in.)		Rotation* at Tube Supports (10^4 radians)		Deflection* (in.) from and at Position		
		Floating End	Fixed End	Floating End	Fixed End	A	B	C
I	cold	-0.006	-0.0005	0.34	-0.71	-0.0006	+0.0004	+0.0009
	hot	-0.026	-0.0020	6.12	-3.07	+0.0095	+0.0106	+0.0095
II	**	-0.084	-0.0045	23.20	-7.16	+0.0327	+0.0332	+0.0277
III	cold	-0.084	-0.0045	23.20	-7.16	+0.0327	+0.0332	+0.0277
	hot	-0.104	-0.0060	28.99	-9.54	+0.0429	+0.0435	+0.0362

*Deflections (measured from nozzle centerline) are positive upwards; clockwise rotations are negative.
**Loading independent of temperature.

The calculations indicated that the upward bowing in the reflector region is considerably offset by the downward displacement of the tube caused by its own weight. Thus it appears that only modest clearances between the through-tube and the reflector liner will be required to accommodate such effects. Although these numerical results are subject to certain refinements, they should provide a reasonably accurate picture for the loading conditions assumed.

The stress in the through-tube as a result of the bowing is small, being less than 600 psi for the cases considered.

4. Physics Experiments and Analysis

a. Reactivity Effect of Beryllium Displacement. An experiment was performed in the AARR Critical Facility to estimate the reactivity effect of displacing beryllium, in the reflector near the reactor core, by water. With the adjacent peripheral control blade (No. 3) at its position of

full withdrawal, the reactivity effect of removing a beryllium slab, 2 in. (thick) x 10 in. (wide) x 19 in. (high), was determined to be -(1.8 ± 0.2)%. This corresponds approximately to the removal of one-sixth of the temporary beryllium annular zone.

The reactivity-control worth of the associated peripheral control blade was measured both with and without the beryllium block in place. For this one blade, the total control worth of blade plus beryllium replacement is estimated to be 2.3%, in comparison with a worth of 1.4% measured for the blade with the beryllium present. The principal purposes of these measurements were: (a) to estimate the additional reactivity shutdown margin if a core package, consisting of a full reactor core plus control blades, were loaded into a medium which included the permanent but not the temporary beryllium; and (b) to study the merits of a combined motion of absorber and beryllium as a reactivity control device.

Control-blade-interaction measurements were made with various groupings of control blades. For the closest grouping of three blades, namely, two adjacent peripheral blades and the common in-core radial blade, the total worth was approximately 30% less than the sum of the measured individual reactivity-control worths. In this same sector, the total worth for the next closest grouping of three control blades was only 10% less than the sum of the reactivity worths of the individual blades. With a closely grouped set of three control blades in this sector, the control worth of an isolated blade on the opposite side of the core was slightly smaller than its worth when the reactor was controlled with a more nearly symmetric grouping of control blades.

With the present (1173/1347) core loading and the oversized internal thermal column (ITC), an experiment was carried out to study possible improvements in the measurement of the peak unperturbed thermal-neutron flux in the ITC per watt of fission power. The excess reactivity was controlled entirely by lowering the level of the water to ~3/4 of the active height of the fuel zone. The absolute fission rate of a punching from a fuel foil provided the normalization. In earlier measurements, the normalization was to a foil placed in an aluminum stringer in the water channel between two fuel plates. The estimated value of the unperturbed peak flux in the 100%-H_2O ITC is (3.8 ± 0.3) x 10^7 n-cm/cm^3-sec per watt of fission power--in this special loading, with an oversized ITC and with ~1/4 of the fuel zone above the water.

b. Theoretical Studies. Computations have been made for the reactivity effect of removing a ring of beryllium at the inner edge of the beryllium reflector. This corresponds to the much smaller experimental perturbation discussed above, where a 2-in.-thick slab of beryllium was removed from one of the six faces of the outer radial boundary of the fuel zone. The calculated result of replacing a full 2-in.-thick ring of beryllium

by water is 8.4%. Both in the experiment and in the calculation there was no water in the beryllium zone, in contrast with the design-reference reflector where a water volume fraction of 0.1 has been assigned to the temporary-beryllium zone. Also, the reference temporary-beryllium zone is somewhat thicker than 2 in.

A theoretical study has been made of the changes in reactivity and in the experimenters' fluxes of thermal neutrons which would result from a change in the reference thickness of the annular fuel zone. To simplify the analysis, the thicknesses and the compositions of the graded-fuel zones were held fixed, and only the thickness of the ungraded portion of the core was varied. The ITC was invariant, both in dimensions and in composition. The inner radius of the beryllium reflector was varied to correspond to the changes in core radius, but the thicknesses and compositions of the various reflector zones were unchanged.

The thickness of the fuel zone has a marked effect on the values of peak neutron flux, per unit fission power, in the experimental facilities. This is a composite of three principal effects. When the fuel zone thickness is decreased but the total power is held constant: (i) the power density near the inner and outer flux traps is increased; (ii) the mean optical distance between the source and the receptor is decreased; and (iii) the probability of leakage of high-energy source neutrons is increased. Figure 25 shows the effect of core thickness on experimental fluxes, both for the

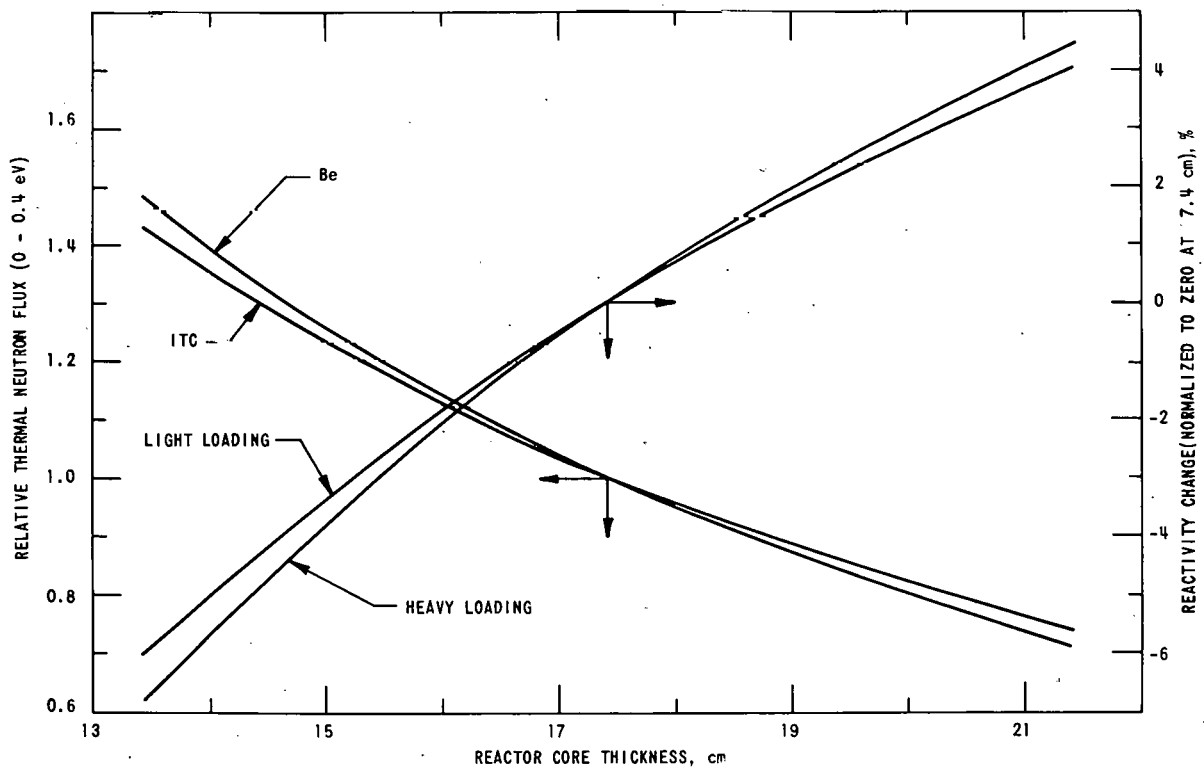

Fig. 25. Effect of Core Thickness on Reactivity and Thermal-neutron Flux

design reference AARR, and, for comparison, for a much lighter (uniform) fuel loading. Only one curve is shown for the percentage change in the peak flux in the ITC since this curve for the reference loading is scarcely distinguishable from the corresponding curve for a fuel loading only 1/4 as large. Note also that, over the entire range of thicknesses, the percentage change in the peak flux in the beryllium is almost the same as the percentage change in the peak flux in the ITC.

Figure 25 also shows the change in reactivity resulting from the change in core thickness. Note that there is little difference in the curves for the two different fuel loadings. Note also that each centimeter reduction in core thickness would cause a loss of ~$1\frac{1}{2}$% in reactivity. Therefore, a reduction in the reactor core thickness would mean that at fixed power the peak experimenters' fluxes would be increased but at a substantial cost in increased peak power density and in reactivity. For example, a 4-cm reduction in core thickness was found to correspond to a one-third reduction in core volume, a one-half increase in the average power density, a 40% increase in the peak power density, and a 35% increase in the peak thermal-neutron flux in the ITC--at an initial cost of 6.7% in reactivity, which would be compounded by an increased loss in reactivity per 1000 MWd of operation.

Another parameter of considerable importance in the optimization of the AARR core design is the degree of radial flattening of power density in the core. The importance of having high power density near the radial boundaries of the fuel zone has been studied in a somewhat more general way, in terms of the relative contributions to experimental fluxes from fission-spectrum sources at various radial locations (see Progress Report for November 1965, ANL-7123, pp. 71-73, and for January 1966, ANL-7152, pp. 79-80). Clearly, a source neutron near a radial boundary of the core is a very much more effective contributor to the fluxes in facilities near that boundary. On the other hand, that neutron contributes almost nothing to fluxes in facilities near the other radial core boundary. Since, in AARR, there are experimental facilities near both core boundaries, it is necessary to keep the power density high near both boundaries. Computations have shown that reduction in power at the edges of the core and an accompanying increase in power density in the central portion of the core offer such cancellations that the peak thermal-neutron fluxes in the ITC and in the beryllium would be changed by only a few percent. However, the additional grading of fuel which would be required to achieve this additional flattening of power density would decrease the excess reactivity available for core operation. Not only would the reactivity of the fresh core be decreased, but the average reactivity loss per 1000 MWd of operation would be increased. This double penalty on core life due to additional power flattening makes it undesirable to reduce significantly the power peaking in the fuel zone of the AARR reference core.

V. NUCLEAR SAFETY

A. Research and Development

1. Coolant Dynamics

a. Coolant (Water) Expulsion Studies. Delays in computer programming have not yet allowed calculation of the expulsion velocities observed from high-speed motion pictures.

Attempts to develop a theoretical model which describes transient film boiling of a partially confined liquid continue. Although the conservation equations which rigorously describe the process have been formulated, it has not yet been possible to obtain an analytical solution without making assumptions which severely limit the applicability of the model. Since the pressure rapidly increases in the vapor due to the increasing vapor temperature as well as the inertial effects of the liquid, vaporization cannot be assumed to occur at a constant temperature as is usually done. The vaporization temperature increases with the pressure and thus is a function of time which is unknown a priori. This observation also implies that there are at least two opposing phenomena controlling the rate of vapor growth, i.e., the increasing temperature increases the vapor production but also increases the vapor pressure; the increasing vapor pressure tends to retard vapor production by raising the effective liquid boiling point.

b. Superheat Experiment. This experiment is designed to measure the degree of liquid superheat required to initiate nucleate boiling in sodium under various conditions simulating a reactor environment. Typical parameters will be systematically varied to determine their independent and combined effects upon the liquid superheat necessary to initiate nucleation. The parameters to be examined are: (a) pressure, (b) dissolved gas content, (c) heat flux, (d) surface characteristics, and (e) the pressure-temperature history of the system.

All instrumentation has been installed and calibrations are being conducted. An X-ray system incorporating a fluoroscope will be used to calibrate the liquid-level probe. The first data should be available very shortly.

Assembly of the initial superheat experiment is complete, and the dump tank has been filled with sodium. The final checkout of the system is forthcoming.

c. Sodium Expulsion Experiment. In this experiment, it is planned to investigate the mechanism of coolant expulsion in a simulated reactor environment. Hence, this experiment includes the measurement of the void distribution, expulsion velocities, pressure transients, and liquid superheats during coolant expulsion.

Construction of the support structure for the initially stagnant sodium expulsion experiment is underway. Final details on the design of the actual expulsion tube are being resolved, and assembly will commence shortly.

Purchase of the programmed electron-beam heater has been delayed, since only one vendor has submitted a bid. Invitations to bid were sent out a second time to a larger number of companies. It appears that a 4-6-month delivery schedule will be encountered.

2. Fuel Meltdown Studies with TREAT

a. Oxide Fuel. A 1.67-kg batch of 13% enriched UO_2 cylinders, 0.383 cm in diameter, has been obtained with an oxygen-to-uranium ratio of 2.00. Approximately 260 g has been set aside for assembly into sixteen half-length EBR-II-type sodium-bonded or sodium-logged pins. Eight of the pins are to be sealed, sodium-bonded samples, with four to be run to a nominal 1 a/o burnup and the other four to be run to a nominal 3 a/o burnup. The remaining eight are to be of the gas-bonded type, with intentionally defected cladding to permit sodium logging of the fuel during the bonding of the pins to the irradiation capsules. These eight pins are specified to receive a nominal 2 a/o burnup.

The six UO_2 pins irradiated to a nominal burnup of 6 a/o (see Progress Report for August 1966, ANL-7249, p. 76) have been inspected by neutron radiography, and the radiochemical determination of integrated flux during irradiation has been completed. Pin 15 is being encapsulated to undergo a transient TREAT exposure. Pin 16 has been selected for destructive examination. The remaining four are reserved for future transient experiments. Burnup values are given in Table XXI.

TABLE XXI. Burnup Values from Monitor Wires

Pin	Burnup (a/o)	Pin	Burnup (a/o)
15	6.6	18	7.6
16	6.2	19	5.6
17	7.4	20	5.7

b. Loop Meltdown Experiments with 7-pin Clusters. Two clusters of 7 EBR-II Mark-I pins were run in meltdown experiments using the Mark-I integral sodium loop. Each cluster consisted of a 9% enriched pin, surrounded by a ring of six 7% enriched pins. Tantalum neutron absorbers were attached to each test section to shape the sample power distribution axially. Reactor irradiation conditions are given in Table XXII.

The first loop has been returned to Illinois for removal of the test section and inspection of the samples. The shipping coffin is being returned to Idaho for the second loop.

TABLE XXII. Transient Irradiation Conditions for 7-pin Clusters

Cluster No.	Initial Sodium Flow (m/sec)	Reactor Period (sec)	Reactor Energy (MW/sec)	Maximum Central Pin Energy* (J/g Fuel)
1	4	0.15	125	398
1	4	0.11	338	1070
2	0	0.15	125	398
2	0**	0.11	407	1290

*For the axial central region.
**Significant transient-induced flows occurred.

c. High-temperature Heat of Vaporization of Sodium. The heat of vaporization of sodium is needed as a function of temperature for analyses of transient accidents. Available data on sodium were evaluated to be used for calculating the sodium heat of vaporization at high temperatures (i.e., in the range between uranium melting point and the sodium critical point). Examination of high-temperature data on density of saturated sodium vapor and liquid[30] disclosed large scatter, sufficient to warrant careful reanalysis of the data and to check the reported heat of vaporization values based on those data.

Extrapolation of the liquid sodium density data of Stone et al.[31] and of Dillon[30] by means of a Rowlinson plot[32] gave the following relationship:

$$\frac{\rho_L - \rho_c}{\rho_c} = 3.7255\left(\frac{T_c - T}{T_c}\right)^{0.6089}, \qquad (1)$$

where ρ_L is liquid density, ρ_c the critical density (0.206 g/cc), T the temperature, and T_c the critical temperature (2573°K).

Equation (1) and low-temperature sodium vapor data[31] were used to construct a rectilinear diameter plot. For $T \leq 1650$°C, the calculated liquid densities and those reported by Dillon[30] were in excellent agreement; above $T \geq 1650$°C, the calculated liquid densities were below those by Dillon. For temperature above those given by Stone, vapor densities were obtained directly from the rectilinear diameter plot.

The Clapeyron equation was used to determine the heats of vaporization:

[30]Dillon, I. G., Nelson, P. A., and Swanson, B. S., ANL-7025 (1965).
[31]Stone, J. P. et al., NRL-6128 (1964).
[32]Rowlinson, J. S., Liquids and Liquid Mixtures, Butterworth's Scientific Publications, Ltd., London (1959), Ch. 5.

$$\frac{dp}{dT} = \frac{\Delta H_v}{T\left(\frac{1}{\rho_v} - \frac{1}{\rho_L}\right)}, \qquad (2)$$

where

ΔH_v = heat of vaporization;

p = equilibrium vapor pressure.

The pressure equation[33]

$$\log_{10} p = 4.521 - \frac{5220.46}{T}$$

was differentiated with respect to temperature and substituted into Eq. (2), which now becomes

$$\Delta H_v = \frac{(2.303)(5220.46)\ PK}{T}\left[\frac{1}{\rho_v} - \frac{1}{\rho_L}\right](0.022997)\ \frac{cal}{g\text{-mole}},$$

where K, a conversion factor equals 24.218 cal/liter-atm.

Results are shown in Table XXIII.

TABLE XXIII. Heats of Vaporization of Sodium

	ΔH_v (cal/g-mole)			ΔH_v (cal/g-mole)	
T (°K)	Calculated	Determined from Dillon[30]	T (°K)	Calculated	Determined from Dillon[30]
1273.15	27700.0	24189.85	2073.15	6568.24	8188.94
1473.15	10720.0	19887.53	2373.15	4968.36	3085.10
1773.15	6890.25	13830.57			

B. TREAT

1. Operations

Two seven-pin clusters of EBR-II pins, one with and one without flow, were irradiated in packaged sodium loops. Preliminary analysis of temperature, flow, and pressure data indicates that some of the fuel pins failed during each test. The loops have been returned to Argonne, Illinois, for disassembly and inspection.

[33]Bonilla, C.F., et al., Trans, Am. Soc. for Metals 55, 877 (1962).

2. Large TREAT Loop

Modifications to the loop necessary to correct the problems discovered during the first pressure test (see Progress Report for June 1966, ANL-7230, p. 68) were completed. Other minor modifications required to reduce thermal expansion stresses were also completed. The entire loop was successfully retested at a pressure of 180 psig.

Installation of thermal insulation was completed, and final connection and checkout of electrical heaters is in progress. The loop will be ready for sodium filling after it has been subjected to one heating cycle to operating temperature and then leak tested at room temperature.

C. Chemical and Associated Energy-transfer Problems

1. Heat Capacity of Liquid UO_2

The high-temperature heat capacity of UO_2 is of importance in fast reactor safety calculations. The general approach to be used for determination will be to encapsulate the UO_2 in tungsten, heat by induction, and measure the heat content by conventional drop calorimetry. Although calculations show cooling-curve methods to be less likely to succeed than the method outlined above, a few experimental tests of the cooling-curve methods will also be made. It is hoped that temperatures from the melting point of UO_2 (2800°C) to near the melting point of tungsten (~3400°C) can be explored.

In initial work the suitability of tungsten as an encapsulation material at temperatures significantly above the melting point of UO_2 was investigated. Tests have been carried out using a wide variety of sources of tungsten, and in no case was any gross attack by the UO_2 observed. The capsules, after heating, were cut open, polished, and examined metallographically. In many cases a metallic precipitate was seen in the oxide (see Fig. 26). The capsule for this experiment was made from wrought tungsten tubing and the encapsulated material was heated to about 3350°C for 1-2 min. Metallographic examination indicated that the precipitated material was tungsten; however, positive identification was made by electron-microprobe analysis.

The material from the experiment at 3350°C was analyzed to determine whether or not the O:U ratio had changed during heating. No change from the initial composition was detected.

Almost all the equipment needed for carrying out the heat-capacity measurements has been ordered, and design and construction of the vacuum chamber in which the heating will be carried out has begun. In addition, capsules of various shapes have been designed to improve uniformity of heating. Several capsule types will be tested before a final choice is made.

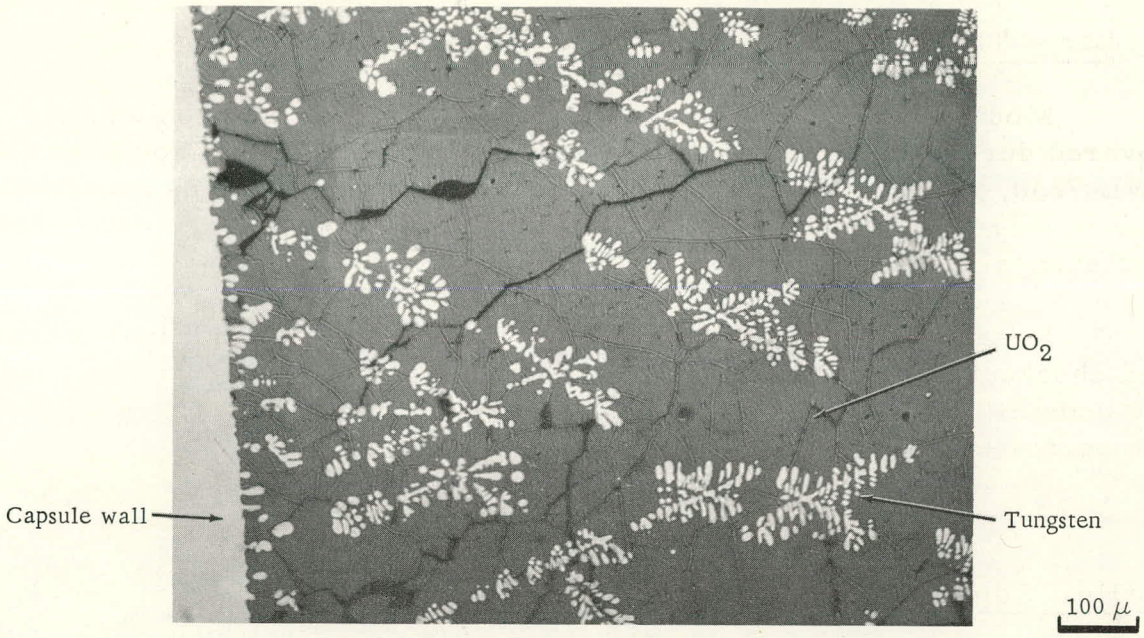

Fig. 26. Section of Tungsten Capsule Containing UO_2 after Heating to 3350°C for 1-2 min

2. Fuel-migration Studies

Determination of the extent of fuel migration and segregation in mixed uranium-plutonium fuels is important in assessing to what extent Doppler broadening as a shutdown mechanism may be affected by axial or radial redistribution of fissile and fertile materials. Redistribution of plutonium and fission products may also lead to localized melting in the event of a moderate reactor transient. It is planned to investigate the behavior of mixed fuels such as uranium and plutonium oxides, carbides, oxycarbides, and nitrides in a thermal gradient. Segregation and migration within fuel samples will be determined by chemical, metallographic, and electron-microprobe analyses.

A thermal-gradient furnace and associated vacuum system for use in a plutonium glovebox has been assembled. Preliminary experiments with UO_2-CeO_2 sample pellets are in progress. To date, samples of UO_2-30 m/o CeO_2 (approximately 3/8 in. in diameter and 1/2 in. long) have been maintained in thermal gradients of ~1000°C/cm for periods of 100 and 500 hr. A UO_2-15 m/o CeO_2 sample has been heated for 100 hr in a similar temperature gradient. On completion of these preliminary experiments the apparatus will be moved into a glovebox and experiments with UO_2-PuO_2 fuels will commence.

Analytical data are not yet available on the heated urania-ceria samples. However, ceramographic examination indicates that pore migration toward the hotter end of the sample has taken place. Figure 27 shows the longitudinal cross section of the UO_2-30 m/o CeO_2 pellet heated for 100 hr. Large pores near the top are evident; unheated samples show more uniform distribution of pores and, in general, have much smaller pores.

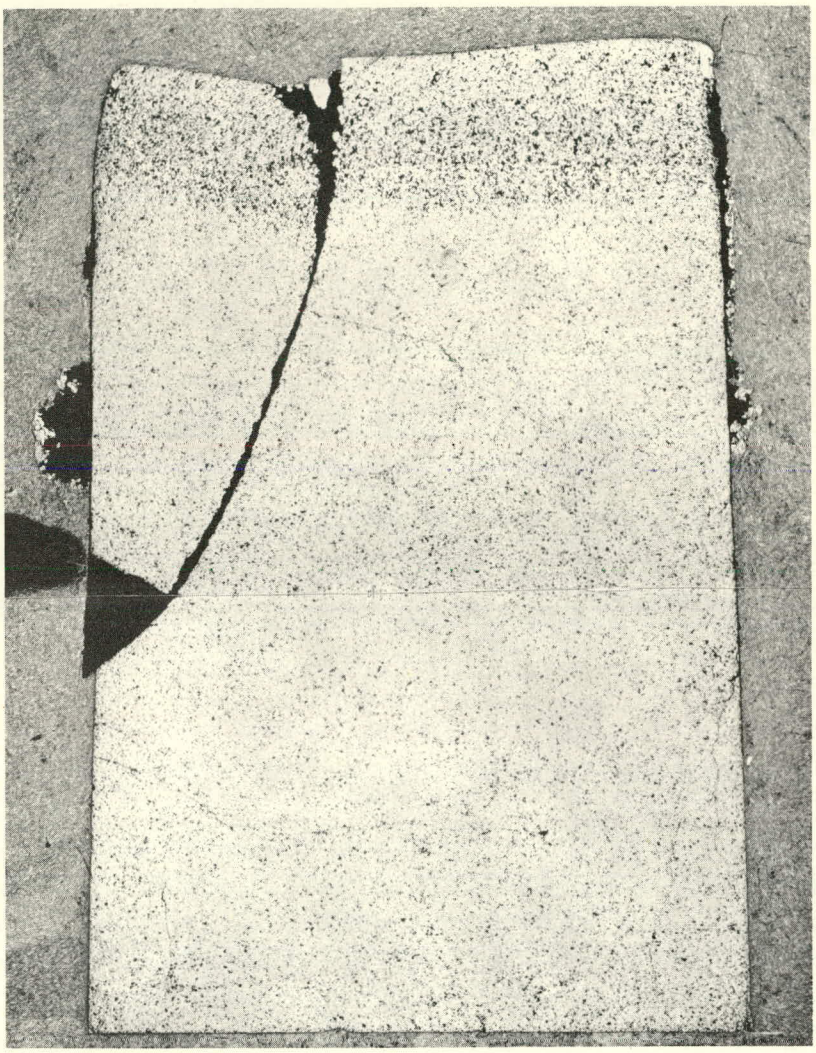

11X

Fig. 27. Longitudinal Cross Section of a UO_2-30 m/o CeO_2 Pellet Heated in Thermal-gradient Furnace for 100 hr

D. Containment

1. Primary Containment by Energy Absorption

An idealized nuclear reactor system with spherical symmetry, which simulates a typical sodium reactor installation, has been analyzed for energy release. A fluid dynamical analysis was performed to determine the effect that the destructive component produces on the concrete primary containment vessel. From this effect, the rate of strain to which the embedded high-strength steel strands are subjected can be determined. The analysis was performed on a system both with and without a reactor vessel. The von Neumann-Richtmeyer pseudoviscous technique was used to obtain the numerical solution. The strain rate to which the strands are

subjected are: (a) 12.32 sec^{-1} for the system without the reactor vessel, and (b) 9.77 sec^{-1} for the system with the reactor vessel. Experimental tests show that for strain rates of the order 10 sec^{-1}, the ultimate strength and total elongation for high-strength steel bars differ from the values obtained from static testing (10^{-3} sec^{-1}) by less than 3%. It can be seen by the reduction in the strain rate that the reactor vessel is a good energy-absorbing device and should be considered as part of the primary containment system.

E. Plutonium Volatility Safety

1. Disposal of Gaseous Fluoride Volatility Reagents

Experiments have continued on the development of methods for the disposal of waste fluorine from the fluoride volatility process, using fluidization techniques. Activated alumina has been shown to be a highly effective material for removing fluorine from process gas streams. The reaction between fluorine and alumina is characterized by an initial period during which the fluorine concentration in the off-gas from the fluid-bed reactor remains at a relatively constant value, less than 50 ppm, and by a breakthrough period in which the fluorine concentration increases rapidly to greater than 50 ppm. The results of a factorially designed experiment to investigate the effects of process variables on the capacity of activated alumina for fluorine (g F_2/g activated alumina) were reported previously (see Progress Report for August 1966, ANL-7249, p. 60). Recent work, in which the ranges of several process variables were extended beyond those employed previously, has shown that increasing the concentration of fluorine in the feed gas from 5 to 75 v/o has no effect on the capacity of activated alumina for fluorine. It was also observed that operation of the fluid-bed reactor at gas velocities greater than 1.65 times the minimum fluidizing velocity leads to slightly lower fluorine capacity. In the course of this work, fluorine capacities as high as 0.8 g F_2/g activated alumina were achieved. The theoretical capacity (complete conversion to aluminum fluoride) is 0.95 g F_2/g activated alumina.

Two other solid reagents, limestone and soda ash, have been evaluated for fluorine disposal. At a fluorine breakthrough defined at 200 ppm of fluorine in the off-gas, the capacity of soda ash was 0.32 g F_2/g soda ash (90% theoretical) while the capacity of limestone was 0.045 g F_2/g limestone (12% theoretical). Since the results for soda ash appear promising, a factorially designed experiment is planned to investigate the effects of independent process variables on the capacity of soda ash for fluorine.

VI. PUBLICATIONS

Papers

The Kinetics of Oxidation of Uranium between 300 and 625°C
L. Baker, Jr., and J. D. Bingle
J. Nucl. Mater. 20(1), 11-21 (July 1966)

Review of Metal-Water Reaction Studies for Reactor Safety Analyses
L. Baker, Jr.
Am. Chem. Soc. 152nd Mtg., New York, September 11-16, 1966, Abstracts of Papers, R-22

The Ignition of Uranium
L. Baker, Jr., J. G. Schnizlein, and J. D. Bingle
J. Nucl. Mater. 20(1), 22-38 (July 1966)

The Use of Bromine Pentafluoride in the Reprocessing of Low-Enrichment Nuclear Reactor Fuels
J. J. Barghusen, M. J. Steindler, D. Ramaswami, and A. A. Jonke
Am. Chem. Soc. 152nd Mtg., New York, September 11-16, 1966, Abstracts of Papers, R-42

Fluidized Bed Disposal of Fluorine
J. T. Holmes and A. A. Jonke
Am. Chem. Soc. 152nd Mtg., New York, September 11-16, 1966, Abstracts of Papers, R-45

Chemical Reactions Accompanying a Hypothetical Loss of Coolant in a Water-Cooled Power Reactor
R. O. Ivins, J. C. Hesson, and R. E. Wilson
Am. Chem. Soc. 152nd Mtg., New York, September 11-16, 1966, Abstracts of Papers, R-23

The Reaction of Gaseous Bromine Pentafluoride with Uranium Compounds
R. L. Jarry and M. J. Steindler
Am. Chem. Soc. 152nd Mtg., New York, September 11-16, 1966, Abstracts of Papers, R-41

Lithium Hydride Systems. Solid-Liquid Phase Equilibria for the Ternary Lithium Hydride-Lithium Chloride-Lithium Fluoride System
C. Johnson, E. Hathaway, and C. E. Crouthamel
J. Chem. Eng. Data 11(3), 372-374 (July 1966)

New Pyrochemical Process for Fast Breeder Reactor Fuels.
I. Process Chemistry
J. B. Knighton, W. Knoch, and R. K. Steunenberg
Am. Chem. Soc. 152nd Mtg., New York, September 11-16, 1966, Abstracts of Papers, R-9

A Study of Aluminum-Water Reactions at High Temperature Using a Laser
L. Leibowitz and L. W. Mishler
Am. Chem. Soc. 152nd Mtg., New York, September 11-16, 1966, Abstracts of Papers, R-24

Electrochemistry of the Lithium Hydride Cell
J. A. Plambeck, J. P. Elder, and H. A. Laitinen
J. Electrochem. Soc. 113, 931-937 (September 1966)

The Ignition of Binary Alloys of Uranium
J. G. Schnizlein, L. Baker, Jr., and J. D. Bingle
J. Nucl. Mater. 20(1), 39-47 (July 1966)

Condensed Phase Equilibria in the System MoF_6-UF_6
L. E. Trevorrow, M. J. Steindler, and D. V. Steidl
Am. Chem. Soc. 152nd Mtg., New York, September 11-16, 1966, Abstracts of Papers, O-47

New Pyrochemical Process for Fast Breeder Reactor Fuels.
II. Uranium Transport Experiments
W. J. Walsh, I. O. Winsch, R. D. Pierce, and L. Burris, Jr.
Am. Chem. Soc. 152nd Mtg., New York, September 11-16, 1966, Abstracts of Papers, R-10

Isothermal Studies of the Stainless Steel-Steam Reaction
R. E. Wilson and C. Barnes, Jr.
Am. Chem. Soc. 152nd Mtg., New York, September 11-16, 1966, Abstracts of Papers, R-25

A Critical Evaluation of Fast Fission Cross Sections
W. G. Davey
Conf. on Neutron Cross Section Technology, Washington, D. C., March 22-24, 1966. USAEC Report CONF-660303, Book 2, pp. 796-808

Dynamic Vibrations and Stresses in Elastic Cylinders and Spheres
G. Cinelli
Proc. 5th Natl. Congr. Applied Mechanics, University of Minnesota, June 1966. ASME, New York, 1966, p. 110 Abstract

Discussion: Maximum Two-Phase Vessel Blowdown from Pipes by F. J. Moody
H. K. Fauske
J. Heat Transfer 88(3), 294 (August 1966)

Synthesis of Optimal Control System for Nuclear Reactors with Generalized Temperature Feedback
I. Kliger
Nuclear Electronics, Proc. IAEA Symp., Bombay, November 22-26, 1965. Intern. Atomic Energy Agency, Vienna, 1966, pp. 443-460

Combined Thermal Convective Magnetohydrodynamic Flow
R. M. Singer
Appl. Sci. Res. 12, 375-404 (1966)

The Chemical Binding Effects on the Resonance Line Shapes of Uranium-238 in a UO_2 Lattice
C. R. Adkins, P. J. Persiani, R. N. Hwang, and J. J. Kaganove
Conf. on Neutron Cross Section Technology, Washington, D.C., March 22-24, 1966. USAEC Report CONF-660303, Book 1, pp. 134-145

Measurement of the $Li^6 + B^{10}$ Neutron Absorption Cross Sections by the Shell Transmission Method
S. A. Cox
Conf. on Neutron Cross Section Technology, Washington, D.C., March 22-24, 1966. USAEC Report CONF-660303, Book 2, pp. 701-712

Sensitivity of Fast Reactor Parameters to Cross Section Uncertainties
H. H. Hummel
Conf. on Neutron Cross Section Technology, Washington, D.C., March 22-24, 1966. USAEC Report CONF-660303, Book 2, pp. 809-820

The Effect of Randomness on Group Cross Sections. II.
C. N. Kelber and P. H. Kier
Nucl. Sci. Eng. 26, 67-72 (September 1966)

Effects of $(n,\gamma n)$ Processes on Fast Neutron Capture and Inelastic Spectra
P. A. Moldauer
Conf. on Neutron Cross Section Technology, Washington, D.C., March 22-24, 1966. USAEC Report CONF-660303, Book 2, pp. 613-622

A Comparison of Multilevel and Single Level Effects for a Fissionable Isotope
E. M. Pennington
Conf. on Neutron Cross Section Technology, Washington, D.C., March 22-24, 1966. USAEC Report CONF-660303, Book 2, pp. 997-1003

Passive Adapter Circuit Drives Decade Scaler
K. G. Porges
Electronic Design 14(21), 92 (September 13, 1966)

Low Flux Determination of Capture-to-Fission Ratio
W. C. Redman and M. M. Bretscher
Conf. on Neutron Cross Section Technology, Washington, D.C., March 22-24, 1966. USAEC Report CONF-660303, Book 2, pp. 1092-1097

Inelastic Scattering--A Compendium
A. B. Smith
Conf. on Neutron Cross Section Technology, Washington, D.C., March 22-24, 1966. USAEC Report CONF-660303, Book 1, pp. 577-598

ANL Reports

ANL-6832 EXAMINATION OF EBWR CORE-1A FUEL
R. Carlander

ANL-6964 BORAX-V NEUTRONICS
J. T. Hagen and R. W. Goin

ANL-7127 IMPROVEMENTS IN CONSOLIDATION AND FABRICATION OF VANADIUM-20 w/o TITANIUM (TV-20)
W. R. Burt, Jr., W. C. Kramer, F. J. Karasek, and R. M. Mayfield

ANL-7137 COMPARATIVE COST STUDY OF THE PROCESSING OF OXIDE, CARBIDE, AND METAL FAST-BREEDER-REACTOR FUELS BY AQUEOUS, VOLATILITY, AND PYROCHEMICAL METHODS
M. Levenson, V. G. Trice, Jr., and W. J. Mecham

ANL-7142 LABORATORY INVESTIGATIONS IN SUPPORT OF FLUID-BED FLUORIDE VOLATILITY PROCESSES. Part X. A Literature Survey on the Properties of Tellurium, Its Oxygen and Fluorine Compounds
D. R. Vissers and M. J. Steindler